MIC2020

20th Machining Innovations Conference for Aerospace Industry

PROCEEDINGS

New Production Technologies in the Aerospace Industry

December 2nd 2020 at the
Hannover Centre for Production Technology (PZH)
in Garbsen, Germany

MANUFACTURING INNOVATIONS NETWORK

IFW
Institut für Fertigungstechnik und Werkzeugmaschinen

CIRP sponsored conference

Preface

Olaf Lawrenz
Chairman of the Manufacturing Innovations Network e. V.,
Head of Varel/Bremen Site, Premium AEROTEC GmbH

Prof. Dr.-Ing. Berend Denkena
Member of the Board of the Manufacturing Innovations Network e. V.,
Head of Institute of Production Engineering and Machine Tools, Leibniz Universität Hannover

The aerospace industry has always been driven by challenges, which often result in innovation. Both, the products and the manufacturing processes are constantly evolving, leading to new standards and technologies, not only in aerospace industry. In the centuries of development, research and industry have always been faced with new challenges, and one of the main challenges in 2020 is the Covid-19 pandemic. The Covid-19 pandemic has hit not many industries as hard as the aerospace industry. Companies are faced with major challenges and have to rethink their business strategy. Meeting these challenges requires intensive exchange between experts and good interdisciplinary cooperation. The Machining Innovations Conference is an excellent opportunity to get updated about new trends, technologies and the latest developments in the aerospace industry. Modern technological development within this sector makes it possible to respond to the challenges of society and to enable an economic and sustainable production. The MIC2020 20th Machining Innovations Conference for Aerospace Industry is presented from the Institute of Production Engineering and Machine Tools in cooperation with the Manufacturing Innovations Network e.V. and takes place at the Hannover Centre for Production Technology (PZH, Garbsen, Germany). Renowned experts from industry and research will present the latest trends, newest know-how and research results in 18 speeches. This years scientific session is sponsored by the International Academy for Production Engineering (CIRP). The contributions to the scientific session are also published in MIC Proceedings by SSRN.

Hannover, December 2020

Olaf Lawrenz

Berend Denkena

Contents

Keynote Speeches

Making Aerospace Manufacturing ready for the post COVID future

Manfred Hader,
Senior Partner,
Roland Berger


Roland Berger
Making Aerospace Manufacturing ready for the post-COVID future
MIC Conference
MANUFACTURING INNOVATIONS NETWORK
02 December 2020

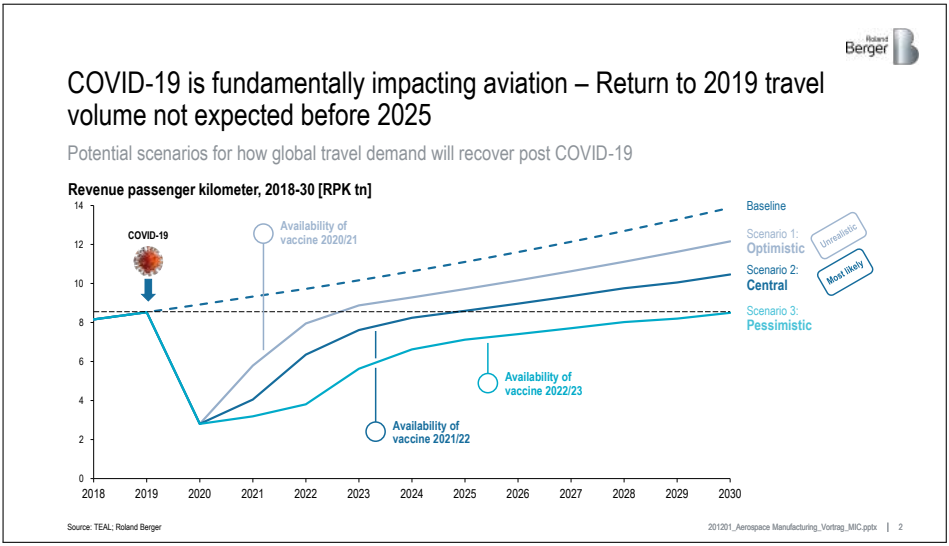
Roland Berger
COVID-19 is fundamentally impacting aviation – Return to 2019 travel volume not expected before 2025
Potential scenarios for how global travel demand will recover post COVID-19
Revenue passenger kilometer, 2018-30 [RPK tn]
14
12
10
8
6
4
2
0
2018
2019
2020
2021
2022
2023
2024
2025
2026
2027
2028
2029
2030
COVID-19
Availability of vaccine 2020/21
Availability of vaccine 2022/23
Availability of vaccine 2021/22
Baseline
Scenario 1: Optimistic
Unrealistic
Scenario 2: Central
Most likely
Scenario 3: Pessimistic
Source: TEAL; Roland Berger
201201_Aerospace Manufacturing_Vortrag_MIC.pptx | 2

COVID-19 is also impacting key industry trends and will require aerospace COOs to revisit their strategy to prepare manufacturing for the future

Key Aerospace trends affected by COVID-19


Launch of the next generation aircraft


Drive towards sustainability


Consolidation within aerospace


Emergence of Chinese OEMs


(De-)globalization of footprint


Automation

How to make **Aerospace Manufacturing** ready for the **future**?

Source: TEAL; Roland Berger

Manufacturing of the future will take place in smaller, more local & universal factories to cope with by COVID-19 accelerated challenges and trends

Key areas for manufacturing of the future

General challenges for manufacturing
- Demographics
- Global instability
- Sustainability
- ...

Key aerospace trends
- Dramatically increased overcapacities
- COVID-19 induced acceleration

Future aerospace factories are ...

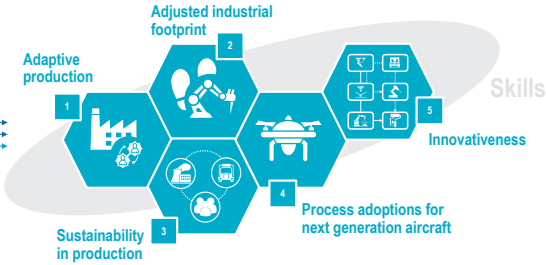

...smaller, more local & more universal

Source: Roland Berger

1 Adaptive production

Roland Berger

Companies must re-think their approach to "adaptiveness", i.e. make the production more resilient, flexible and state-of-the-art

Production system re-design for adaptive production

1 Focus on resilience	2 Provide high flexibility	3 Cost efficiency requirements	4 Embrace new technologies
Being able to cope with (sudden) change without failing to deliver on promises	Being able to seamlessly adjust to fluctuations/ mid-term changes in demand	Being able to produce at low costs while maintaining high quality & short delivery times	Being able to offer state-of-the art processes & technologies to fulfill customer wishes
Agility	Adaptability	Digitization	Autonomous factory
Robustness	Scalability	Automation	Processes & Technologies

No focus on output maximization anymore *– the* ***new target*** *is to reach higher levels of* ***robustness, flexibility*** *and* ***competitiveness***

Source: Airbus; PTC; VW; Bosch Rexroth; MTU Aero Engines DLR; Safran; Roland Berger; interviews

2 Adjusted industrial footprint

Roland Berger

Local supply chains must be the backbone of a resilient industrial footprint – Orders to be shifted based on available capacity & customer needs

Three steps towards resilient supply chains

Adaptable factories in strategic regions

- **Small and highly adaptable assembly lines** close to strategic customers
- **Inventories** to cope with temporary supply shortages

Local supply chains close to the assembly lines

- **Local-for-local suppliers**
- **Just-in-Time** or even **Just-in-Sequence** delivery of parts
- Fulfill **local content requirements**

Integration of suppliers from best cost countries

- Close **monitoring of suppliers** with artificial intelligence
- **IT integration & seamless data transfer** (e.g. smart components)

Source: Roland Berger; interviews

3 Sustainability in production

Companies not integrating sustainability topics into their production will face serious pressure from customers in the future

Contribution of production to sustainability

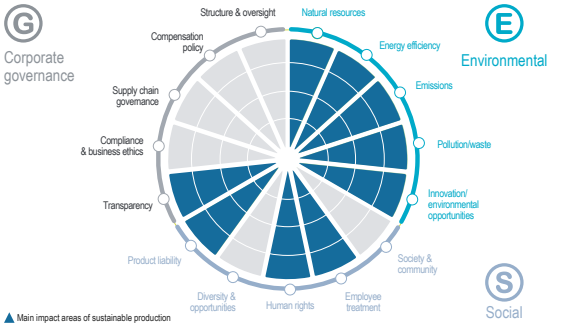

▲ Main impact areas of sustainable production

- **In the context of the Aerospace industry, mainly environmental aspects are affected through sustainable production**
- **Efficiency projects and sustainability projects need to go hand-in-hand**
- **Production always has to respect human rights and treat workers correctly**

Source: Roland Berger

3 Sustainability in production

There are many challenges with respect to sustainability in aerospace production – Multiple solutions to be explored

Examples of solutions for sustainability challenges during production (non-exhaustive)

Supply chain	(E) Select responsible raw material suppliers by using environmental performance indicators (E) Encourage a geographically concentrated suppliers-base around integrated sites which could limit CO2 emissions (S) Ensure that suppliers respect labor and human rights and comply with international laws (G) Allow a constant quality control and traceability in the overall aircraft value chain (e.g. through a connected IT architecture between the OEM & suppliers)
Energy & resources (incl. raw materials)	(E) Use of (raw) materials that could be easily recyclable (E) Minimize (raw) material waste (e.g. by casting parts close to final shape) and recycle material waste (e.g. metal chips) (E) Switch to recycled or "grow-back" material e.g. producing cabin interior elements (E) Use of renewable energy solutions (E) Optimize machine park by replacing energy-consuming equipment (e.g. with air-source heat pumps, solar panels)
Production processes	(E) Use of eco-friendly surface treatment (e.g. laser alloying) and painting/coating – Limit number of coating processes (E) Avoid the use of phthalates, beryllium, antimony, BFR[1], and PVC[2] representing the main hazardous chemicals in the production of electronics (S) Improve health and safety procedures to ensure zero accidents in production sites (S) Ensure that labor and human rights are monitored and respected in production sites
Products	(E) Use eco-friendly fabrics for seat covers (E) Encourage modularity by generalizing standards between OEMs and suppliers (E) Encourage the use of onboard systems allowing the addition of new features through software upgrade (extending the lifetime and reducing obsolescence)

1) Brominated flame retardant; 2) Polyvinyl chloride

Source: Desk research, Roland Berger

4 Process adoptions for next generation aircraft

Manufacturing needs to get involved in the cross-functional development of future products to avoid costly challenges during production ramp-up

Manufacturing involvement into new product development

Digital twin

> **Connectivity** of assets, systems and operators on premise and **along the entire supply chain** via IoT-platforms to enable e.g. analytics, AI etc.
> **Modell-based definition** (e.g. up-to-date, digital and consistent data)
> High **transparency at any time** (e.g. producibility, costs, changes)

UAM mass production

> Be ready for **ramping-up UAM** production – master at the same time a **step change with respect to costs**
> Acquire required **production technologies**, build up **qualifications** and get **EASA/FAA certifications** for new manufacturing processes

Aircraft design for alternative propulsion

> **Electric propulsion** promises to make **aviation sustainable** but requires **design changes** – **hydrogen** based **propulsion** requires a large and pressure resistant liquid hydrogen storage that might be located in the fuselage

Enabler
- Standardized customization (Modularization)
- Design for Manufacturing

Implications for operations

> **Manufacturing know-how needs to be integrated into the design process** to ensure full producibility and automatability
> Industry 4.0 requires **fully digital products**
> Alternative propulsion systems require a **paradigm shift also in aircraft design & production**

Source: Roland Berger; interviews

5 Innovativeness

Aerospace manufacturers should enhance production with capabilities for new products and leverage free capacities in new markets

Product portfolio management

ENHANCEMENT
New products

New mobility
Urban Air Mobility (UAM), hyperloop transportation, …

New propulsion systems
Hydrogen/alternative fuels, electric planes, …

New materials & structures
Flexible wings, …

Source: techxplore

DIVERSIFICATION
New markets and industries

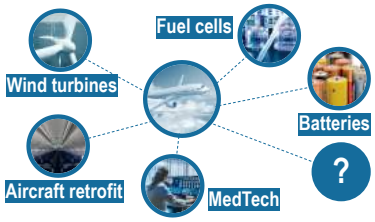

Use the downtime to prepare the production system for new products – Change is always harder in a running system

Explore new opportunities to utilize manufacturing capacity, e.g. enter aircraft retrofit or non-aviation markets

Source: Roland Berger; interviews

We recommend to take actions now to make legacy programs future proof & to use COVID as opportunity to get ready for the future of manufacturing

Roadmap for Aerospace manufacturing

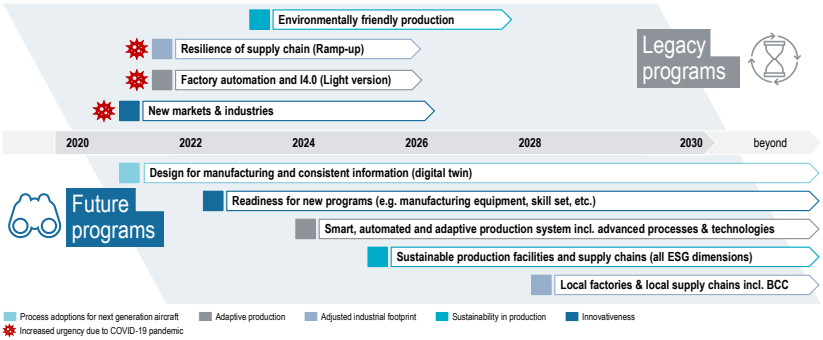

Source: Roland Berger; Interviews

Availability of the right skills is the key success factor for future readiness – Hence, this topic must be high on every corporate agenda

Key skills for manufacturing of the future

Type of skill-set

1 Core technology and process skills
Core STEM and process proficiency

2 Product and industry knowledge
Product and portfolio lifecycle including go-to-market models

3 Leadership and people skills
Management, leadership and team development

Functional focus

- Programme Management
- Engineering
- **Operations**
- **Supply Chain**
- Quality

Key skills

Aerospace players can focus on developing **skills in three main areas** within the field of **manufacturing to emerge stronger** after the **COVID-19 crisis**

Non-exhaustive

Production footprint and supply chain
- Local Supply Ch.
- Digital Twin of supply chain
- Balanced footprint
- Double Sourcing
- Connectivity along supply chain

Advanced production systems
- Automation
- Additive Manufacturing
- Digital Twin of manufacturing site
- Focus factory
- New materials & production processes

Alternative product concepts
- New & sustainable materials
- Hygienic materials
- Thermoplastics
- All-/More-Electric
- "Smart Skin"

Source: BDLI; Roland Berger

Please contact our global experts for further insights and personal discussions about the aerospace factory of tomorrow

Manfred
Hader

Senior Partner

+49 160 744 4327
Manfred.Hader@
rolandberger.com

Dr. Bernhard
Langefeld

Partner

+49 160 744 6143
Bernhard.Langefeld@
rolandberger.com

Dr. Stephan
Baur

Principal

+49 160 744 8041
Stephan.Baur@
rolandberger.com

Johannes
Kube

Senior Consultant

+49 160 744 4410
Johannes.Kube@
rolandberger.com

Roland Berger
THINK:ACT

Digitale Vernetzung in der Flugzeugfertigung - leichter gesagt als getan

Jürgen Nolte,
Vice President,
Siemens Vertical Aerospace


„Digitale Vernetzung in der Flugzeugfertigung – leichter gesagt als getan…“
Frei verwendbar
Jürgen Nolde, Siemens AG


Die Flugzeugindustrie und Covid-19 –
Restrukturierung und Veränderungen in der Supply Chain
SIEMENS
Herausforderungen der Flugzeugindustrie
• Überbrücken der momentanen Phase geringer Nachfrage bei weiterhin funktionierender Supply Chain, schnelle Anpassung an das “New Normal”
Veränderungen in der Zuliefererlandschaft
Insourcing
Reduzierung der Fixkosten, Ausschöpfung der existierenden Ressourcen.
Konsolidierung
Vertikale und horizontale Konsolidierung – Optimierung der Produktionskapazitäten
Restrukturierung
Anpassen der Kapazitäten an künftige Produktionsraten

Siemens in Aerospace – mehr als nur CNC

SIEMENS

Digital Industries

Data Backbone, Digital Twin product, production, performance, end to end manufacturing……

- Transparenz
- Speed

Support

Service, Shop Floor Digitalisierung, Integral Plant Maintenance, consulting….

Best in Class Automation

CNC Steuerungen, Roboter, Assembly, Composite, AM, Krane…

Verbesserung der Fertigungs-transparenz

Smart Infrastructure
Safety, Air, Energy Management

Siemens in Aerospace – weltweite Aufstellung

SIEMENS

Corporate Account Managers (CAM) – Global Account Managers (GAM)

AIRBUS	D. Rabeneck	BOEING	D. Green	Rolls-Royce	Rob Poyner
SAFRAN	C. Camus	GE Aviation	R. Vanmarcke	BAE SYSTEMS	R. Edwards

28 Account Manager in 13 Regionen

6 Corporate Account Manager

HQ Team – Koordinierung, Technik, Events


Erfolgreiche Projekte in Automatisierung und Software in Aerospace
SIEMENS
BOEING
AIRBUS
GENERAL DYNAMICS
UAC
PILATUS
SUKHOI
BOMBARDIER
Commercial Aviation
NORTHROP GRUMMAN
BAE SYSTEMS
GENERAL ATOMICS
BOEING
LOCKHEED MARTIN
Defense Aerospace
SAFRAN
Rolls-Royce
GE Aviation
Pratt & Whitney
Engines and Propulsion
RAFAEL
MOOG
Collins Aerospace
Raytheon
SPIRIT
Supplier & Avionics
SPIKE AEROSPACE
ERION
Supersonic market
ULA
SPACEX
VECTOR
NORTHROP GRUMMAN
arianegroup
Launch Vehicles
BOEING
SNC
Bell
SPACEX
Manned and Unmanned Space Systems
BYE AEROSPACE
SIEMENS
AIRBUS
zipline
Electric and start-up markets

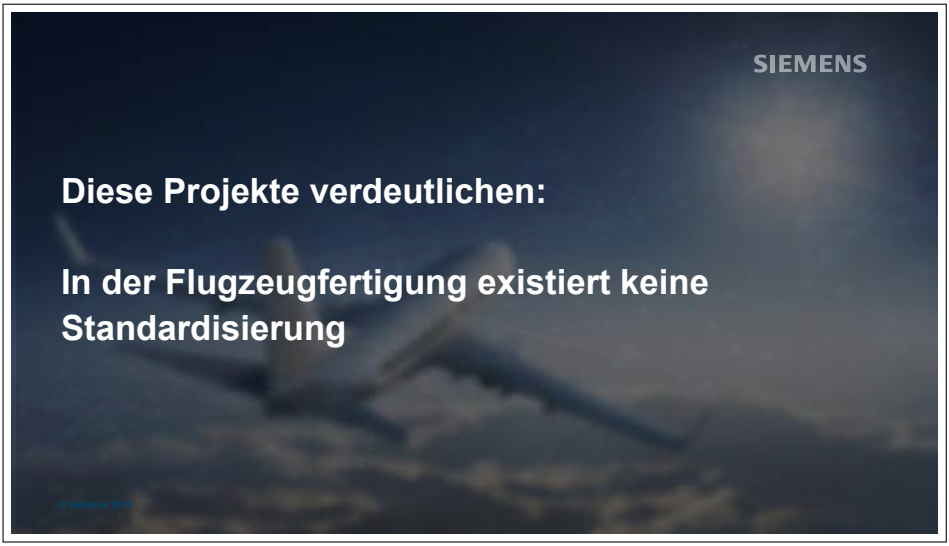
SIEMENS
Diese Projekte verdeutlichen:
In der Flugzeugfertigung existiert keine Standardisierung
© Siemens 2017

SIEMENS

Extrem lange Produktionszyklen

Boeing 747- 53 Jahre Produktion

Lockheed Hercules C130- 64 Produktionsjahre

B52- 68 Jahre

Panavia Tornado-im 41. Jahr…

SIEMENS

Höchste Fertigungskomplexität

SIEMENS

Zertifizierte Prozesse

SIEMENS

Die Aerospace “Brownfield” Werke blockieren I4.0 Anwendungen

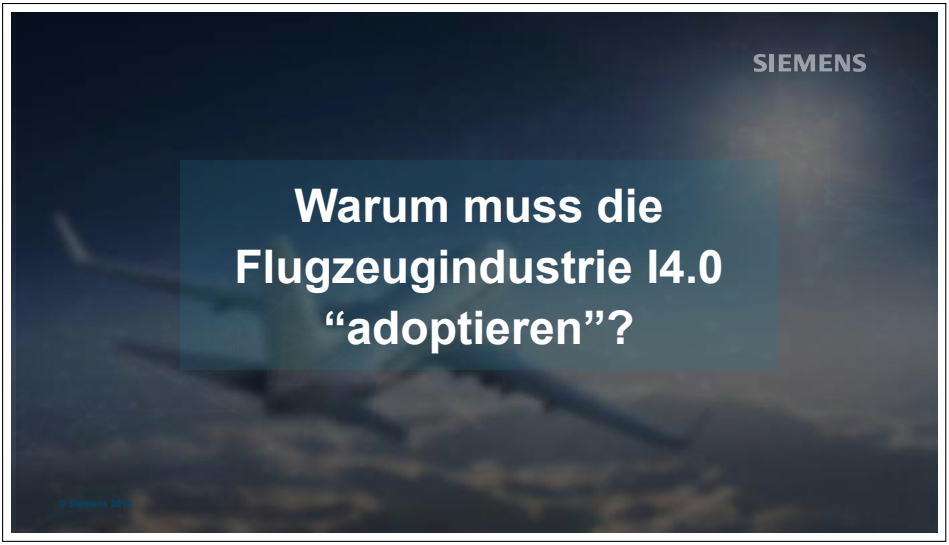
SIEMENS
Warum muss die Flugzeugindustrie I4.0 “adoptieren”?

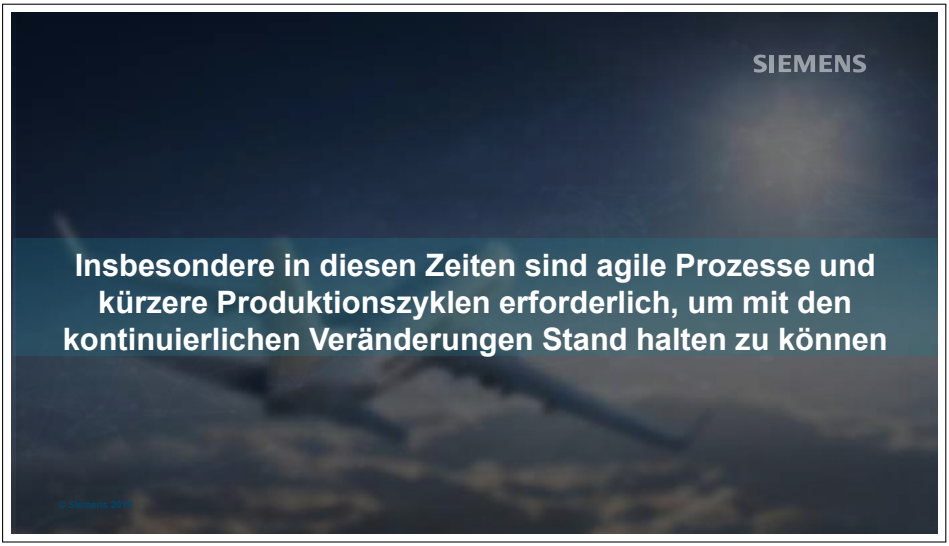
SIEMENS
Insbesondere in diesen Zeiten sind agile Prozesse und kürzere Produktionszyklen erforderlich, um mit den kontinuierlichen Veränderungen Stand halten zu können


SIEMENS
Design, Prototyping, Zertifizierung und die Produktion müssen schneller umgesetzt werden

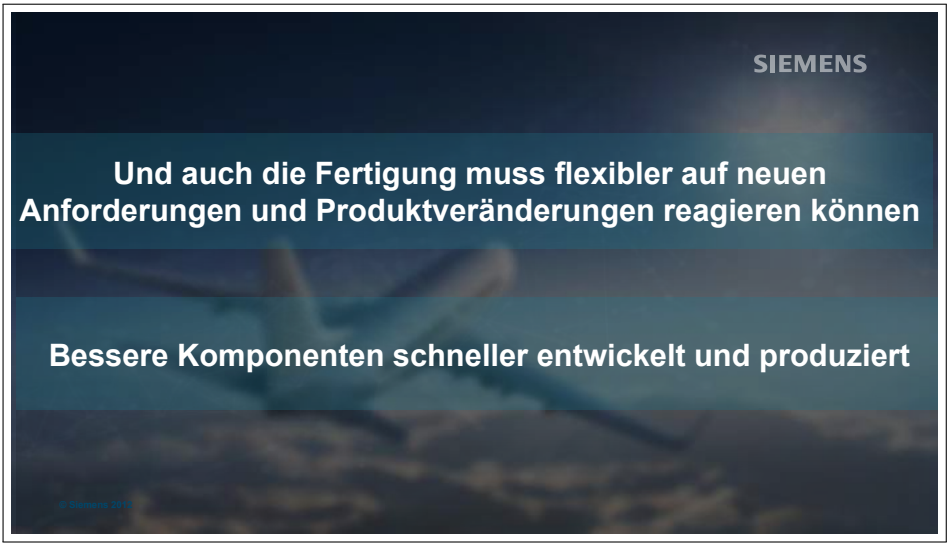
SIEMENS
Und auch die Fertigung muss flexibler auf neuen Anforderungen und Produktveränderungen reagieren können
Bessere Komponenten schneller entwickelt und produziert


SIEMENS
Was sind die ersten Schritte in der Standardisierung?


SIEMENS
Die Vernetzung der Fertigungs-kompontenten und Maschinen

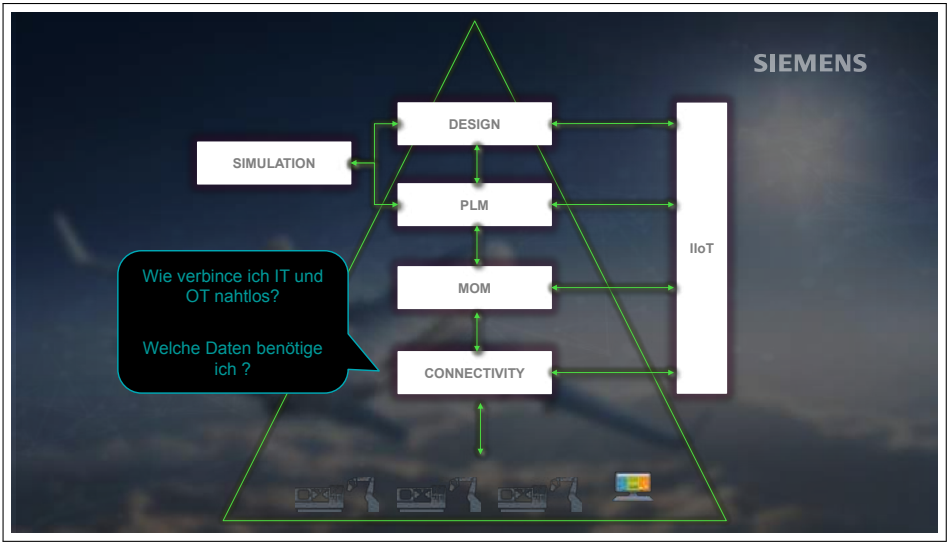
SIEMENS
DESIGN
SIMULATION
PLM
MOM
CONNECTIVITY
IIoT
Wie verbince ich IT und OT nahtlos?
Welche Daten benötige ich ?

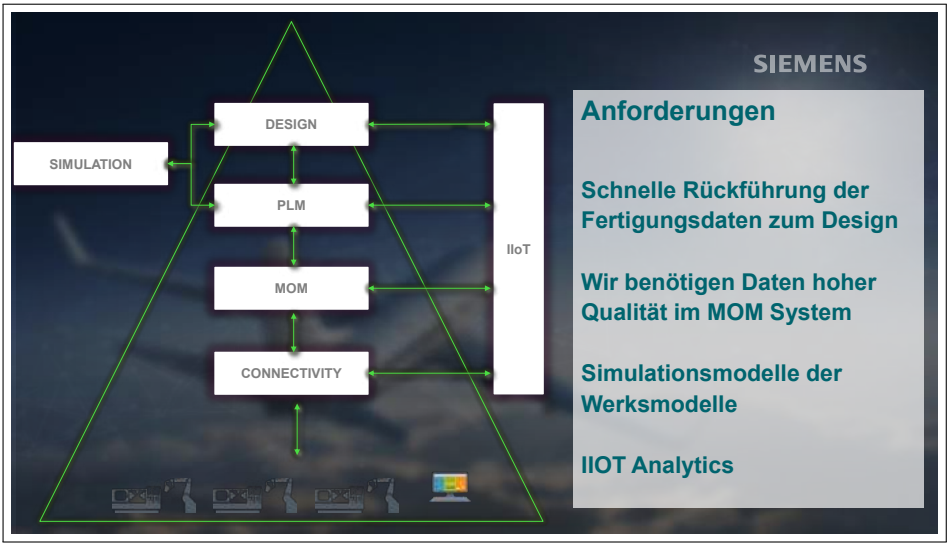
SIEMENS
DESIGN
SIMULATION
PLM
MOM
CONNECTIVITY
IIoT
Anforderungen
Schnelle Rückführung der Fertigungsdaten zum Design
Wir benötigen Daten hoher Qualität im MOM System
Simulationsmodelle der Werksmodelle
IIOT Analytics

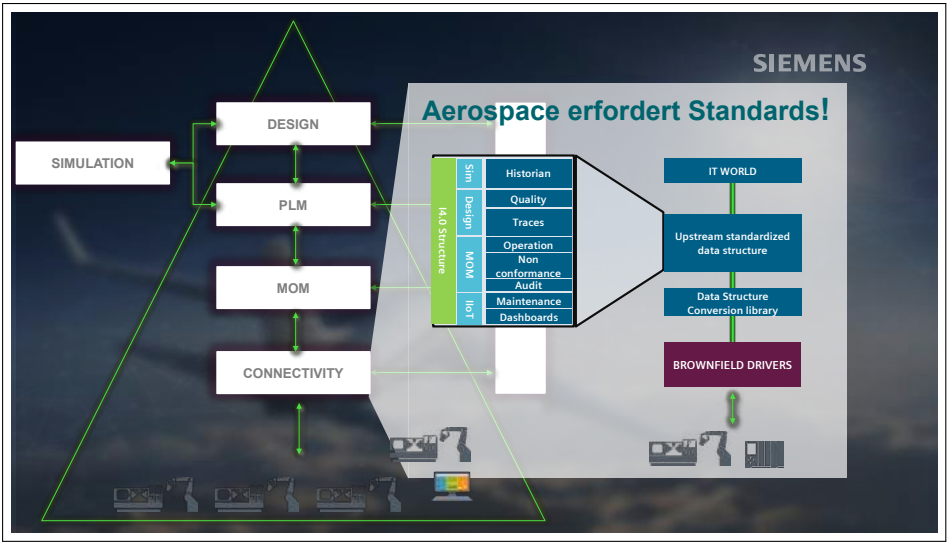
SIEMENS
Aerospace erfordert Standards!
SIMULATION
DESIGN
PLM
MOM
CONNECTIVITY
I4.0 Structure
Sim
Design
MOM
IIoT
Historian
Quality
Traces
Operation
Non conformance
Audit
Maintenance
Dashboards
IT WORLD
Upstream standardized data structure
Data Structure Conversion library
BROWNFIELD DRIVERS


SIEMENS
Standards in Aerospace
IT WORLD
Upstream standardized data structure
Data Structure Conversion library
BROWNFIELD DRIVERS

Aerospace Digital Interoperability Labor

SIEMENS

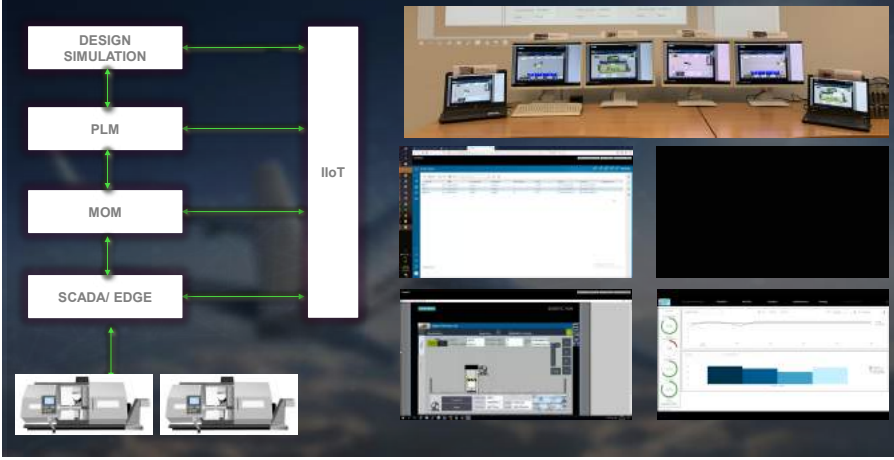

Aktuelle MIN Projekte – eine Möglichkeit für den Start von Standardisierung in Aerospace

SIEMENS

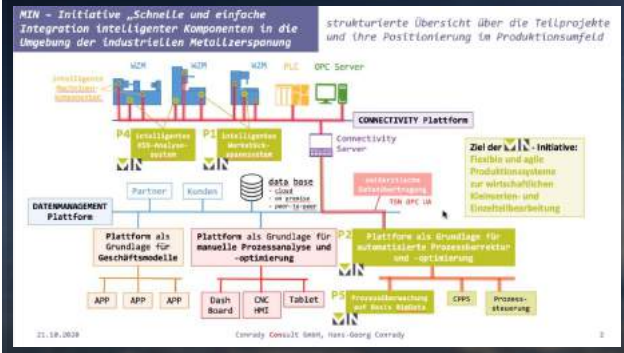

Wir unterstützen gern

Optimization and digitalization of the metallic additive manufacturing process chain at Airbus Helicopters

Luis Martin Diaz,
Vice President Head of Industrial Service Centers Germany,
Airbus Helicopters



MIC 2020 Optimization and digitalization of the metallic additive manufacturing process chain at Airbus Helicopters

Dr. Luis Martin Diaz
Vice President - HO Industrial Service Centers Germany

AIRBUS

AGENDA

1| AIRBUS HELICOPTERS
2| END-TO-END METALLIC AM PROCESS
3| DIGITALIZATION
4| CONCLUSION AND Q&A

AIRBUS

AIRBUS Helicopters

[Airbus Amber]

A unique global presence!

Main Sites:
- France: Marignanne
- Germany: Donauwörth

19,751 employees in 2019

6.9 bn € turnover in 2019

to serve 3,050 operators

29 Customer Centres and affiliated sites

in 150 countries

4 December 2020 MIC 2020 Optimization and digitalization of the metallic additive manufacturing process chain at Airbus Helicopters

AIRBUS

Civil Helicopters

[Airbus Amber]

Single

Light twin

Twin medium

Medium/Heavy

AIRBUS

Military Helicopters

[Airbus Amber]

Light helicopters

Helicopters Medium weight class

Helicopters medium weight/ heavy class

Special helicopters

AIRBUS

Technology demonstrators

[Airbus Amber]

VSR700

RACER

CityAirbus

AIRBUS

HELICOPTERS [Airbus Amber]

3D-Printing at Airbus Helicopters in Donauwörth
Metallic Additive Manufacturing (Titanium)

- Machine: EOS M400-4
- 4-Laser System (simultaneously) to increase productivity
- Automatic powder refilling system
- Build chamber: 400x400x400(64l)
- Material: Ti64 (Titanium powder)

9 December 2020 MIC 2020 Optimization and digitalization of the metallic additive manufacturing process chain at Airbus Helicopters AIRBUS

HELICOPTERS [Airbus Amber]

3D-Printing at Airbus Helicopters in Donauwörth
Metal 3D-Printing (Titanium)

43% weight savings for our first 3D printed titanium parts

More than 3200 Parts printed

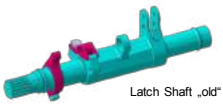
Latch Shaft „old“

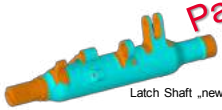
Latch Shaft „new“


Latch Shaft „old“


Latch Shaft „new“

10 December 2020 MIC 2020 Optimization and digitalization of the metallic additive manufacturing process chain at Airbus Helicopters AIRBUS

HELICOPTERS

[Airbus Amber]

ROADMAP [PRODUCTS AND PROCESSES]

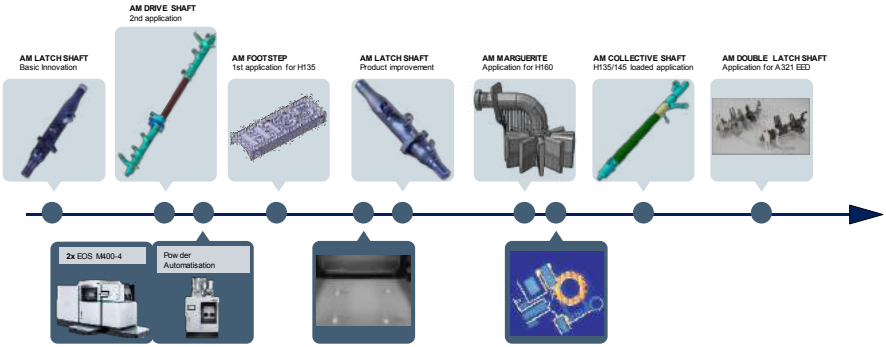

AM Metal Outlook

The unique manufacturing depth and design/industrialization know-how allows AH to develop and improve the AM process chain end-to-end and so identify and implement business case driven AM applications.

AIRBUS

HELICOPTERS

[Airbus Amber]

What are we learning?

About the potential of this technology for Aerospace

- Weight
- Recurring costs
- Performance

About the end-to-end Process of Metallic AM

- Core competences
- Interdependencies
- Strategic approach

About the maturity of the Metallic AM Aerospace Industry

- Promises vs. reality
- Understanding of Aerospace requirements
- Caution vs. fear

AIRBUS

HELICOPTERS [Airbus Amber]

Strategy: industrialization as core competence, in a context of full understanding of qualification requirements

Industrialization of additively manufactured applications

design stress	support nesting	print, OT, depowder	post print	machining	post machining	means of process security	application qualification	data mgt.

Design4AM means to customise the design to the print and all subsequent process elements as well as enhancement of process elements to allow an efficient and qualifiable design solution

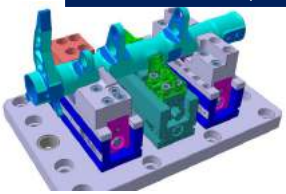

AIRBUS

HELICOPTERS [Airbus Amber]

End-to-End Process

	Powder Supply	Powder Bed Fusion	Stress relief Heat treatment	Part Separation	Removal of Support Structure	Dry blasting	Hot Isostatic Pressing (HIP)	High Rate Etching	CT Testing	Machining	Etching & Dye-Penetrant test
Where	external	internal	internal	internal	internal	internal	external	internal	external	internal	internal

Interdependency of capability to automatize the removal of the support structures with the design of the part and robustness of the printing process

AIRBUS

HELICOPTERS [Airbus Amber]

End-to-End Process

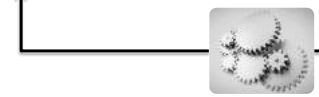

Interdependency between layer thickness and etching process

AIRBUS

HELICOPTERS [Airbus Amber]

End-to-End Process

Interdependency between wall thickness and clamping strategy for machining

AIRBUS

HELICOPTERS

[Airbus Amber]

End-to-End Process

	Powder Supply	Powder Bed Fusion	Stress relief Heat treatment	Part Separation	Removal of Support Structure	Dry blasting	Hot Isostatic Pressing (HIP)	High Rate Etching	CT Testing	Machining	Etching & Dye-Penetrant test
Where	external	internal	internal	internal	internal	internal	external	internal	external	internal	internal

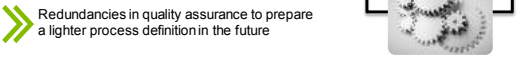

Redundancies in quality assurance to prepare a lighter process definition in the future

AIRBUS

HELICOPTERS

[Airbus Amber]

DIGITALIZATION APPROACH FOR METALLIC PRINTING

Focus on big-data & data analytics to establish co-relation on complete process

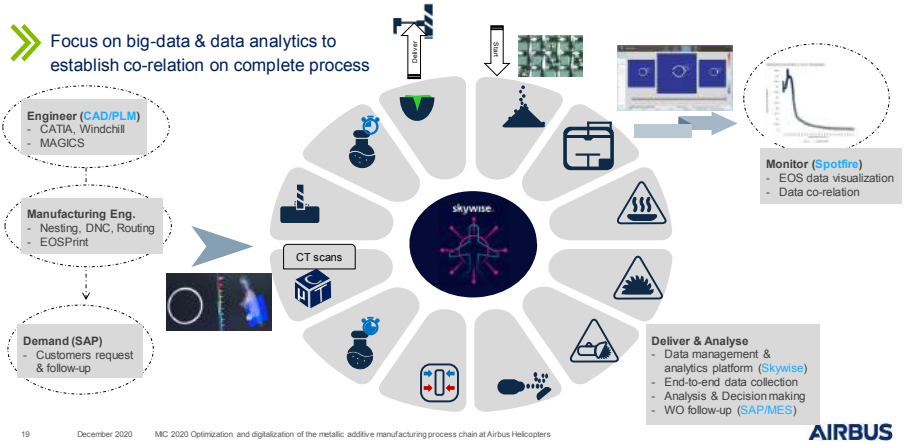

AIRBUS

HELICOPTERS

[Airbus Amber]

HOW DIGITALIZATION ADDS VALUE

In-depth monitoring during printing with Optical Thermography will result in reduced NDT => process simplification and reduced costs eg. OT Drive shaft

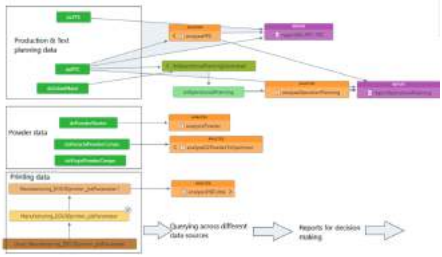

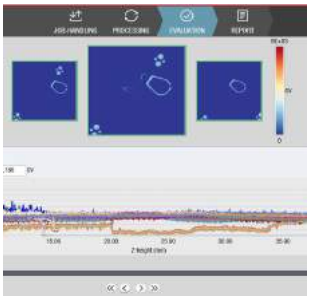

Tracking all production relevant data and co-relating them helps us understand process dependencies – eg. Powder to Part oxygen values

AIRBUS


[Airbus Amber]
4| CONCLUSION AND Q&A
22 December 2020 MIC 2020 Optimization and digitalization of the metallic additive manufacturing process chain at Airbus Helicopters

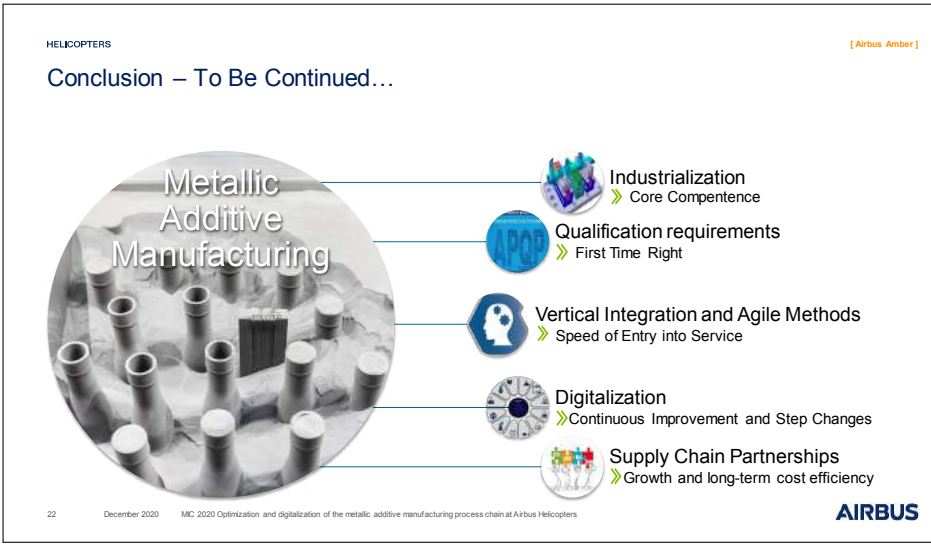
HELICOPTERS
[Airbus Amber]
Conclusion – To Be Continued…
Metallic Additive Manufacturing
Industrialization
» Core Compentence
Qualification requirements
» First Time Right
Vertical Integration and Agile Methods
» Speed of Entry into Service
Digitalization
» Continuous Improvement and Step Changes
Supply Chain Partnerships
» Growth and long-term cost efficiency
22 December 2020 MIC 2020 Optimization and digitalization of the metallic additive manufacturing process chain at Airbus Helicopters
AIRBUS


Questions
Online discussion 12/03/20 from 2:00pm to 3:00pm
Contact us:
Dr. Luis Martin Diaz
HO ISC Germany
Frank Rethmann
HO ISC 3D Printing
23 December 2020 MIC 2020 Optimization and digitalization of the metallic additive manufacturing process chain at Airbus Helicopters
AIRBUS

SFB 871 - Regeneration komplexer Investitionsguter Systemdemonstrator

Nicolas Nübel,
Research Assistant,
Leibniz Universität Hannover

Produkt-Regeneration
Sonderforschungsbereich 871
Regeneration komplexer Investitionsgüter
finanziert durch die DFG

SFB 871 – Regeneration komplexer Investitionsgüter
Systemdemonstrator

Hannover, 2. Dezember 2020

Sprecher
Prof. Dr.-Ing. Jörg Seume

Stellvertretender Sprecher
Prof. Dr.-Ing. Berend Denkena

Geschäftsführer
Dipl.-Ing. Philipp Gilge

Koordinator Systemdemonstrator
Nicolas Nübel M. Sc.

Leibniz Universität Hannover

Produkt-Regeneration

MIC 2020
Keynote SFB 871

Einleitung
Zustandserfassung
Bewertung
Bearbeitung
Qualitätssicherung
Schlussfolgerung

SFB 871
Systemdemonstrator

N. Nübel
02.12.2020
Folie 2/27

Leibniz Universität Hannover

Komplexe Investitionsgüter

Prokonzept Berlin, HNA

MB Bladeservice

MTU, TFD

- Wenige, unflexible und zum Teil händische Reparaturverfahren
- Erfahrungsbasierte Einzelfallentscheidungen
- Geringe Nutzung wissenschaftlicher Erkenntnisse aus der Neuentwicklung

Aktuelle Regeneration

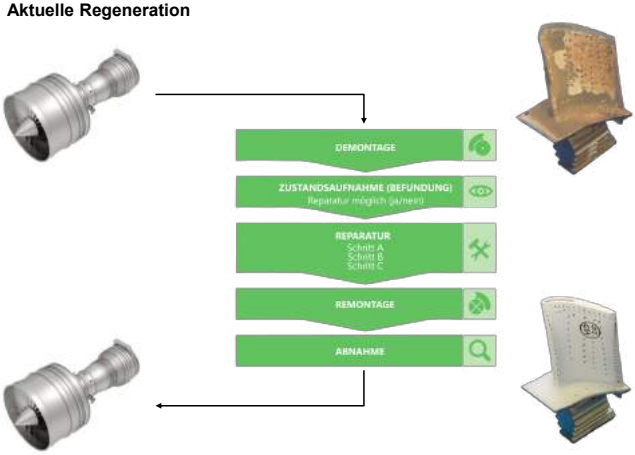

Aktuelle Regeneration

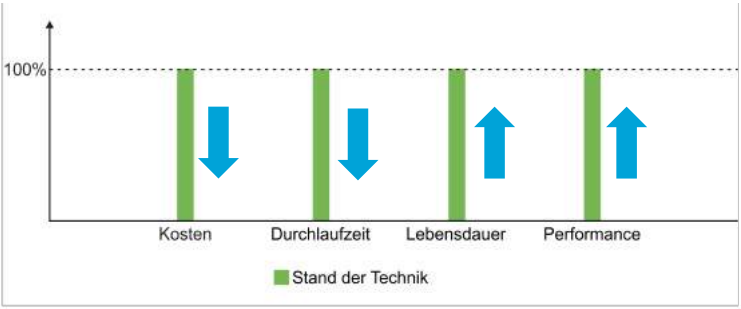

- Keine Kenntnis des produktionstechnischen Aufwands
- Keine Kenntnis des funktionalen Nutzens

→ Ineffiziente Regenerationsmaßnahmen → Verbesserungen

Produkt-Regeneration

MIC 2020
Keynote SFB 871

Einleitung
Zustandserfassung
Bewertung
Bearbeitung
Qualitätssicherung
Schlussfolgerung

SFB 871
Systemdemonstrator

N. Nübel
02.12.2020
Folie 5/27

Leibniz Universität Hannover

Zukünftige Regenerationen

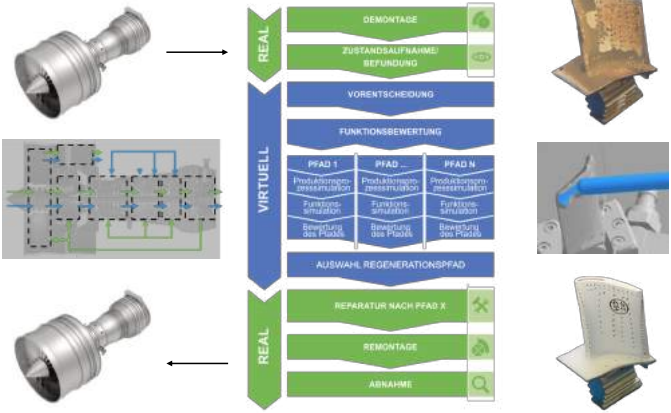

Simulative Bewertung des produktionstechnischen Aufwands und funktionalen Nutzens

- Wissensbasierte Entscheidungen
- Effizientere Regenerationen

Produkt-Regeneration

MIC 2020
Keynote SFB 871

Einleitung
Zustandserfassung
Bewertung
Bearbeitung
Qualitätssicherung
Schlussfolgerung

SFB 871
Systemdemonstrator

N. Nübel
02.12.2020
Folie 6/27

Leibniz Universität Hannover

Einteilung der Regenerationsprozesskette

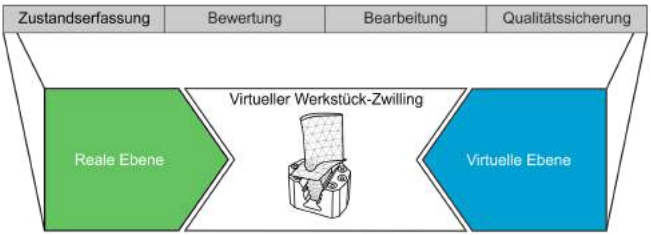

- Virtueller Werkstück-Zwilling als Schnittstelle zwischen realer und virtueller Ebene ermöglicht: Automatisierte Prozesskette

Zustandserfassung
Abgasstrahlanalyse am Flügel

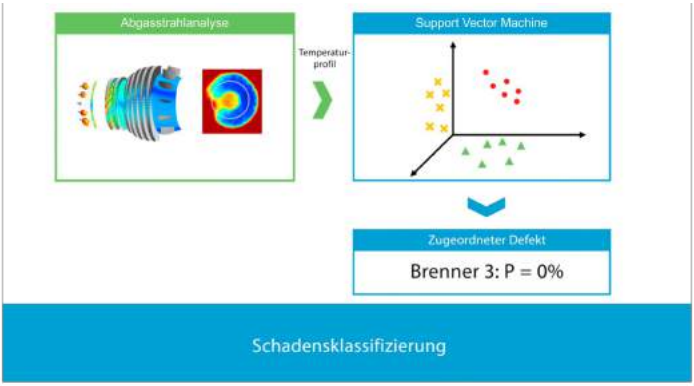

- Abgasstrahlanalyse des Triebwerks am Flügel mittels **B**ackground **O**riented **S**chlieren-Analyse
- Erkennung von Schäden im Heißgaspfad (Brennkammer, Turbine) anhand der Abgasstrahlanalyse

Zustandserfassung
Geometrieerfassung im teilzerlegten Triebwerk

- Schnelle Prüfung in beengten oder schwer zugänglichen Bauräumen
- Zusammensetzung von Einzelmessung zu einem 3D-Modell zur Bewertung des Zustandes

Produkt-Regeneration

MIC 2020
Keynote SFB 871

Einleitung
Zustandserfassung
Bewertung
Bearbeitung
Qualitätssicherung
Schlussfolgerung

SFB 871
Systemdemonstrator

N. Nübel
02.12.2020
Folie 9/27

Leibniz Universität Hannover

Zustandserfassung
Bauteilschonende und sensorische Demontage

- Reduzierung der maximalen Demontagekraft durch Mikrostöße
- Erfassung der zum Austreiben notwendigen Kraft und Frequenz

Produkt-Regeneration

MIC 2020
Keynote SFB 871

Einleitung
Zustandserfassung
Bewertung
Bearbeitung
Qualitätssicherung
Schlussfolgerung

SFB 871
Systemdemonstrator

N. Nübel
02.12.2020
Folie 10/27

Leibniz Universität Hannover

© Leibniz University Hannover 2020

Zustandserfassung
Intelligenter Werkstückträger

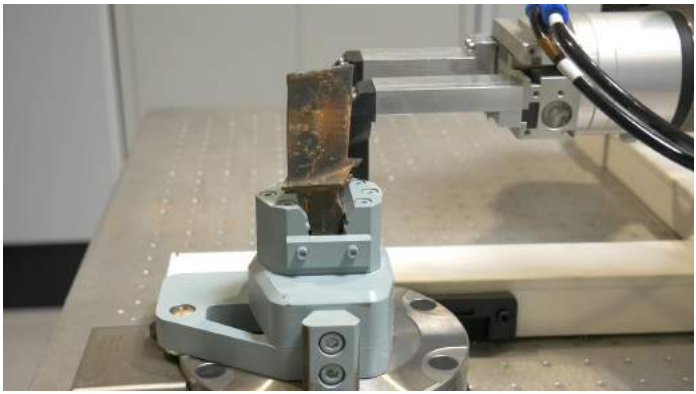

- Einsetzen der Schaufel in einen intelligenten Werkstückträger
- Einmessfreies Werkstückhandling durch Nullpunktspannsysteme in allen Prozesszellen

Zustandserfassung
Handhabung des Werkstückträgers

- Mobiles Handhabungssystem zur flexiblen Verkettung der Zellen
- Einfache Integration weiterer Prozesszellen in die Prozesskette

Zustandserfassung
Zerstörungsfreie Prüfung des Bauteilzustandes

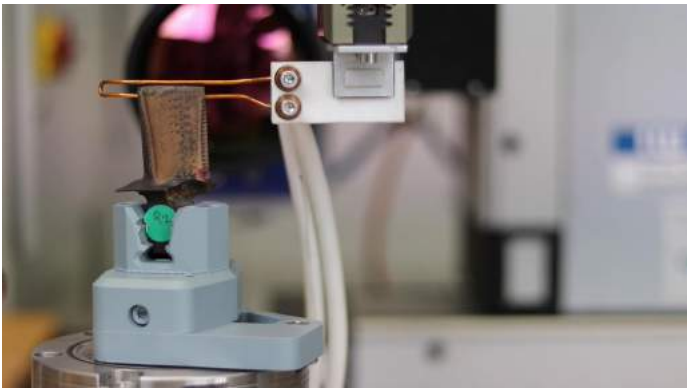

- Klassifizierung von lokalen Defekten sowie Materialcharakterisierung im Bauteil-Mehrschichtsystem
- Detektion von Rissen durch Hochfrequenzinduktionsthermografie

Zustandserfassung
Multiskalige Geometrieerfassung der relevanten Schaufeloberfläche

- Ausrichtung der Messwerte im prozessübergreifenden Koordinatensystem
- Zusammenführen der Einzelmessungen über stochastisches Muster und Werkstückträger

Bewertung
Parametrisierung der Schaufel

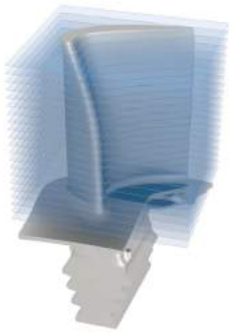

Nr.	Parameter	Einheit	Eulerradius
1	Radialspalt	mm	0,48
2	Vorderkantenradius	mm	1,61
3	Staffelungswinkel	°	40,45
4	Skelettlinienlänge	mm	84,71
5	Sehnenlänge	mm	53,81
…	…	…	…
17	Hinterkanten-Metallwinkel	°	65,98

- Bestimmen von jeweils 17 Parametern in 20 Schnittebenen
- Durchführung der notwendigen Simulationen anhand von Parametern in einem vorgelagerten Prozess

Bewertung
Berücksichtigung von Wechselwirkungen auf das Gesamtsystem

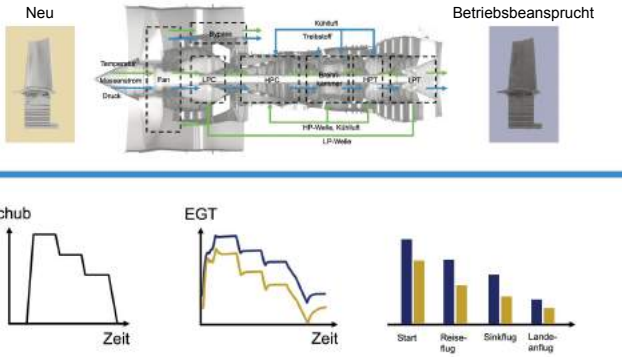

- Berücksichtigung von Geometrieveränderungen und lokalen Rauheiten auf der Schaufel
- Bestimmung der Performancekennzahl: **E**xhaust **G**as **T**emperature (EGT)

Bewertung
Bestimmung der Restlebensdauer

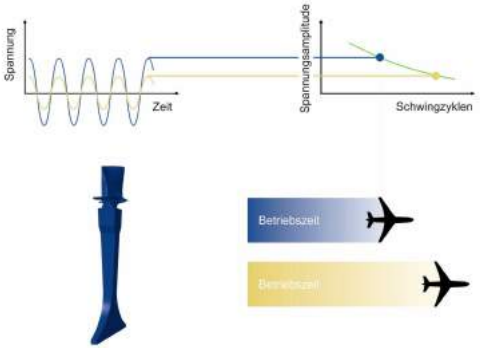

- Geänderte Geometrie (Radialspalt) ▶ Berechnung der Schwingspannung
- Hier: Verkürzung der Lebensdauer der Schaufel durch die höheren Spannungen

Bewertung
Bestimmung des kritischen Risswachstums

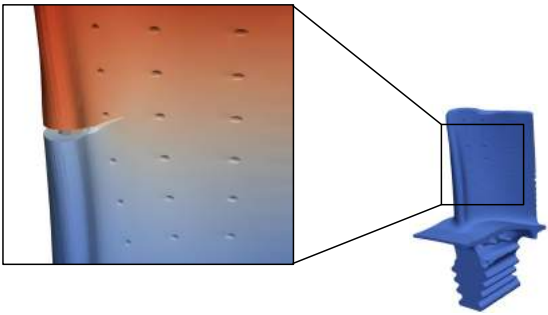

- Thermomechanisch gekoppelter dynamischer Rissfortschritt
- Berechnung der durch den Rissfortschritt reduzierten Lebensdauer

Bewertung
Berücksichtigung der Kundenwünsche

Güte	Performance EGT Margin	Lebensdauer	Max. Durchlaufzeit Regeneration
A	35 K	20.000 Flugzyklen	1 Tage
B	30 K	15.000 Flugzyklen	2 Tage
C	25 K	12.000 Flugzyklen	3 Tage

- Kundenindividuelle Gewichtung der Zielgrößen
- Bessere Planbarkeit der Auslastung der Prozesskette durch Gütestufen

Bewertung
Prognose des Regenerationsergebnisses

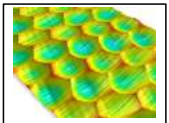

Prozesswissen und –simulationen

Pfad Nr.	Performance EGT Margin	Lebensdauer	Kosten
1	0 K	0 Flugzyklen	0
2	32 K	20.000 Flugzyklen	5.000 €
3	30 K	16.000 Flugzyklen	2.100 €
4	18 K	14.000 Flugzyklen	300 €

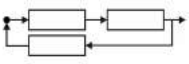

Qualitätsregelkreis Prozesskette

- Abgleich von Prozess- und Funktionssimulationen mit Erfahrungswerten vergangener Regenerationen
- Prognose der pfadabhängigen Regenerationsergebnisse, Kosten und Prozesszeiten

Bewertung
Auswahl des Regenerationspfades

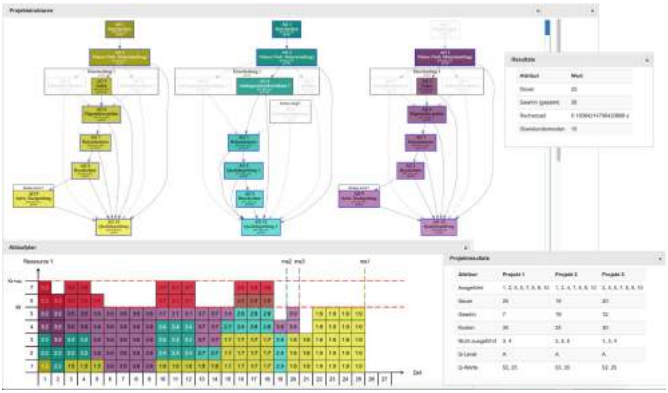

- Berücksichtigung der Kundenwünsche und technischen Randbedingungen
- Optimierung der Bearbeitungsreihenfolge in der Prozesskette

Produkt-Regeneration

MIC 2020
Keynote SFB 871

Einleitung
Zustandserfassung
Bewertung
Bearbeitung
Qualitätssicherung
Schlussfolgerung

SFB 871
Systemdemonstrator

N. Nübel
02.12.2020
Folie 21/27

Leibniz Universität Hannover

Bearbeitung
Additiver Aufbau der Schaufelspitze

- Einkristalliner Materialauftrag durch Temperaturgradienten beim Laserstrahlschweißen
- Aufmaß für nachfolgende spanende Rekonturierung

Produkt-Regeneration

MIC 2020
Keynote SFB 871

Einleitung
Zustandserfassung
Bewertung
Bearbeitung
Qualitätssicherung
Schlussfolgerung

SFB 871
Systemdemonstrator

N. Nübel
02.12.2020
Folie 22/27

Leibniz Universität Hannover

© Leibniz University Hannover 2020

Bearbeitung
Simulationsgestützte Planung der Rekonturierung

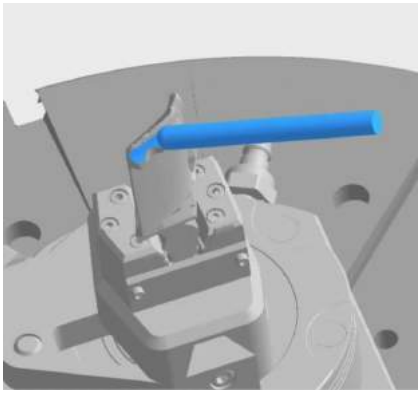

- Extrapolation der Schaufelform in den beschädigten Bereich
- Simulative Identifikation der optimalen Werkzeugwege und Prozessparameter

Produkt-Regeneration

MIC 2020
Keynote SFB 871

Einleitung
Zustandserfassung
Bewertung
Bearbeitung
Qualitätssicherung
Schlussfolgerung

SFB 871
Systemdemonstrator

N. Nübel
02.12.2020
Folie 23/27

Leibniz Universität Hannover

Bearbeitung
Geschickte Rekonturierung

- Erfassung der Abdrängung durch ortsaufgelöste Steifigkeitsmodelle und Prozesskraftmessung
- Reaktive Kompensation mittels Magnetführung verringert die Formabweichung

Produkt-Regeneration

MIC 2020
Keynote SFB 871

Einleitung
Zustandserfassung
Bewertung
Bearbeitung
Qualitätssicherung
Schlussfolgerung

SFB 871
Systemdemonstrator

N. Nübel
02.12.2020
Folie 24/27

Leibniz Universität Hannover

© Leibniz University Hannover 2020

Bearbeitung
Endkonturnahe Turbinenschaufelregeneration

- Kombiniertes Löten/Alitieren zur Verkürzung der Beschichtungsprozesskette
- Applikation von Lot/MCrAlY/Al durch thermisches Spritzen mit anschließender Wärmebehandlung

Produkt-Regeneration

MIC 2020
Keynote SFB 871

Einleitung
Zustandserfassung
Bewertung
Bearbeitung
Qualitätssicherung
Schlussfolgerung

SFB 871
Systemdemonstrator

N. Nübel
02.12.2020
Folie 25/27

Leibniz Universität Hannover

Qualitätssicherung
Vergleich der regenerierten Schaufel mit den Kundenanforderungen

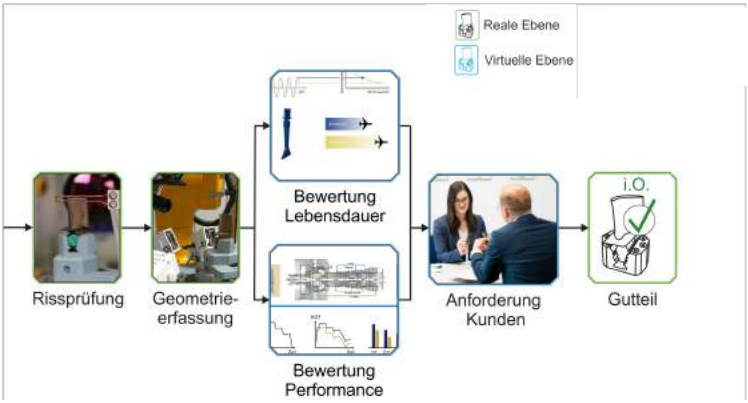

Produkt-Regeneration

MIC 2020
Keynote SFB 871

Einleitung
Zustandserfassung
Bewertung
Bearbeitung
Qualitätssicherung
Schlussfolgerung

SFB 871
Systemdemonstrator

N. Nübel
02.12.2020
Folie 26/27

Leibniz Universität Hannover

Schlussfolgerungen

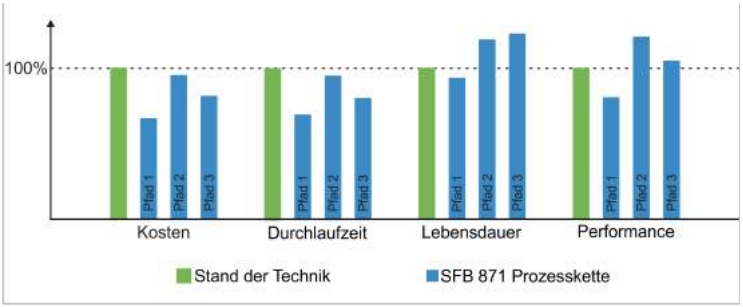

- Verbesserung sowohl der einzelnen Regenerationsschritte als auch Optimierung der Prozesskette
- Grundlegendes Verständnis ermöglicht wissensbasierte Entscheidungen bei der MRO

Sprecher:
Prof. Dr.-Ing. Jörg Seume
Seume@tfd.uni-hannover.de

Stellvertretender Sprecher:
Prof. Dr.-Ing. Berend Denkena
Denkena@ifw.uni-hannover.de

Geschäftsführer:
Dipl.-Ing. Philipp Gilge
Gilge@tfd.uni-hannover.de

Koordinator Systemdemonstrator:
Nicolas Nübel M. Sc.
Nuebel@ifw.uni-hannover.de

Produkt-Regeneration
Sonderforschungsbereich 871
Regeneration komplexer Investitionsgüter
finanziert durch die DFG

Leibniz Universität Hannover

Session 1 - New Technologies in Machining

Influence of the crystallographic orientation of a directionally solidified nickel based superalloy on macroscopic grinding forces

Adina Grimmert,
Research Assistant,
MTU Aero Engines AG

Gefördert durch:
Bundesministerium für Wirtschaft und Energie
aufgrund eines Beschlusses des Deutschen Bundestages

Influence of the crystallographic orientation of a directionally solidified nickel-based superalloy on macroscopic grinding forces

20th Machining Innovations Conference for Aerospace Industry – 12/02/2020

Adina Grimmert, Dr. Lisa Dankl, Prof. Dr.-Ing. Petra Wiederkehr*

*Virtual Machining, TU Dortmund University

Proprietary Notice

Outline

- MTU Aero Engines AG
- Motivation
- Objective and Approach
- Test-planning and set-up
- Comparison of forces regarding the orientation
- EBSD Analysis
- Conclusions

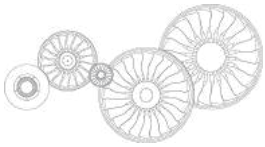

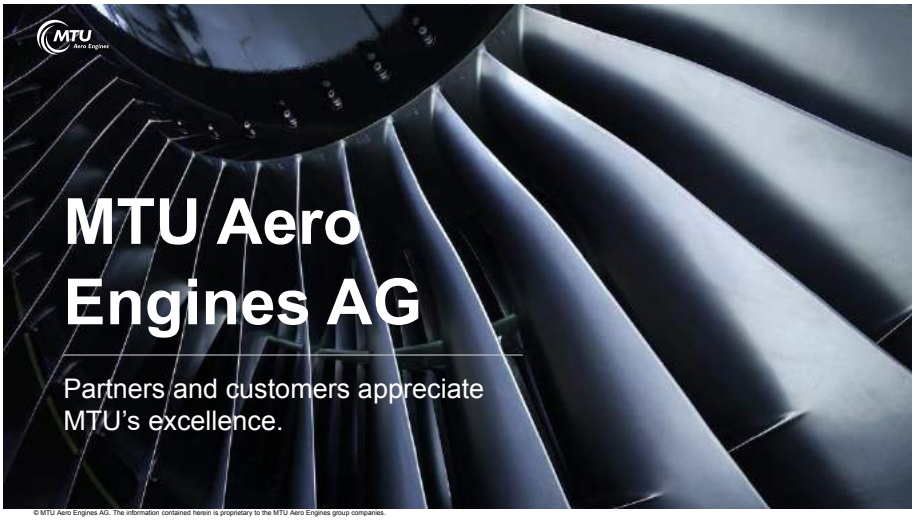

MTU Aero Engines AG in numbers

About MTU Aero Engines AG

Design, development, production and **support of aircraft engines** in all thrust categories
Commercial business: 30% of aircraft have MTU technology on board
Military business: full system capability, for more than 80 years
Commercial MRO: worldwide leader in customized engine service solutions
MRO portfolio: 1,000 shop visits per year for more than 30 different engine types
People: More than 10,000 engine experts at 16 locations
Technology: 150 technology projects, 400 patents and 200 invention disclosure reports per year
Fiscal year 2019: Revenue € 4.63 billion, EBIT adj. € 0.76 billion

~ twelvefold* increase in share value since 2005

* Basis: 30 December 2019

MTU focuses on five core engine competencies - three core components and on unique manufacturing and maintenance processes

Manufacturing

Maintenance

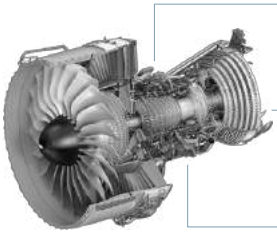

High-pressure compressor (HPC)

Low-pressure turbine (LPT)

Turbine center frame (TCF)

Motivation – Profile grinding processes

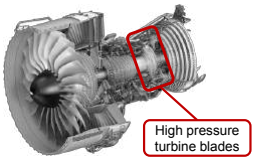

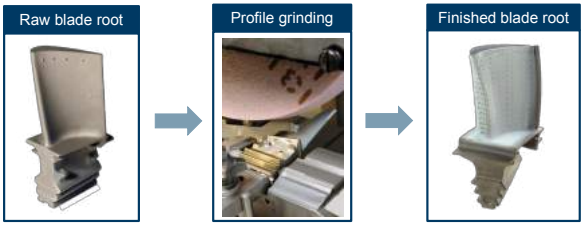

- Removing several millimeters of stock material by grinding
- High depth of cut values result in high process forces
- Evaluation of macroscopic process forces to pre-design the process and avoid overloading

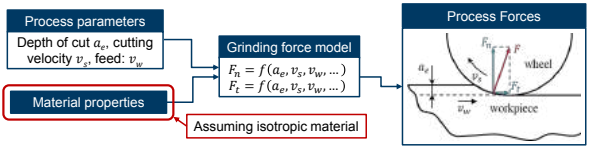

Motivation – Directionally solidified alloys in aerospace industry

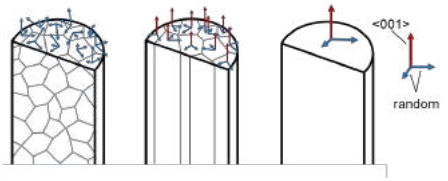

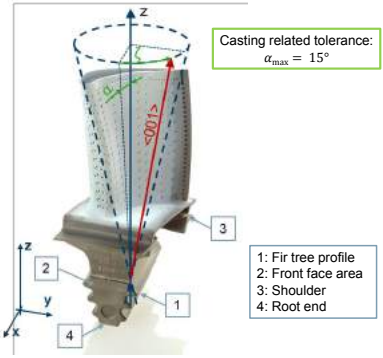

- Blades are directionally solidified by investment casting process
- Mechanical properties differ with direction of solidification
- Grinding of different profiles results in various grinding directions with respect to the solidification direction
- Literature shows an effect of crystallographic orientation for micro-cutting processes

Objective and Approach

Objective:

Do the anisotropic mechanical properties of the material have an influence on the macroscopic grinding forces?
Does the crystallographic orientation of the material have to be implemented in the grinding force model?

Approach:

- Preparing grinding samples of MAR 247 with various grinding directions with respect to the solidification direction
- Grinding forces measurements
- Analyzing the grinding forces with respect to the orientation
- Evaluating the scattering of the crystallographic orientation with Electron BackScatter Diffraction (EBSD)

Test-planning and set-up – Preparation of grinding samples

- Generating grinding samples out of a directionally solidified MAR247 block
- Grinding samples were extracted from a block by wirecutting
- Resulting in four different grinding directions with respect to crystallographic orientation

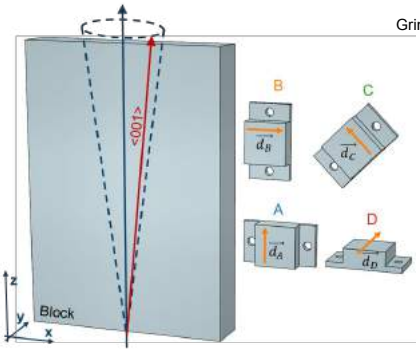

Grinding direction:

$$\vec{d}_A = \begin{pmatrix} 0 \\ 0 \\ 1 \end{pmatrix}, \quad \vec{d}_B = \begin{pmatrix} 1 \\ 0 \\ 0 \end{pmatrix}, \quad \vec{d}_C = \begin{pmatrix} -1 \\ 0 \\ 1 \end{pmatrix}, \quad \vec{d}_D = \begin{pmatrix} 0 \\ 1 \\ 0 \end{pmatrix}$$

Grinding in xz-plane

Test-planning and set-up – Experimental test set-up

- Each parameter set was used for one sample of each orientation (A, B, C, D)
- Parameter set 7 is the initializing parameter set to generate a similar initial surface

Parameter set	a_e [mm]	v_w [mm/min]	v_s [m/s]	Grinding direction
1	0.4	400	30	down
2	0.4	100	20	up
3	1	400	10	up
4	0.05	1000	10	up
5	1	400	20	down
6	0.05	100	20	down
7*	0.05	200	20	down

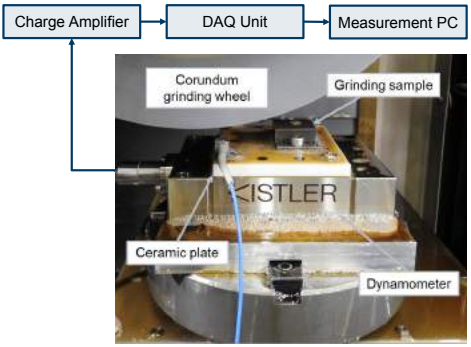

Comparison of forces regarding the orientation (1)

Parameter set 2

a_e = 0.4 mm
v_w = 100 mm/min
v_s = 20 m/s
up-grinding

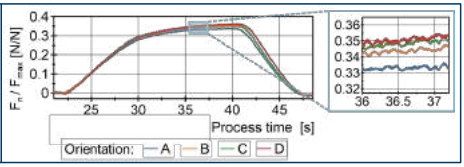

Parameter set 3

a_e = 1 mm
v_w = 400 mm/min
v_s = 10 m/s
up-grinding

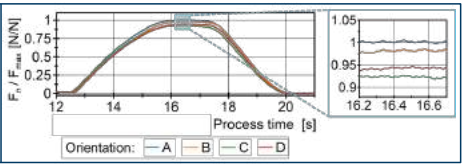

Post-processing of signals

- Filtering the signals according to dynamometer's eigenfrequencies:
  - $f_{cutoff,n} = 860\ Hz$
  - $f_{cutoff,t} = 245\ Hz$
- Compensation of coolant forces
- Calculating centered moving average for visualizing offsets:

$$f(F_i) = \frac{1}{2N+1} \sum_{k=i-N}^{i+N} F_k \qquad m - N > i > N$$

- Normalizing forces with respect to highest measured force F_{max}

Comparison of forces regarding the orientation (2)

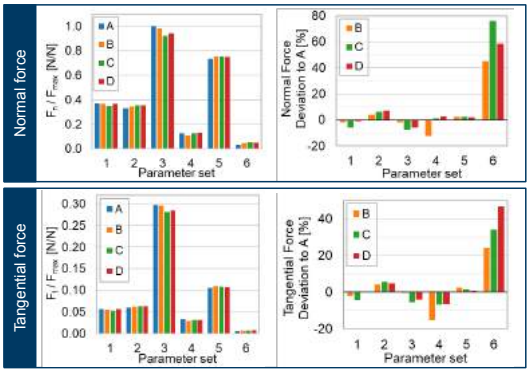

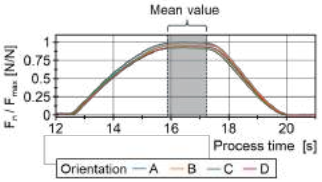

- Comparing mean value of forces of full cut
- Percentage of the deviation calculated to the corresponding value of orientation A

No trend visible which orientation led to highest or lowest forces

EBSD Analysis – Scattering of the crystallographic orientation

Preparation of EBSD sample

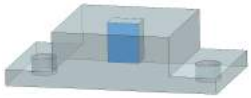

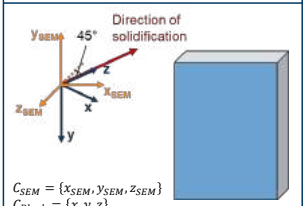

$C_{SEM} = \{x_{SEM}, y_{SEM}, z_{SEM}\}$
$C_{Block} = \{x, y, z\}$

Area mapping of crystallographic orientation with EBSD

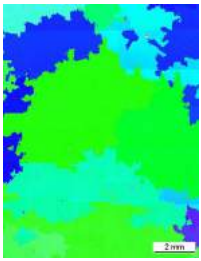

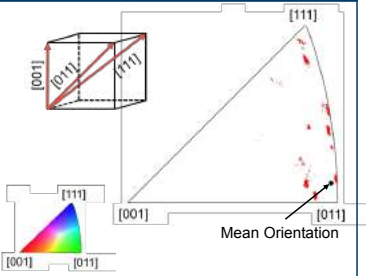

- Mean orientation as expected close to [011] corresponding to a 45° deviation to z_{SEM}
- Red data points show significant scattering and numerous grains oriented close to [111]

Conclusions

- Analysis of forces showed no correlation of the crystallographic orientation and the grinding direction
- Possible reasons for the findings:
  - EBSD analysis showed significant scattering of the direction of solidification of the columnar grains in the material
  - Scattered orientations paired with multiple grains of the wheel being in engagement at the same time
- For future studies a similar analysis for a single-crystal material would be of interest
- Direction of solidification will not be implemented to the macroscopic force model for directionally solidified materials

Thank you for your attention.

Mail to:
adina.grimmert@mtu.de

These investigations were kindly funded as a part of the „*InvernTurb*“ project by the Luftfahrtforschungsprogramm VI (*LuFoVI-1*)

Gefördert durch:
Bundesministerium für Wirtschaft und Energie
aufgrund eines Beschlusses des Deutschen Bundestages

A New Flank Face Design Leading to an Improved Process Performance when Drilling High Temperature Nickel Base Alloys

Milan Bücker,
Research Assistant,
TU Dortmund

technische universität dortmund

20th Machining Innovations Conference for Aerospace Industry
December 2nd 2020, Hannover, Germany

ISF

A New Flank Face Design Leading to an Improved Process Performance when Drilling High-Temperature Nickel-Base Alloys

Milan Bücker, M.Sc.
Dr.-Ing. Ekrem Oezkaya
Ulf Hensler, B.Sc.
Prof. Dr.-Ing. Prof. h.c. Dirk Biermann

Outline

ISF

- **Motivation and Objectives**
- Preinvestigations
- Implementation of the New Design
- Experimental Validation
- Conclusions and Outlook

2

Motivation and Objectives

Workpiece Material: Inconel 718 (NiCr19Fe19Nb5Mo3)

- Typical fields of application:
  - Turbine disks in aircraft engines
  - Turbo chargers
  - Industrial turbines
- Characteristics:
  - Oxidation resistant up to T = 1000 °C
  - High temperature strength up to T = 650 °C
  - High work hardening tendency
  - Low thermal conductivity

Source: SpaceX

Source: Siemens

3

Motivation and Objectives

Consequences for the Drilling of Inconel 718

- Critical heat dissipation from the point of action
- High thermal loads in the drilling tool
- Abrasive and adhesive wear on the cutting edge
- Limited productivity

→ **Impact on workpiece quality and surface integrity**

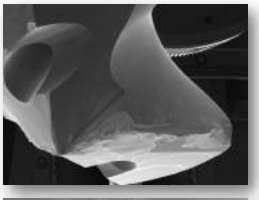

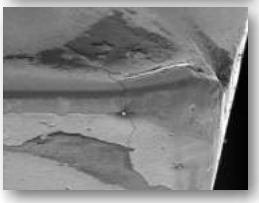

4

Outline

- Motivation and Objectives
- **Preinvestigations**
- Implementation of the New Design
- Experimental Validation
- Conclusions and Outlook

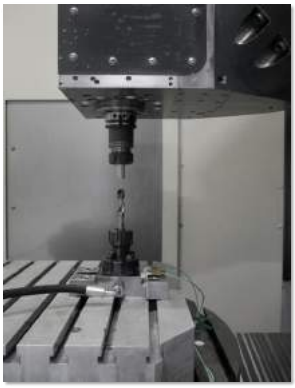

5

Preinvestigations

Flank Face Modification (Generation 1) – Development

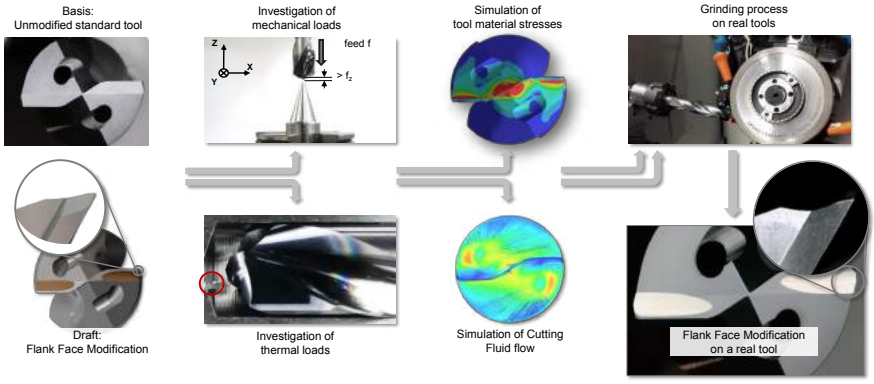

6

Preinvestigations

ISF

Flank Face Modification (Generation 1) – Manufacturing

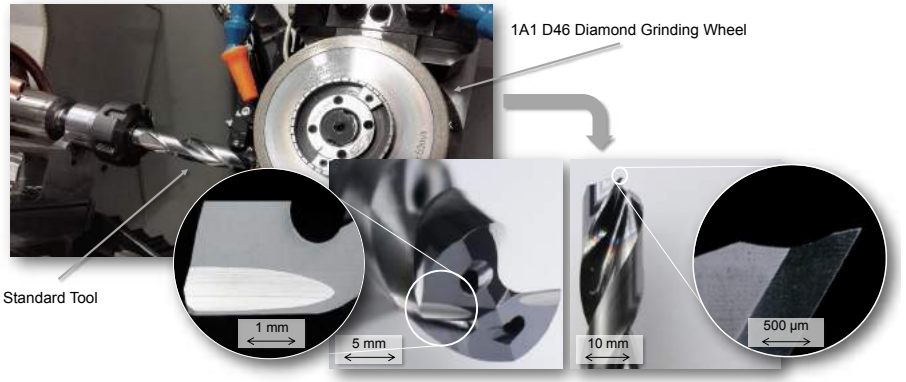

7

Preinvestigations

ISF

Flank Face Modification (Generation 1) – Impact on Tool Life

Tool Type:	varied	**Cutting Speed.:**	varied	**Cutting Fluid:**	Emulsion (10 %)
Workpiece Mat.:	Inconel 718	**Feed:**	varied	**Fluid Pressure**	p_{fluid} = 55 bar

Standard tool  **Flank Face Mod. Gen. 1** 

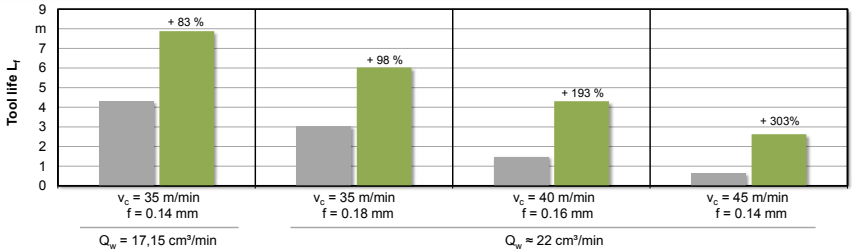

8

Preinvestigations

ISF

Flank Face Modification (Generation 1) – Impact on Surface Integrity

Tool Type:	varied	**Cutting Speed.:**	v_c = 35 m/min	**Cutting Fluid:**	Emulsion (10 %)
Workpiece Mat.:	Inconel 718	**Feed:**	f = 0.14 mm	**Fluid Pressure**	p_{fluid} = 55 bar

Standard tool  **Flank Face Mod. Gen. 1** 

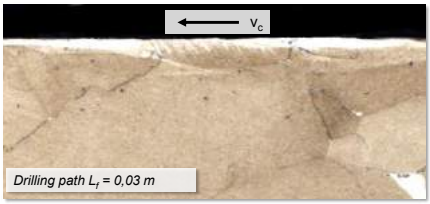

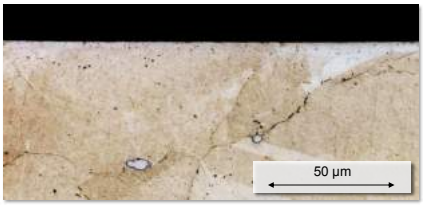

9

Preinvestigations

ISF

Flank Face Modification (Generation 1) – Impact on Drilling Torque

Tool Type:	varied	**Cutting Speed.:**	v_c = 35 m/min	**Cutting Fluid:**	Emulsion (10 %)
Workpiece Mat.:	Inconel 718	**Feed:**	f = 0.14 mm	**Fluid Pressure**	p_{fluid} = 55 bar

Cutting edge width: 130 µm 150 µm 180 µm 200 µm

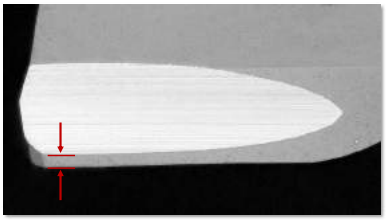

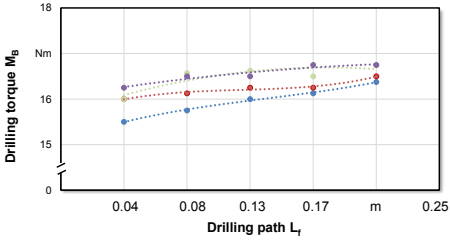

10

Preinvestigations

Conclusions from Previous Investigations

- Effects of a Flank Face Modification:
  - Increase in tool lives
  - Decrease of subsurface influences
  - Distinctive benefits at high cutting speeds
- End of tool lives often reached by cutting edge chipping
- Indications of high thermal stress at the cutting edges

→ **Objective:**
Further development of the Flank Face Modification

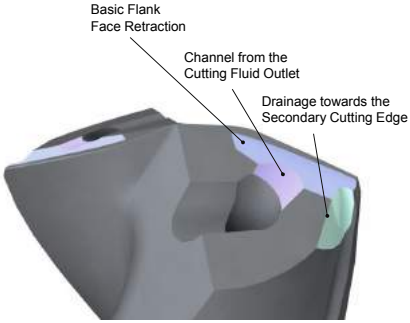

11

Outline

- Motivation and Objectives
- Preinvestigations
- **Implementation of the New Design**
- Experimental Validation
- Conclusions and Outlook

12

Implementation of the New Design

Implementation of the Flank Face Modification – Generation 2

- Creating further flow channels by grinding
- Directing the cutting fluid
  - Towards the cutting edge
  - Closer the point of action

Standard Tool	Flank Face Modification Gen. 1	Flank Face Modification Gen. 2

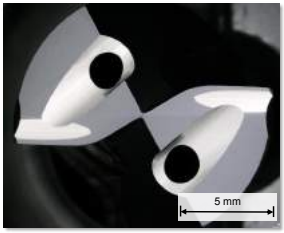

13

Implementation of the New Design

Implementation of the Flank Face Modification – Generation 2

- Creating further flow channels by grinding
- Directing the cutting fluid
  - towards the cutting edge
  - closer to the point of action

Channel towards Cutting Fluid Outlet	Cutting Fluid Drainage	Flank Face Modification Gen. 2

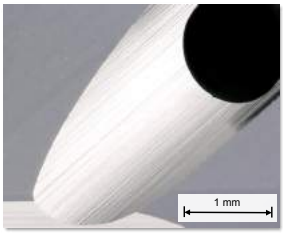

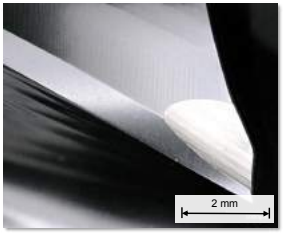

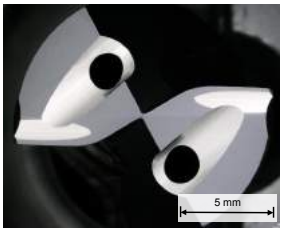

14

Implementation of the New Design

Computational Fluid Dynamics Simulation

Simulation Software:	ANSYS CFD	**Fluid Pressure:**	p = 55 bar	Fluid Flow Velocity
Rotational Speed.:	ω = 83.36 rad/s	**Mass Flow:**	$\dot{m}$ = 0.6 kg·s^{-1}	0 25 50 m/s 100

Standard Tool	Flank Face Modification Gen. 1	Flank Face Modification Gen. 2

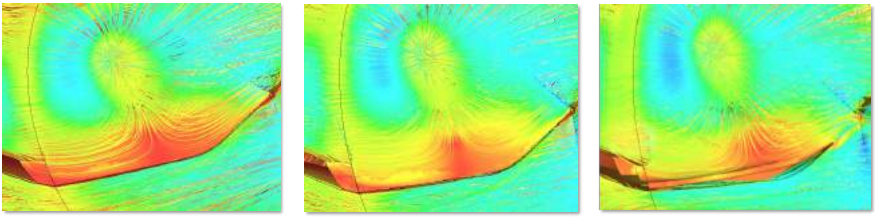

15

Outline

- Motivation and Objectives
- Preinvestigations
- Implementation of the New Design
- **Experimental Validation**
- Conclusions and Outlook

16

Experimental Validation

ISF

Tool Lifes Comparison

Tool Type:	varied	**Cutting Speed.:**	v_c = 45 m/min	**Cutting Fluid:**	Emulsion (10 %)
Workpiece Mat.:	Inconel 718	**Feed:**	f = 0.14 mm	**Fluid Pressure**	p_{fluid} = 55 bar
Standard Tool		**Mod. Gen. 1**		**Mod. Gen. 2**	

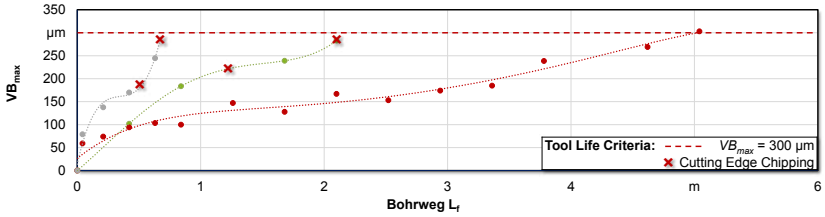

17

Experimental Validation

ISF

Reduction of Cutting Fluid Residues

Tool Type:	varied	**Cutting Speed.:**	v_c = 45 m/min	**Cutting Fluid:**	Emulsion (10 %)
Workpiece Mat.:	Inconel 718	**Feed:**	f = 0.14 mm	**Fluid Pressure**	p_{fluid} = 55 bar
Mod. Gen. 1				**Mod. Gen. 2**	

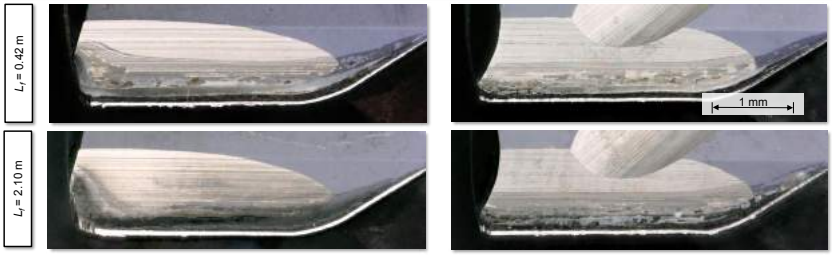

18

Experimental Validation

Decrease of Workpiece Material Adhesion

Tool Type:	varied	**Cutting Speed.:**	v_c = 45 m/min	**Cutting Fluid:**	Emulsion (10 %)
Workpiece Mat.:	Inconel 718	**Feed:**	f = 0.14 mm	**Fluid Pressure**	p_{fluid} = 55 bar

Mod. Gen. 1 **Mod. Gen. 2**

19

Outline

- Motivation and Objectives
- Preinvestigations
- Implementation of the New Design
- Experimental Validation
- **Conclusions and Outlook**

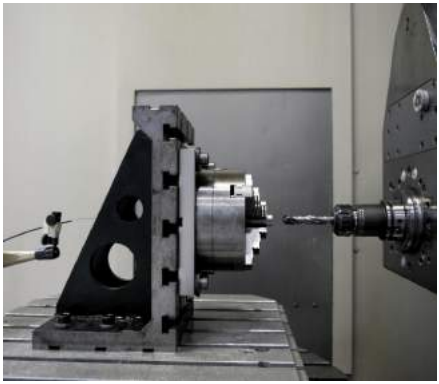

20

Conclusions and Outlook

Flank Face Modification Gen. 2

Summary

- Further increase of tool life
- Significant reduction of
  - Cutting fluid residues
  - Workpiece material adhesions
- Prediction of higher cutting fluid flow

Future work

- Investigation of temperature reduction
- Experimental validation of cutting fluid flow improvements
- Implementation of alternative designs by solid carbide milling
- Variation of workpiece materials

21

Thank you for your kind attention!

Milan Bücker, M.Sc.
Institute of Machining Technology

Baroper Str. 303
44227 Dortmund
Germany

+49 231 755 2662
milan.buecker@tu-dortmund.de
www.isf.de

Acknowledgements

This paper is based on investigations of the project
"Investigations on optimization of the cutting edge of twist drills for the machining of the high temperature resistant nickel base alloy Inconel 718"
which is kindly supported by the German Research Foundation (DFG).

DFG Deutsche Forschungsgemeinschaft
Project no. 327 963 939

Machining technology and PVD coatings for milling thin structural parts of Inconel 718

Heiko Frank,
Business Area Manager,
GFE - Gesellschaft für Fertigungstechnik und Entwicklung Schmalkalden e.V.

GFE – Gesellschaft für
Fertigungstechnik und Entwicklung
Schmalkalden e.V.

Machining technology and PVD coatings for milling thin structural parts of Inconel 718

H. Frank, M. Schiffler , F. Welzel, T. Maul (GFE Schmalkalden e.V.)
T. Cselle, A. Lümkemann (Platit AG)

Project partners:

20th Machining Innovations Conference for Aerospace Industry 2020 (MIC 2020), December 2nd 2020, Hannover, Germany

Agenda

1. Motivation
2. Experimental work
   - Work piece material, cutting tools, cutting parameters
   - carbide and cutting edge
3. Development of suitable tool coatings
4. Cutting tests: trochoid rough milling and pre-finish milling
   - Determination of optimal coatings
   - Correlation between coating analysis, wear tests and machining
   - Cooling lubricant conditions
5. Final tool comparison
6. Summary and conclusions

1. Motivation

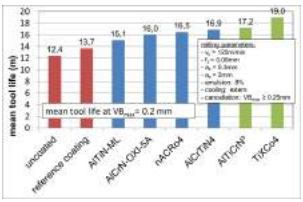

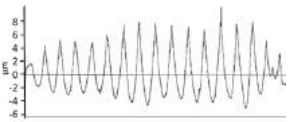

- Results from the previous investigations:
  - Peripheral milling of Inconel 718 with ball end mills
  - With a suitable coating (TiXCo4) including pre- and post-treatment up to 40% increase in tool life compared to the reference coating
- Milling of blisk components in the field test
- Roughness profiles of the blisk blades: chatter marks as a result of component and tool vibrations → faster tool wear and unsuitable surfaces.

Agenda

1. Motivation
2. Experimental work
   - Work piece material, cutting tools, cutting parameters
   - carbide and cutting edge
3. Development of suitable tool coatings
4. Cutting tests: trochoide rough milling and pre-finish milling
   - Determination of optimal coatings
   - Correlation between coating analysis, wear tests and machining
   - Cooling lubricant conditions
5. final tool comparison
6. Summary and conclusions

2. Experimental work

Goals:

- Improvement of the coating adhesion
- Improvement of the mechanical stability of the layers
- Improvement of the impact strength and vibration resistance of the layers
- Optimization of the cooling lubricant conditions

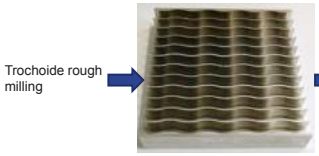

Work piece material:

- Inconel 718 in aerospace quality 200 mm x 200 mm x 36 mm

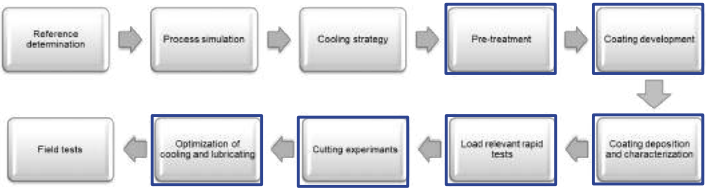

2. Experimental work: work piece, cutting tools, cutting parameters

Cutting tools (for rough milling and pre-finishing):

- Torus cutters with a central internal cooling (Ø 1,5 mm)
- Diameter: 10mm
- Number of cutting edges: z = 5
- Corner radius: 1 mm
- Cutting length: 22mm
- Overall length: 72mm

Used coolant and lubricant:

- Blaser Swisslube B-Cool 9665
- Blaser Swisslube Vasco 7000

Parameter	Trochoide rough milling	Pre-finishing
Cutting speed v_c	90 m/min	150 m/min
Tooth feed f_z	0.21 mm	0.075 mm
Engagement width a_e	0.1 mm	0.3 mm
Depth of engagement a_p	12 mm (2x offset in depth)	22 mm
Cutting arc angle	15°	-

Machining center:
DMU 125 P duoBlock

2. Experimental work: carbide and cutting edge

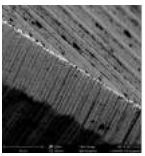

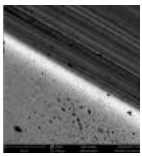

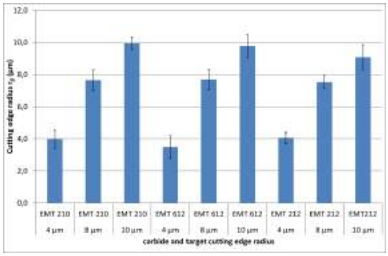

- Used carbides (EXTRAMET)
  - EMT 210
  - EMT 212
  - EMT 612
- Cutting edge rounding by drag grinding with DF-3 Tools system from OTEC Präzisionsfinish GmbH
- Used granules:
  - HSC1/300
  - H4/400
- Target for cutting edge radii:
  - 4 µm; 8 µm and 10 µm

2. Experimental work: carbide and cutting edge

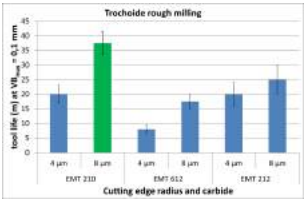

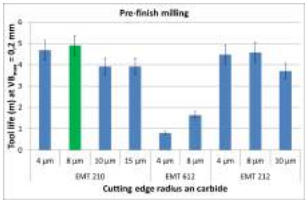

- **Trochoide rough milling of Inconel 718**:
  - Tools from EMT 210 with a cutting edge radius of about 8 µm → highest tool life
- **Pre-finish milling of Inconel 718:**
  - Tools from EMT 210 with a cutting edge radius of about 8 µm → highest tool life
  - Differences between EMT 210 and EMT 212 are not so high than with rough milling.

Agenda

1. Motivation
2. Experimental work
   - Work piece material, cutting tools, cutting parameters
   - carbide and cutting edge
3. Development of suitable tool coatings
4. Cutting tests: trochoide rough milling and pre-finish milling
   - Determination of optimal coatings
   - Correlation between coating analysis, wear tests and machining
   - Cooling lubricant conditions
5. final tool comparison
6. Summary and conclusions

3. Development of suitable tool coatings

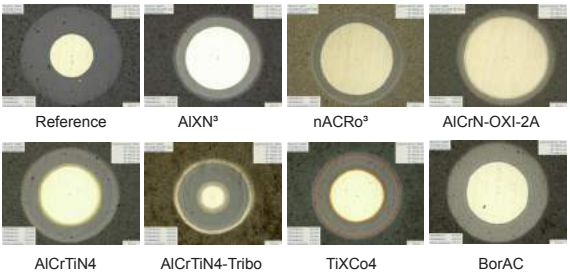

- Improvement of ductility by nano-structured and nano-layered coatings
- Improvement of the thermal resistance and wear resistance by oxygen or silicon-containing coatings
- Reduction of friction by smooth coatings (post-treatment) or C-based top layer
- Reduction of internal stresses by boron-containing layers
- Variation of the coating architecture, structure, composition and thickness

3. Development of suitable tool coatings

Coating Analytic methods:

- Coating structure and thickness (calotte grinding)
- Hardness and modulus of elasticity (PICODENTOR HM 500, Helmut Fischer GmbH)
- Coating adhesive strength (scratch test built, GFE)
- Coefficients of friction against 100Cr6 (MCR 302 rheometer, Anton Paar)
- Residual stress (XRD measurements)

Load-relevant rapid tests:

- Calotte grinding tests (KaloMax NT)
- Micro impact tests (Micro Materials Limited, UK)
- Vibrational friction wear tests (SRV, Optimol Instruments)

Example: Calotte grinding tests with KaloMax NT

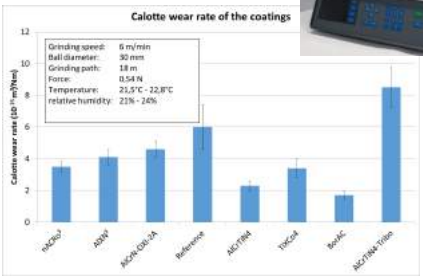

3. Development of suitable tool coatings

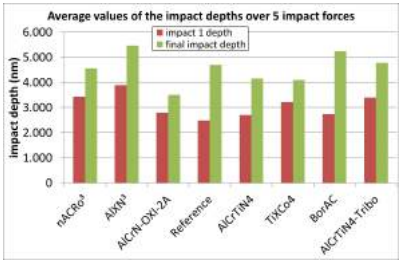

Example: Micro impact test for determination of crack and wear resistance

- Accelerating a small diamond impact ball against a coated substrate
- Measuring of impact depth

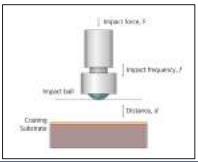

Accelerating load	Various from 1 N to 2 N
Acceleration distance	40 µm
Test duration	5 minutes
Number of impact event per test	75
Number of test repeats	5
Probe geometry	20 µm (diamond)
Measured parameter	Probe depth in to sample

- Reference coating, AlCrTiN4: high cracking resistance (low impact 1 depth)
- AlCrN-OXI-2A, TiXCo4, AlCrTiN4: high crack propagation resistance (low final impact depth)

→ Micro-impact tests are a suitable method for predicting the behavior of coatings and coated tools (fast coating screening)

Agenda

1. Motivation
2. Experimental work
   - Work piece material, cutting tools, cutting parameters
   - carbide and cutting edge
3. Development of suitable tool coatings
4. Cutting tests: trochoide rough milling and pre-finish milling
   - Determination of optimal coatings
   - Correlation between coating analysis, wear tests and machining
   - Cooling lubricant conditions
5. final tool comparison
6. Summary and conclusions

4. Cutting tests: trochoide rough milling and pre-finish milling

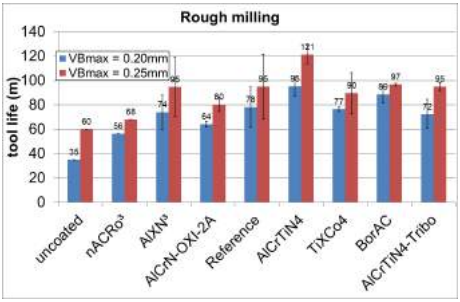

Roughing technology parameters:
v_c = 90 m/min
f_z = 0.21 mm
a_e = 0.1 mm
a_p = 12 mm (2x)
coolant: B-Cool 9665

tools:
Torus cutters Ø10 x 22 / R1
EMT 210 / KV 8 µm
coatings: various (see x-axis)
post-treatment: drag grinding / wet blasting
workpieces:
Inconel 718 (200 mm x 200 mm x 36 mm)

- Relevant conditions:
  - 8 different PVD coatings
  - Post-processed by drag grinding
  - Comparison with uncoated tools
  - Trochoide rough milling of undulating grooves.
- AlCrTiN4:
  - Longest tool life (22% or 27 higher than the reference coating) (because of high Cr content).
  - Tool life in comparison to uncoated milling tools is increased by a factor of 2.0 to 2.7.

→ **The AlCrTiN4 coating is clearly recognizable as a favorite for trochoide rough milling**.

4. Cutting tests: trochoide rough milling and pre-finish milling

Rough milling

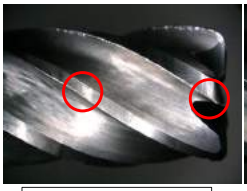

Mag. x 20
milling length 120 m:
AlCrTiN4-coating

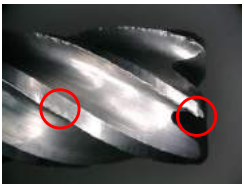

Mag. x 20
milling length 120 m:
BorAC-coating

- large differences in cutting edge wear, especially at the cutting corner
- significantly more wear with the BorAC coating than with AlCrTiN4.
- Typical wear progress in trochoide rough milling:
  - Begin with built-up cutting edges
  - Micro cut-outs
  - Cut-outs on the rake faces
  - Chipping on the open areas
  - Total failure due to cut-outs on all cutting edges or broken cutting corners

4. Cutting tests: trochoide rough milling and pre-finish milling

Technology optimization in pre-finish milling

Problem: sudden wear due to insufficient cooling

Solution: Slidable wave-shaped bar

Result:
Constant wear, longer tool life

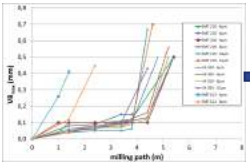

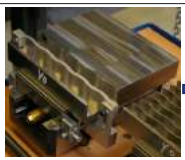

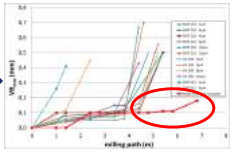

Coating optimization

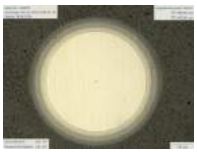

AlCrN-OXI-2A
thicker core layer

BorCo: BorAC
+ TiSiN top layer

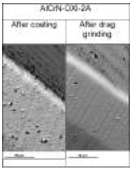

4. Cutting tests: trochoide rough milling and pre-finish milling

Pre-finish milling

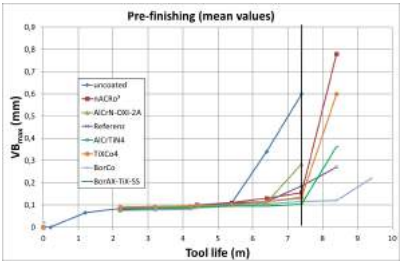

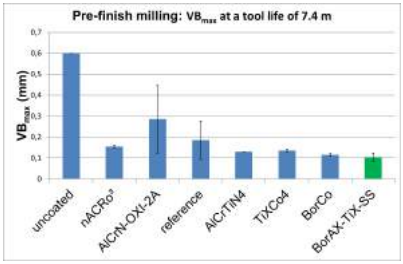

Pre-finishing technology parameters:
v_c = 150 m/min
f_z = 0.075 mm
a_e = 0.3 mm
a_p = 22 mm

Cutting tools:
Torus cutter Ø10 x 22 / R1
EMT 210 / KV 8 µm
Coatings: different
Post-treatment: drag grinding / wet blasting
Workpiece:
Inconel 718 (200 mm x 200 mm x 36 mm)

➢ BorAX-TiX leads to lowest wear.

Voltage- and Current-Measurement Based Force Estimation in Broaching Using Synchronous Motor Drive

Kazumasa Miura,
Post Doc,
RWTH Aachen University

Voltage- and Current-Measurement Based Force Estimation in Broaching Using Synchronous Motor Drive

Kazumasa Miura, Tobias Seelbach, Thorsten Augspurger,
Daniel Schraknepper, and Thomas Bergs

Laboratory for Machine Tools and Production Engineering (WZL)
RWTH Aachen University, Germany

20th Machining Innovations Conference for Aerospace Industry 2020 (MIC 2020), December 2nd 2020, Hannover, Germany

Introduction

Target of process monitoring
- Wear monitoring
- Detection of tool breakage
- Estimation of workpiece quality
- Adaptive force control

Typical signals for process monitoring
- Tool-path trajectory
- Spindle speed
- Acceleration
- Acoustic emission
- Temperature
- **Cutting force**

2

Our indirect measurement approach based on external voltage and current measurement

Simulation-approach

Engagement conditions

Workpiece & tool models

Process Parameters

Cutting Force Simulator

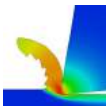

Simulated force

Integration

Indirectly-measured force

Motor voltage

Motor current

Other-servo signals

Machine model

Indirect Force Estimator

Estimated force

Monitoring-approach

Main advantages

- **Indirect measurement of absolute cutting force**
- **Tooth**-condition monitoring
- Retrofitting solution

3 © Werkzeugmaschinenlabor WZL

WZL | RWTH AACHEN UNIVERSITY

Use case 1

Indirect measurement of absolute cutting force

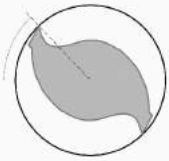

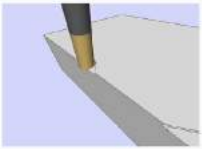

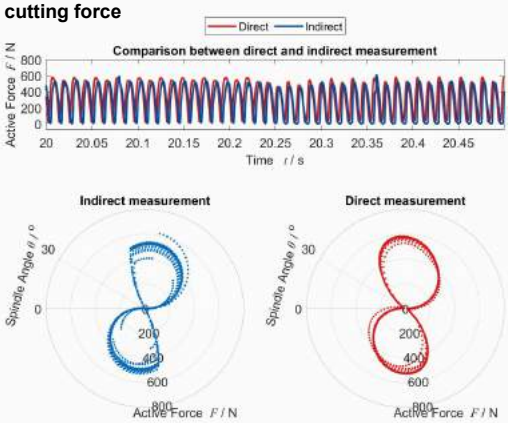

Use case 2
Tooth condition monitoring

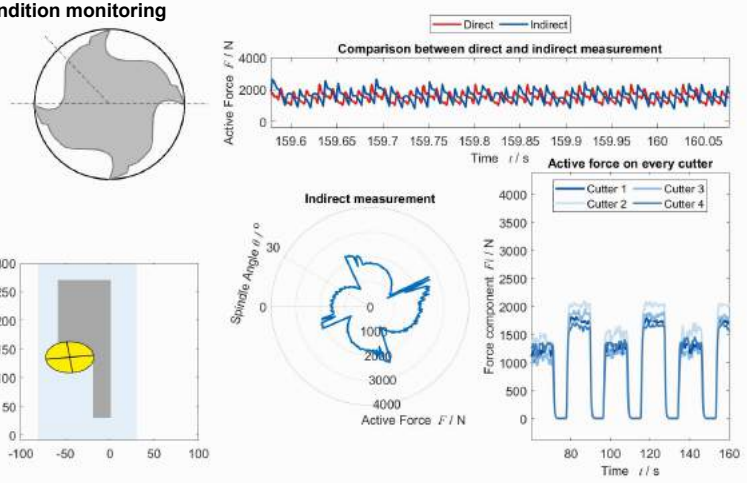

Use case 3
Adaptive force control

Target of this study

How we model the relationship between the cutting force and motor current?

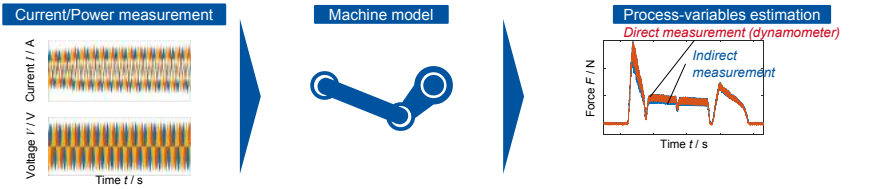

- The motor-current signal is well-acknowledged in the past studies to reflect the effect of the cutting force.
- To measure **the absolute force** indirectly, we need to model the relationship between the motor-current and cutting force.
- For this purpose, a force dynamometer is usually used to identify this relationship.
- However, in some situations (e.g., large broaching machines), we cannot use a dynamometer because of its hardware costs and its installation difficulty.
- This study utilizes additional **voltage measurement** to identify this relationship and measures the cutting force indirectly.

7 © Werkzeugmaschinenlabor WZL

Target machine and process

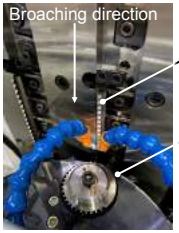

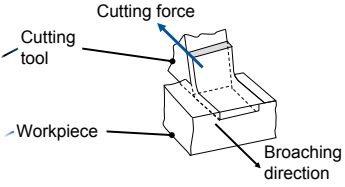

Forst external broaching machine

- Maximal output of 80 kN
- Cutting velocity of up to 150 m/min
- Vertical broaching
- AC synchronous-motor drive

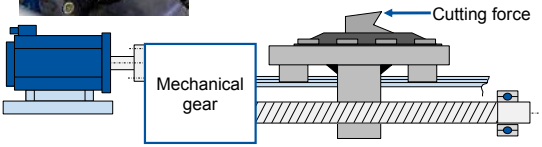

8 © Werkzeugmaschinenlabor WZL

Indirect force measurement based on the motor current

- Motion equation of the drive system

$$Mv' = G_r \cdot \tau - F_\mathrm{f} - F_{cut}$$

- Motor torque τ is mechanically designed to have a linear relationship to the motor current i_q

$$\tau = K_t \cdot i_\mathrm{q}$$

- Consider that the broaching process has a constant velocity

$$F_{cut} = G_r \cdot K_t \cdot i_\mathrm{q} - F_\mathrm{f}$$

Identifications of torque constant K_t and friction effect F_f are required.

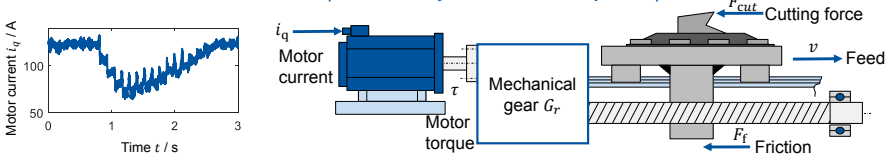

Energy conversion

When a motor rotates with a rotation speed of ω_e and a motor current of i_q,

- Motor torque τ

$$\tau = K_t \cdot i_\mathrm{q}$$

- Mechanical power P_m

$$P_\mathrm{m} = \tau \cdot \omega_e$$

- Consider the energy conversion ($P_\mathrm{m} = P_\mathrm{e}$)

$$\Phi = K_t = K_e$$

The current-torque relationship Φ can be identified not by the motor torque τ and motor current i_q, but by the **induced voltage e_q and rotation speed ω_e**

- Back-EMF (electromotive force) e_q
  - Induced voltage generated by the flux change and it depends on the rotation speed

$$e_\mathrm{q} = K_e \cdot \omega_e$$

- Electrical power P_e

$$P_\mathrm{e} = e_\mathrm{q} \cdot i_\mathrm{q}$$

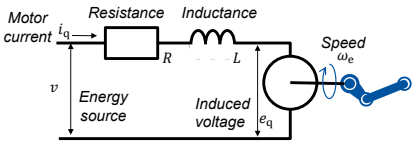

Induced voltage and speed estimations

- Voltage equation of an AC synchronous motor

$$\boldsymbol{v}_{\alpha\beta} = L\boldsymbol{i}'_{\alpha\beta} + R\boldsymbol{i}_{\alpha\beta} + \boldsymbol{e}_{\alpha\beta}$$

$$\boldsymbol{T}_{\alpha\beta} = \sqrt{2/3}\begin{bmatrix}1 & 1/2 & -1/2\\ 0 & \sqrt{3}/2 & -\sqrt{3}/2\end{bmatrix}$$
$$\boldsymbol{i}_{\alpha\beta} = [i_\alpha \quad i_\beta]^T = \boldsymbol{T}_{\alpha\beta}[i_u \quad i_v \quad i_w]^T$$
$$\boldsymbol{v}_{\alpha\beta} = [v_\alpha \quad v_\beta]^T = \boldsymbol{T}_{\alpha\beta}[v_u \quad v_v \quad v_w]^T$$

Induced voltage $\boldsymbol{e}_{\alpha\beta}$ can be estimated by the measured current/voltage $\boldsymbol{i}_{\alpha\beta}, \boldsymbol{v}_{\alpha\beta}$ and motor parameters L, R.

Simplified Motor model

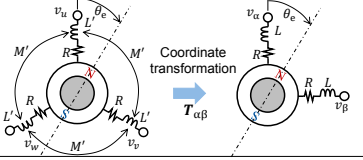

- Induced voltage of an AC synchronous motor

$$\boldsymbol{e}_{\alpha\beta} = \begin{bmatrix}e_\alpha\\ e_\beta\end{bmatrix} = \Phi\omega_e\begin{bmatrix}-\sin\theta_e\\ \cos\theta_e\end{bmatrix}$$

  - Induced voltage signals are sinusoidal waves with a phase shift of 90 degrees from each other.
  - A phase-lock loop (PLL) structure can capture the frequency of these sinusoidal waves.

PLL for the induced voltage calculates the speed ω_e and angle θ_e

PLL structure

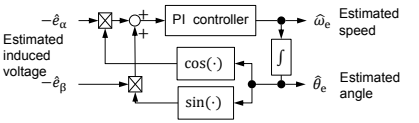

Identifications of torque constant and friction effect for indirect force measurement

- Identification of torque constant Φ
  - Induced voltage of a synchronous motor

$$\boldsymbol{e}_{\alpha\beta} = \begin{bmatrix}e_\alpha\\ e_\beta\end{bmatrix} = \Phi\omega_e\begin{bmatrix}-\sin\theta_e\\ \cos\theta_e\end{bmatrix}$$

$$\Rightarrow \quad -e_\alpha\sin\theta_e + e_\beta\cos\theta_e = \Phi\omega_e$$

  - Least square method against the discrete signals with n samples.

$$\Phi = (A^TA)^{-1}A^TB$$

$$A = [\omega_e[1] \quad \omega_e[2] \quad \dots \quad \omega_e[n]],$$
$$B = [e_q[1] \quad e_q[2] \quad \dots \quad e_q[n]],$$
$$e_q = -e_\alpha\sin\theta_e + e_\beta\cos\theta_e$$

- Identification of friction effect F_f
  - Motor torque of an AC synchronous motor

$$\tau = \Phi(-i_\alpha\sin\theta_e + i_\beta\cos\theta_e)$$

    - Regard $i_q = -i_\alpha\sin\theta_e + i_\beta\cos\theta_e$,
$$\tau = \Phi \cdot i_q$$

  - Motor-current-based force calculation

$$F_{cut} = G_r \cdot \Phi \cdot i_q - F_f$$

    - Assume the friction effect during cutting F_f is the same as that without cutting ($F_{cut} = 0$).
$$F_f = G_r \cdot \Phi \cdot i_q$$

Based on this, this study conducts an identification test, and then indirectly-measures the cutting force.

Broaching test against Inconel 718

Experimental setup

- Cutting tool (13 teeth)
  - Three chip thicknesses h=80 µm, 50 µm, 20 µm
- Process parameters
  - v_c = 5 m/min
- Broaching length
  - 28 mm per cut
  - Total 460 cuts (=12.88 m)
- Used sensors
  - Cutting force measurement
    - Piezoelectric dynamometer Z21289 of Kistler
  - Current/voltage measurement
    - Power analyzer PW3390 of HIOKI
  - Measurement timings

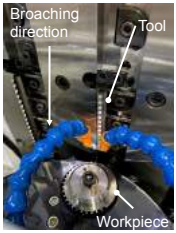

i-th cut	80th	160th	260th	360th	460th
Cutting length [m]	2.24	4.48	7.28	10.08	12.88

Identification test (air-cutting motion)

- Measurement motor signal

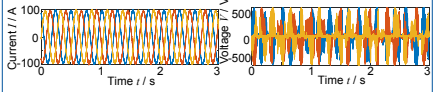

- The identified torque constant by the least mean square method $G_T\Phi$ =145.5 N · A
- The identified friction effect including gravity effect

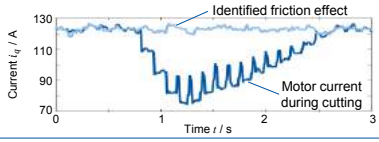

Experimental results of broaching test against Inconel 718

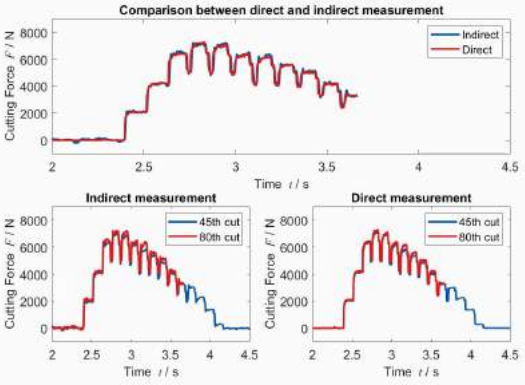

Summary

- This study focused on the indirect measurement of the cutting force based on the motor current in broaching operations using an AC synchronous motor.
- To measure the absolute cutting force indirectly, we need to model the relationship between the motor-current and cutting force.
- Instead of using dynamometers for the identification, this study utilized the additional voltage measurement.
  - Identification of the current-torque relationship through the induced voltage and speed estimations.
  - Identification of the friction effect through angle estimation.
- This study executed a broaching experiment and indirectly-measured the cutting force.

Thank you for your attention.

- Kazumasa Miura, Ph.D.
- Process Monitoring Group
- Laboratory for Machine Tools and Production Engineering WZL
- RWTH Aachen University

☎ +49 241/ 80 28018

✉ k.miura@wzl.rwth-aachen.de

Machining-based thermal error analysis of CFRP structured machine tool

Makoto Kato,
Visiting Lecturer,
Keio University (Japan)

20th Machining Innovations Conference for Aerospace Industry (MIC 2020),
2 December 2020, Garbsen, Germany

Machining-based thermal error analysis of CFRP-structured machine tool

Makoto Kato[a], Yuji Mizoguchi[b], Kazumasa Kono[c], Yasuhiro Kakinuma[a]

a Keio University, Japan
b OKUMA Corporation, Japan
c Makino Milling Machine Co.Ltd, Japan

1

Outline

1	Background & Research purpose
2	Experimental setup of proposed machining tests
3	Experimental results and discussion
4	Conclusions and outlook

Outline

Counterplans for thermal errors

Required form accuracy of machine tools

Dimension error of cutting machine: 10-100 μm

- Thermal influence 75% [1]
- Kinematic errors
- Dynamic forces
- Motion control, etc.

Development phase

- Control environment and cutting conditions
  Using chamber, warm-up operation, etc.
- Compensate by NC with thermal error prediction
  Develop error model, temperature analysis by FEM, etc.
- Reduction thermal errors by designing thermal characteristic
  Apply new structural materials with low thermal expansion coefficient, install effective cooling unit, etc.

CFRP

[1] J. Mayr et al, "Thermal issues in machine tools", CIRP Annals, Volume 61, Issue 2, 2012, Pages 771-791

Application of Carbon Fiber Reinforced Plastic

Mechanical properties of CFRP

- High specific stiffness
- Good dimensional stability
- Damping capability

✓ With anisotropy depending on fiber orientation

Unidirectional / Cross-ply laminates

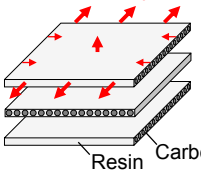

CFRP application in transportation equipment

Arranged fiber orientation gives higher mechanical properties

➢ Proportionally reduce energy consumption

[2] [2] Akihiko Kitano "Characteristics of Carbon-Fiber-Reinforced Plastics (CFRP) and Associated Challenges – Focusing on Carbon-Fiber-Reinforced Thermosetting Resins (CFRTS) for Aircraft", Int J. of Automation Technology, Vol.10, No.3, 2016

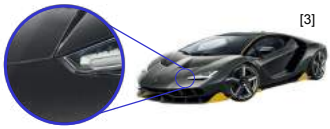

[3] [3] THE 100 HEADS-UP ISSUES #094, "https://www.gqjapan.jp/car/news/20171003/the-100-heads-up-Issues-094", 10 Sep 2017

CFRP-structured machine tool

Prototyped by the Japan Machine Tool Builders' Association

Main spindle CFRP with steel sleeve

Conditions: Spindle rotation at 12,000 min^{-1} for 250 min

Results: Reduce axial thermal expansion to 35%

Ram CFRP in steel square pipe

Conditions: Environment temperature change from 20 to 28 °C for 8 h

Results: 30% reduction in Z-axis direction

Saddle Combine CFRP and aluminum alloy casting

Conditions: Estimation by FEM under the heat generation related to X- and Z-axis feed motion

Results: 30% reduction of the thermal expansion in Z-axis direction

[4] Kono D, Mizuno S, Muraki T, Nakaminami M, A machine tool motorized spindle with hybrid structure of steel and carbon fiber composite, CIRP Annals, Vol. 68, Issue 1 (2019), pp. 389–392.
[5] Kato J, Yoshioka H, Shinno H, Asakura K, Goto S, Usuda K, Hori N, CFRP-wo-tekiyoushita-netuhenkeiyokuseiborunezi-no-seinouhyouka, The Japan Society for Precision Engineering Autumn Conference, B01-4 (2018), pp. 145–146 (in Japanese).
[6] Sugita N, Yoshioka Y, Kakinuma Y, Kono D, Shinkouzouzairyoutekiyousyouenegatakousakukikai-no-kenkyuukaihatu, The Japan Society for Precision Engineering Spring Conference (2019), pp. 211–212 (in Japanese).

CFRP-structured machine tool

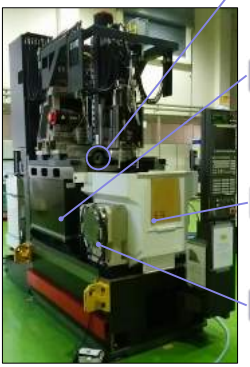

Feed axis CFRP in steel pipe

Conditions: Full stroke feed motion with related structures weight
Results: 69%, 66%, 57% reduction on related X-, Y-, Z-axis direction

Column and Bed CFRP and REC in gray cast iron

Conditions: Environment temperature change from 20 to 28 ºC until being a steady value
Results: 20% reduction in Z-axis direction

Trunnion table (C-axis) CFRP in steel pipe

Conditions: Switching rotation on 300 min^{-1} for 3 h
Results: 62% reduction in the rotational axis direction

Trunnion table (A-axis) CFRP and cast iron with steel sleeve

Conditions: Switching rotation for 3 h
Results: 54% reduction in the direction normal to the plane

[4] Kono D, Mizuno S, Muraki T, Nakaminami M, A machine tool motorized spindle with hybrid structure of steel and carbon fiber composite, CIRP Annals, Vol. 68, Issue 1 (2019), pp. 389–392.
[5] Kato J, Yoshioka H, Shinno H, Asakura K, Goto S, Usuda K, Hori N, CFRP-wo-tekiyoushita-netuhenkeiyokuseiborunezi-no-seinouhyouka, The Japan Society for Precision Engineering Autumn Conference, B01-4 (2018), pp. 145–146 (in Japanese).
[6] Sugita N, Yoshioka Y, Kakinuma Y, Kono D, Shinkouzouzairyoutekiyousyouenegatakousakukikai-no-kenkyuukaihatu, The Japan Society for Precision Engineering Spring Conference (2019), pp. 211–212 (in Japanese).

Tasks of CFRP-structured machine tool

Difficult to enhance uniformly the mechanical characteristics in all directions on machine tools

- ✓ Investigation of machining accuracy by actual cutting tests
- ✓ Certifying the effectivity of CFRP application and the behavior of thermal deformation in a structured machine tool

Research purpose

Machining-based thermal error analysis of CFRP-structured machine tools for high-precision machining

CFRP machine tool

vs.

Base machine

5-axis machine tool
(OKUMA, MILLAC33TU)

Methodology

- Propose a novel machining-based thermal error analysis
- Experimental comparison through machining tests
- Discussion the behavior of thermal expansion and thermal conduction

Outline

1	Background & Research purpose
2	**Experimental setup of proposed machining tests**
3	Experimental results and discussion
4	Conclusions and outlook

Machine tools specifications

All the elements of the CFRP machine tool
- Have the same size
- Designed to realize a static stiffness equivalent / improvement

Table 1 Structures weight

Axis	Base machine	CFRP machine tool
X-axis mass	950 kg	710 kg
Y-axis mass	2050 kg	1190 kg
Z-axis mass	600 kg	490 kg
A-axis inertia	2.8 kgm^2	1.9 kgm^2
C-axis inertia	0.22 kgm^2	0.15 kgm^2

Table 2 Motor specifications

Axis	Travel	Rated power
X feed	340 mm	2.5 kW
Y feed	300 mm	2.7 kW
Z feed	230 mm	4.5 kW
A rotation	-	2.4 kW
C rotation	-	3.7 kW
Spindle rotation	-	26 kW

Machine configuration [CA/YXZ]

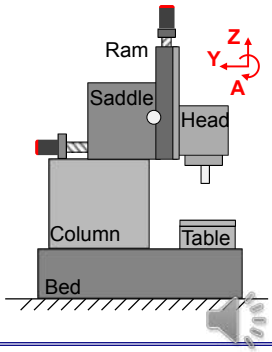

Warm-up operation for experiment

Experimental conditions

- Machining tests were conducted with idle time, assuming setup operation

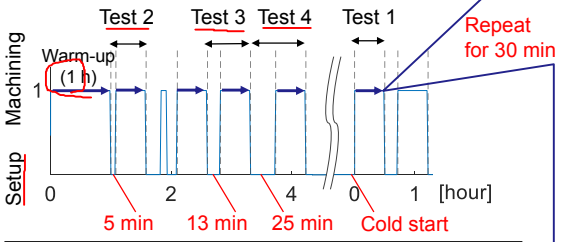

Test	Assumptions	Idle time
1	Cold start	-
2	Automated factories	5 min
3	Setup by operators	13 min
4	Have to wait for other processes	25 min

One cycle behavior of drilling operation (approximately 20 s)

1. Drilling 9 holes on 10 m/min
2. Tool change 40 m/min
3. Positioning 12000 min^{-1} for 10 s

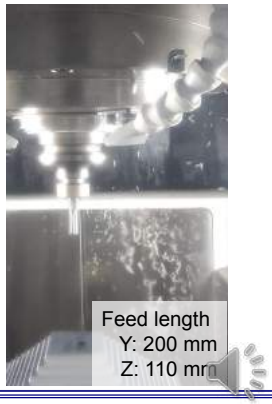

Test piece for machining test

Prepared test piece before machining test

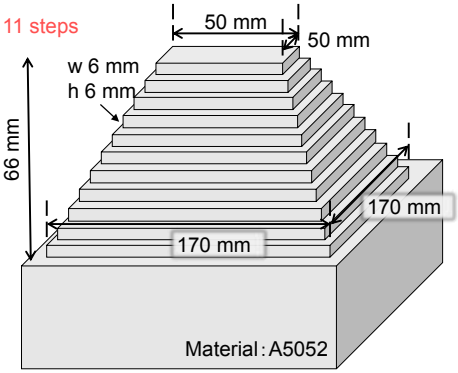

Machined test piece

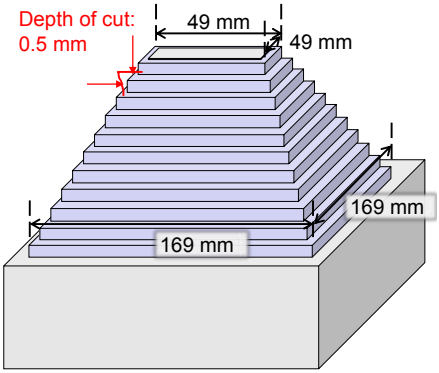

- Thermal errors were indirectly analyzed by measuring the dimensions of the machined test piece.

Machining test procedure

Flowchart of machining test

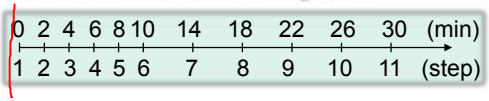

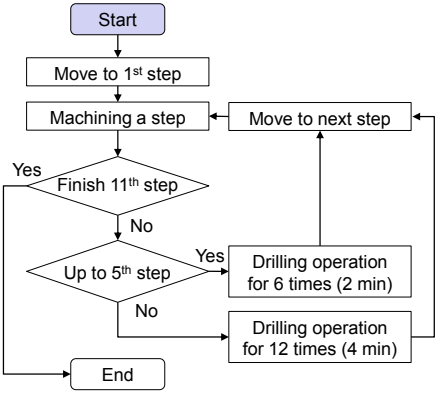

Workshop

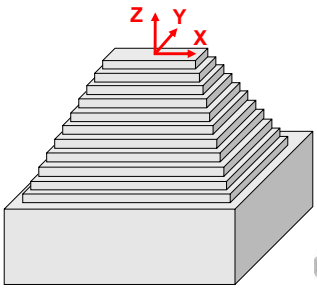

Machining test procedure

Flowchart of machining test

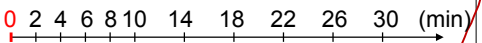

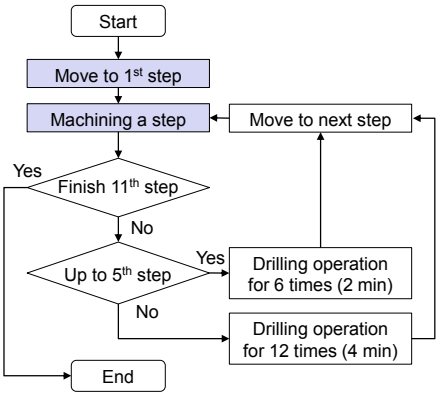

Workshop

Machining a step:	
Cutting width	5.5 mm
Cutting thickness	0.5 mm
Feed rate	4800 mm/min
Feed per tooth	0.1 mm
Cutting type	Down cut

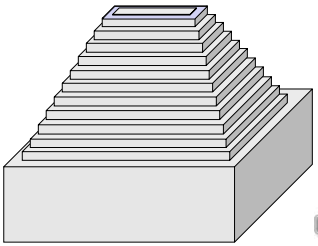

Machining test procedure

Flowchart of machining test

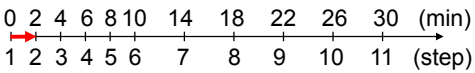

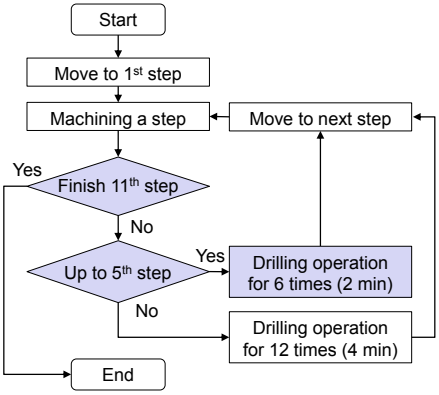

Workshop

Drilling operation

1. Drilling 9 holes on 10 m/min
2. Tool change 40 m/min
3. Positioning 12000 min^{-1} for 10 s

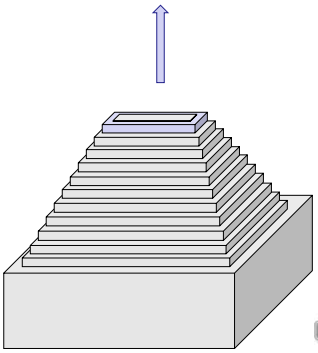

Machining test procedure

Flowchart of machining test

0 2 4 6 8 10 14 18 22 26 30 (min)
1 2 3 4 5 6 7 8 9 10 11 (step)

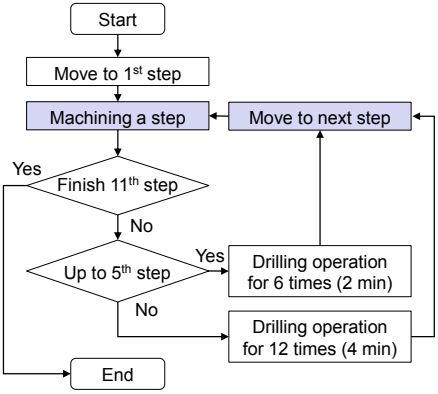

Workshop

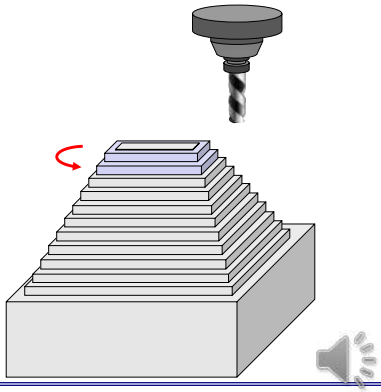

Laboratory for Manufacturing Science, School of Integrated Design Engineering, Keio Univ.

Machining test procedure

Flowchart of machining test

0 2 4 6 8 10 14 18 22 26 30 (min)
1 2 3 4 5 6 7 8 9 10 11 (step)

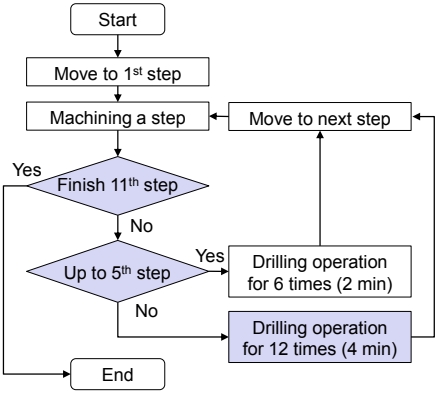

Workshop

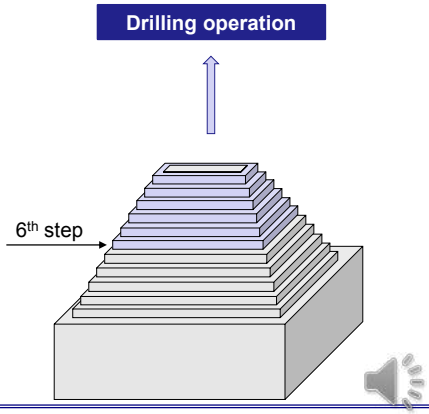

Calibration method for location errors

Measurement of i-th machined square-shape step

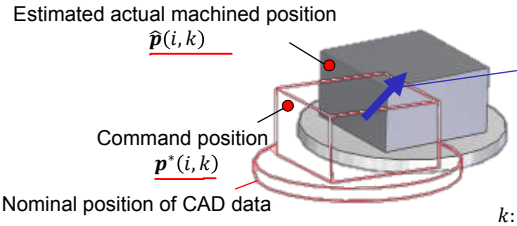

Target in the measurement

Location errors
- Displacement:
  $\Delta x(i), \Delta y(i), \Delta z(i)$
- Inclination:
  $\Delta\alpha(i), \Delta\beta(i), \Delta\gamma(i)$

k: Amount of measurement points

Relation of machined position[7]

$$\begin{bmatrix}\hat{\boldsymbol{p}}(i,k)\\1\end{bmatrix} = \boldsymbol{D_x}(\Delta x(i))\boldsymbol{D_y}(\Delta y(i))\boldsymbol{D_z}(\Delta z(i))\boldsymbol{D_a}(\Delta\alpha(i))\boldsymbol{D_b}(\Delta\beta(i))\boldsymbol{D_c}(\Delta\gamma(i))\begin{bmatrix}\boldsymbol{p}^*(i,k)\\1\end{bmatrix}$$

where: Homogeneous coordinate transformation

$$\boldsymbol{D_x}(\Delta x)\boldsymbol{D_y}(\Delta y)\boldsymbol{D_z}(\Delta z)\boldsymbol{D_a}(\Delta\alpha)\boldsymbol{D_b}(\Delta\beta)\boldsymbol{D_c}(\Delta\gamma) \approx \begin{bmatrix}1 & -\Delta\gamma & \Delta\beta & \Delta x\\ \Delta\gamma & 1 & -\Delta\alpha & \Delta y\\ -\Delta b & \Delta\alpha & 1 & \Delta z\\ 0 & 0 & 0 & 1\end{bmatrix}$$

[7] Ibaraki S, Iritani T, Matsushita T, Calibration of location errors of rotary axes on five-axis machine tools by on-the-machine measurement using a touch-trigger probe, International Journal Machine Tools and Manufacture, Vol. 58 (2012), pp. 44-53.

Calibration method for location errors

Measurement of i-th machined step

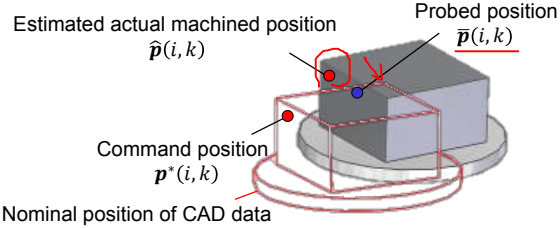

Calibration of location errors[7]

- If location errors Δ are known, machined position $\hat{\boldsymbol{p}}(i,k)$ must be close to probed position $\bar{\boldsymbol{p}}(i,k)$

$$\text{minimize: S} = \sum_{k=1}^{N}\left\{\left(\bar{\boldsymbol{p}}(i,k) - \hat{\boldsymbol{p}}(i,k)\right)\cdot\boldsymbol{n}^*(i,k)\right\}^2$$

- Obtain time behavior of displacement by solving minimization problem in each machined step

[7] Ibaraki S, Iritani T, Matsushita T, Calibration of location errors of rotary axes on five-axis machine tools by on-the-machine measurement using a touch-trigger probe, International Journal Machine Tools and Manufacture, Vol. 58 (2012), pp. 44-53.

Outline

Projection of the measured test pieces on Test 1 (Cold start)

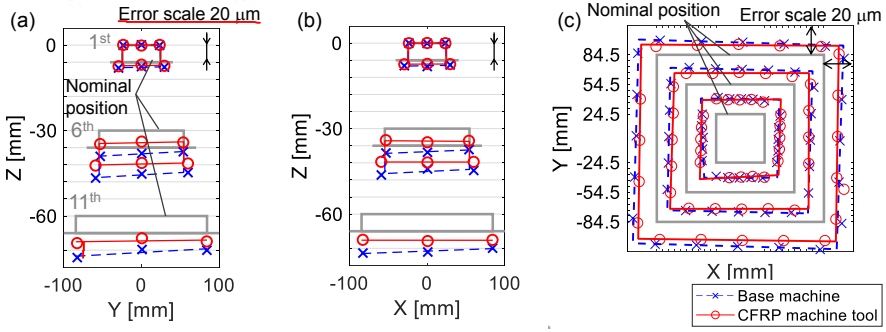

- Errors in the Z-axis were suppressed by low thermal expansion coefficient of each element
- Dimensional errors were caused by tool deflection due to cutting force (because room temperature was controlled)

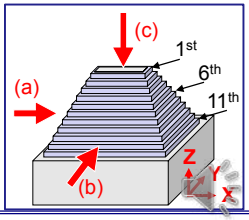

Projection of the measured test pieces on Test 2 (setup for 5 min after warm-up operation)

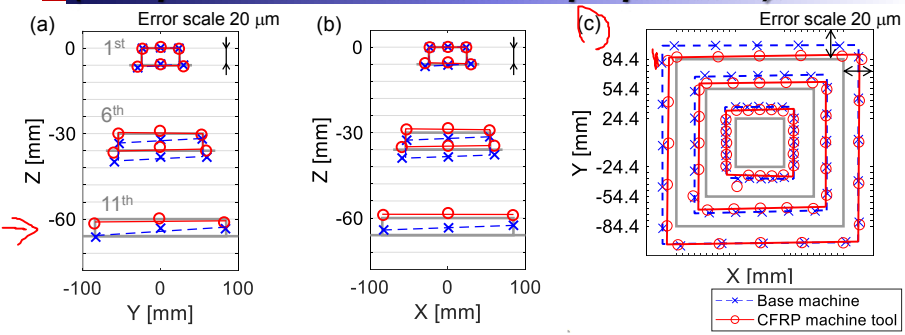

- CFRP machine tool clearly showed high-precision machining properties in the Z-axis
- Base machine were difficult to maintain in a steady state because conventional materials have a smaller time constant for heat conduction
- On the base machine, dimensional errors of square shape became larger in the lower steps

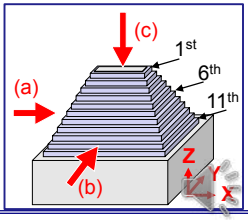

Dimensional errors according to the square shape in Y-axis direction

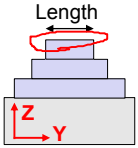

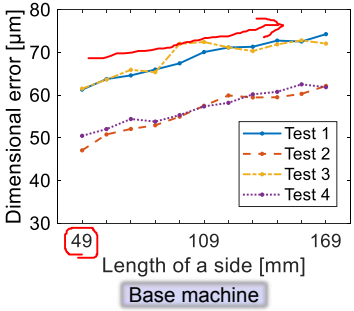

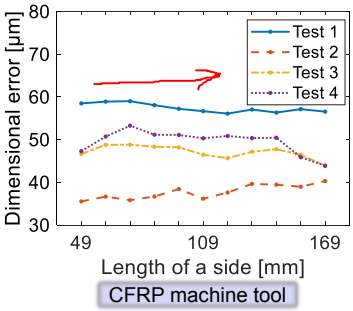

- This increase was not affected by warm-up operation
- Same tendency was also confirmed in the X-axis direction

CFRP machine tool shows high-precision feeding accuracy

Time behavior of thermal error on Z-axis

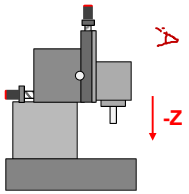

Experimental conditions

Test	Setup operation
1	Cold start
2	5 min
3	13 min
4	25 min

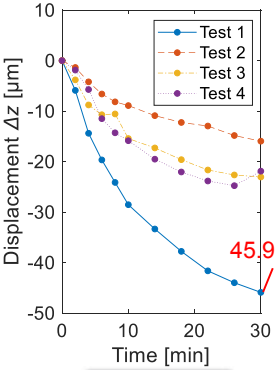

Base machine

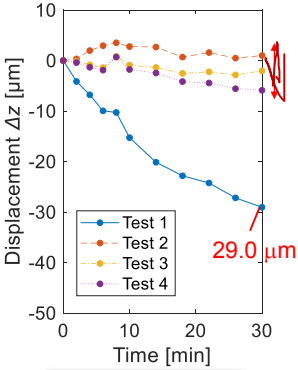

CFRP machine tool

- The displacement was decreased by 36.8% in cold start
- Warm-up operation keeps the displacement less than 5 μm

CFRP machine tool shows high-precision machining accuracy

Time behavior of thermal error on Y-axis

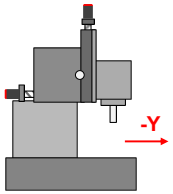

Experimental conditions

Test	Setup operation
1	Cold start
2	5 min
3	13 min
4	25 min

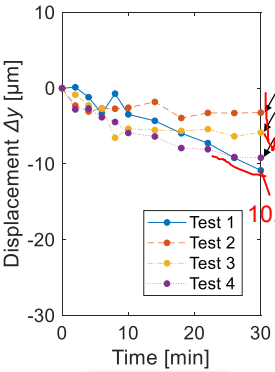

Base machine

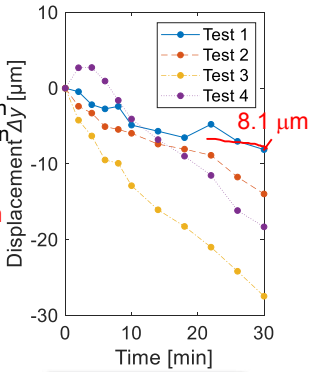

CFRP machine tool

After warm-up operation

- Squareness of the Y-axis to Z-axis on base machine was well adjusted
- Show unique behaviors not a first-order delay system on CFRP machine tool
  - ➢ **Y-axis error is in proportion to Z-axis feed**

Thermal deformation of CFRP machine tool (Discussion of thermal error on Y-axis)

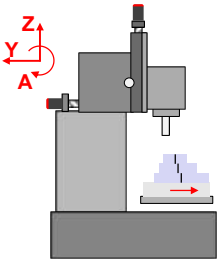

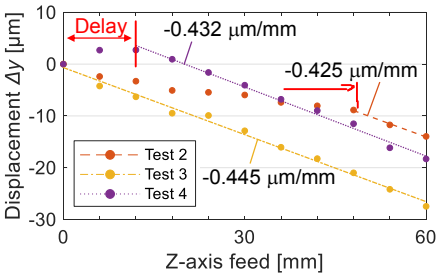

Y-axis error according to Z-axis feed is −0.434 μm/mm (−24.9×10^{-3} deg)

- Warm-up for 1 h was not enough to provide stability
- Setup for 25 min radiated heat, which maintained squareness

CFRP spindle unit shows unique behavior of thermal expansion because of **the mechanical anisotropy of heat conduction**

1. Expansion in the −Z-direction (being stable after warm-up)
2. Inclination in A-axis (**unexpected counter direction**)

Outline

Conclusions and outlook

Machining-based thermal error analysis of CFRP-structured machine tools for high-precision machining

Thermal errors of a CFRP-structured machine tool

- Drilling process for 30 min was analyzed by proposed machining tests
  - ✓ On cold start
    Z-axis direction: Decreased by 36.8%, from 45.9 μm to 29.0 μm
    Y-axis direction: Decreased by 25.7%, from 10.9 μm to 8.1 μm
  - ✓ After warm-up operation
    Z-axis direction: Less than 5 μm
    Y-axis direction: −0.434 μm/mm according to Z-axis feed

Implementation of CFRP application

- Actuators such as Main spindle and Feed axis have big advantages for thermal errors
- Warm-up operation shows the possibility of high-precision machining because CFRP can retain generated heat and can keep thermal deformation in long-term operation
  - ✓ At the same time, compensation methods of A-axis inclination based on temperature measurements is required

Thank you for your kind attention

Makoto Kato, Ph.D. candidate
Department of System Design Enginering, Keio University
Kakinuma Laboratory
Post code: 223-8522
3-14-1, Hiyoshi, Kohoku-ku, Yokohama, Kanagawa, Japan
E-mail: kato@ams.sd.keio.ac.jp

Demonstration on base machine

Machining without warm-up operation of test procedure
- Cold start
- about For 3 min
- Cutting condition is same to machining tests

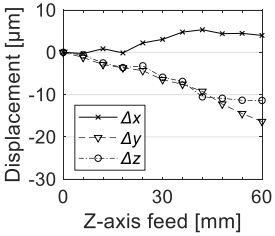

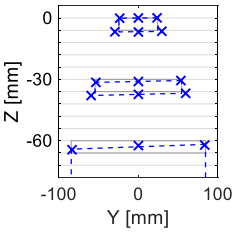

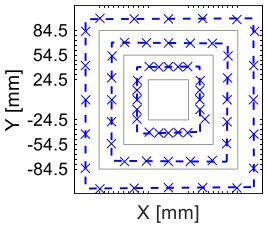

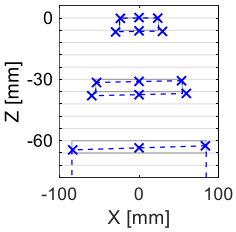

Present Status and Future Directions of Advanced Material Removal Technologies for Aerospace Manufacturing

Ahmad Sadek,
Research Officer,
National Research Council Canada, Montreal

NRC CNRC

NRC.CANADA.CA

20th Machining Innovations Conference for Aerospace Industry 2020 (MIC 2020), December 2nd 2020, Hannover, Germany (Video Presentation)

Present Status and Future Directions of Advanced Material Removal Technologies for Aerospace Manufacturing

A. Sadek, Z. Shi, B. Shi, A. Damir, M. Hassan, M. Meshreki, and H. Attia

Aerospace Manufacturing Technologies Center,
National Research Council, Montreal, QC, Canada

National Research Council Canada | Conseil national de recherches Canada

Canada

Outline

- Introduction
- Advanced Material Removal Technologies for Aerospace Manufacturing:
  - High Performance Superabrasive Grinding
  - Integrated Laser-Assisted Machining (LAM) and Laser Surface Heat Treatment (LSHT)
  - New Sustainable Hybrid Cooling
- Intelligent Tool Condition Monitoring (TCM)
- Virtual Drilling of FRP Composites and Hybrid Stacks: Optimization of Tool Geometry
- Concluding Remarks and future directions.

Introduction

- Material cutting (aerospace & automotive): ~ C$200 bn annual in North American.
- Canada - 3rd globally in civil aircraft production: 700 companies & C$27 bn annual direct revenue.
- Increasing demand for high productivity, high accuracy and environmental impact.

This work presents the recent advances in high-performance cutting technologies (I4.0 aligned):

(i) Superabrasive grinding of difficult-to-cut aerospace materials.

(ii) Integrated laser-assisted machining (LAM) and laser surface heat treatment (LSHT).

(iii) New sustainable hybrid cooling: liquid nitrogen (LN2) + minimum quantity lubrication (MQL).

(iv) Intelligent tool condition monitoring (TCM).

(v) Virtual machining: tool geometry optimization (drilling of composite and hybrid stacks.

Featuring: environmental and economical sustainability, effective digital inter-connectivity and integrated intelligence.

NRC·CNRC

NRC·CNRC

NRC.CANADA.CA

Advanced Material Removal Technologies for Aerospace Manufacturing

- High Performance Superabrasive Grinding
- Integrated Laser-Assisted Machining (LAM) and Laser Surface Heat Treatment (LSHT)
- New Sustainable Hybrid Cooling

National Research Council Canada | Conseil national de recherches Canada

Canada

Introduction to Superabrasive Grinding

- **Superabrasive (SA) grinding:** Grinding with diamond and Cubic Boron Nitride (CBN) abrasives.
- **Advantages of electroplated SA wheels:** (a) long wheel life, (b) a wide range of wheel size, (c) complex wheel profile, (d) suitable for grinding on multi-tasking machining center, (e) Suitable for difficult-to-cut materials such as Ni, Ti-alloys, hard coatings.

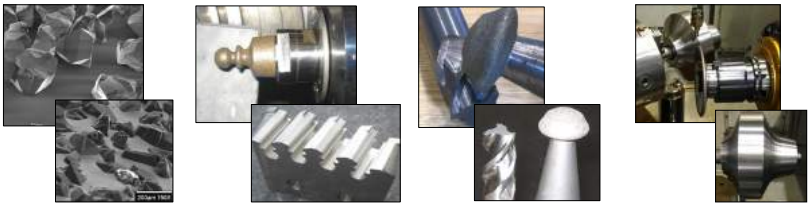

Superabrasive Grinding of Titanium Alloys

- **Objective**
  - Demonstrate the feasibility of grinding Ti-alloys using superabrasive wheels and high pressure grinding fluid for enhanced grinding performance.
- **Challenges**
  - Extremely low thermal conductivity and high chemical affinity to abrasives.
  - Wheel loading and ground surface smearing.
  - Low material removal rates for avoiding wheel loading, typical specific MRR of 2 – 3 mm^2/s with conventional abrasives.
  - High specific energy, high grinding temperatures, and low G-ratio.

Superabrasive Grinding of Titanium Alloys

- **Achievements**
  - A maximum specific MRR of 8 mm^2/s was obtained with a electroplated CBN wheel.
  - Wheel loading and ground surface smearing were eliminated.
  - Low specific energy of 20 – 40 J/mm^3.

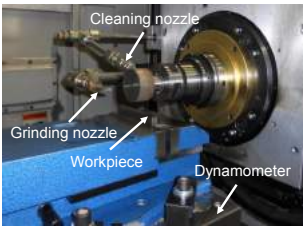

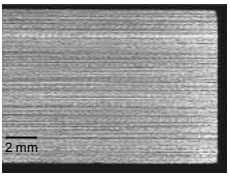

Ground surface

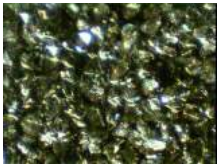

Used wheel surface

Superabrasive Grinding for Extending Wheel Life

- G-ratio: wheel wear resistance index (material removed volume per unit wheel wear volume.
- Conventional G-ratio =1.0 (Ti-alloys, conventional wheels).
- Electroplated CBN wheel, G-ratio = 155.

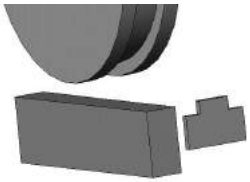

Illustration of radial wheel wear measurement

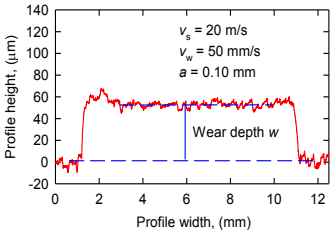

Measured radial wheel wear profile

Superabrasive Grinding of Complex Geometries

- Five-axis grinding with wheels of simple geometries.
- Form grinding with wheels of complex geometries.

A nickel alloy integral bladed rotor (IBR) machined by 5-axis grinding with an electroplated CBN wheel of 10 mm diameter [4].

Fir-tree slots in a nickel alloy ground with a form electroplated CBN wheel of diameter of about 4 – 15 mm. A high speed spindle attachment (75,000 rpm) was used to drive the small wheel.

NRC·CNRC 9

NRC CNRC

NRC.CANADA.CA

Advanced Material Removal Technologies for Aerospace Manufacturing

- High Performance Superabrasive Grinding
- Integrated Laser-Assisted Machining (LAM) and Laser Surface Heat Treatment (LSHT)
- New Sustainable Hybrid Cooling

National Research Council Canada | Conseil national de recherches Canada

Canada

Laser-Assisted Machining (LAM) and Laser Surface Heat Treatment (LSHT)

- **LAM**: machined-surface temperature < 600ºC (prevent microstructure change)
- **LSHT**: heating temperature > 995 ºC (β phase fully or partly transform into a martensitic type of α

  →harder layer on the machined surface.)

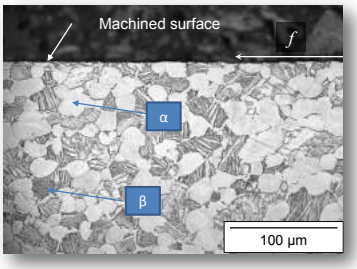

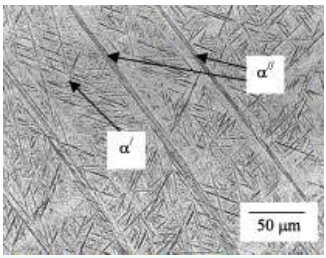

NRC·CNRC

Laser-Assisted Machining (LAM) and Laser Surface Heat Treatment (LSHT)

Model description

- Heat flux: heat exchange window to simulate laser preheating.
- LSHT: tool speed equal to zero

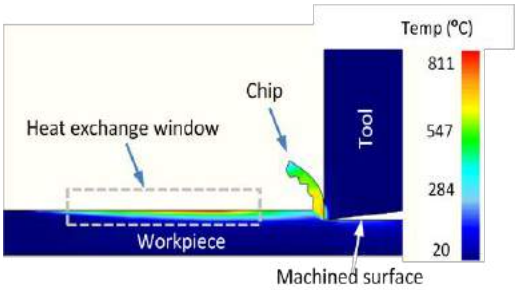

Ti-6Al-4V. v=100 m/min, a_p=0.2 mm

NRC·CNRC 12

Laser-Assisted Machining (LAM) and Laser Surface Heat Treatment (LSHT)

Simulation animation

- Laser beam shooting in front of cutting zone.
- High preheating temperature extensively softens the material
- Cutting force reduced

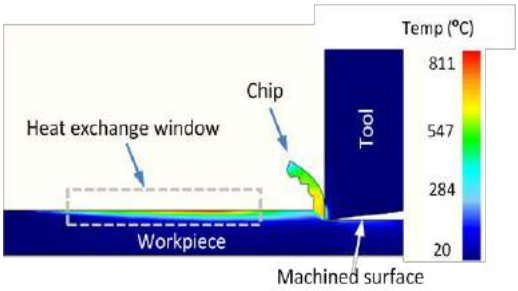

Prediction of Residual Stress (RS)

Optimization of LAM and LSHT process

- ↑ Laser power → Cutting force (Fc) ↓, Machined surface temperature (Ts) ↑.
- LAM: Ts < 600ºC to avoid microstructure change on machined surface→ Optimal net laser power = 520 W → cutting force reduced by 50%
- LSHT: preheating temperature > 995ºC (β transus temperature) → net laser power > 450 W.

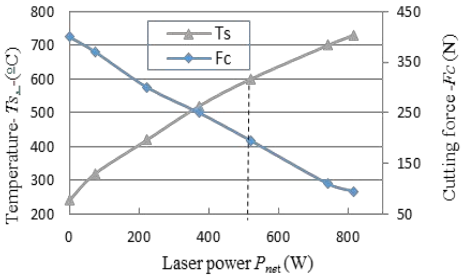

NRC CNRC

NRC.CANADA.CA

Advanced Material Removal Technologies for Aerospace Manufacturing

- High Performance Superabrasive Grinding
- Integrated Laser-Assisted Machining (LAM) and Laser Surface Heat Treatment (LSHT)
- New Sustainable Hybrid Cooling

National Research Council Canada | Conseil national de recherches Canada

Canada

Introduction and Background

- Novel high performance and environment friendly cooling and lubrication solution.
- Potential interest for robotized machining.

Objective:

Understand the fundamentals of the flow characteristics of the two jets and their interaction to optimize the cooling / lubrication strategy.

- Flow simulation (Numerical CFD modeling)
- Experimental investigation and validation

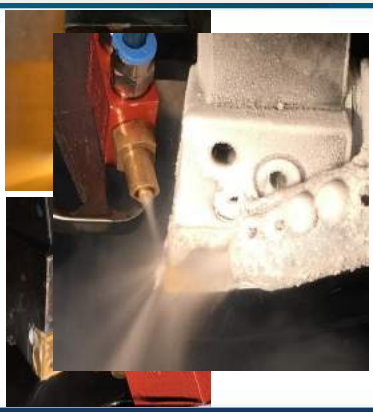

NRC·CNRC 16

Experimental Investigation

Setup and test matrix

› Equipment and material:
- 6-axis Boehringer NG 200 CNC turning center.
- PVD coated CNMP432 (TiAlN/TiN) carbide insert.
- Ti-6Al-4V rods.

› Cutting conditions
- Cutting speed: 56 m/min
- Feed: 0.2 mm/rev
- RDOC: 1.5 mm

- **Tested cooling modes:**
  - *Flood* (6 L/min),
  - *LN2* using external nozzle.
  - *HPC* at 7.86 MPa
  - *Hybrid*: MQL using 2 channel nozzle at 20 mL/min oil flow rate and 30 L/ min air flow rate and LN2 through tool holder.
- **Measured parameters:**
  - Cutting forces, tool wear and Residual stress.

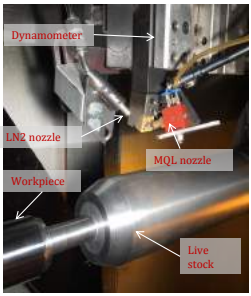

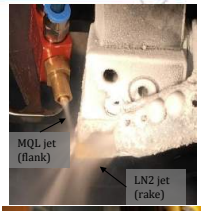

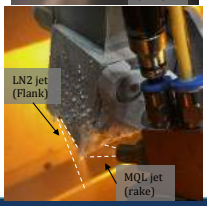

Flow Characterization and Simulation

Case (a): LN2 on rake face
- Turbulence along the jet's edges → accelerated LN2 evaporation.
- High LVF of LN2 on rake face → Efficient heat absorption.
- Low LVF of LN2 (20%) at the tool nose on the flank face.

Case (b): Hybrid (MQL on rake, LN2 on flank through tool holder).
- MQL jet retains LN2 in the cutting area (*cooling blanket*). → higher LVF of LN2 (70%) staying inside the gap in contact with the tool nose and cutting edge.
- LN2 jet reduces the MQL jet temperature (phase change of oil droplets).
- LN2 delivery through the tool holder has significant effect on reducing the insert temperature.

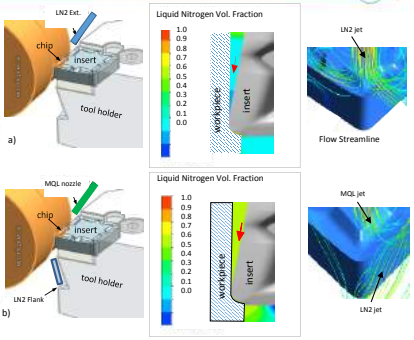

Hybrid cooling strategy has the best cooling effect on the cutting edge that can reduce flank wear.

Results and analysis
Forces

- Hybrid cooling reduces the main cutting and feed forces:
  - 36% and 18% reduction compared to flood.
  - 27% and 9% reduction compared to LN2.
  - 6% reduction compared to HPC.
- Favorable interaction between the LN2 and the MQL jets that increases the VF of LN2 reaching the cutting area, leading to enhanced cooling and lubrication capability.

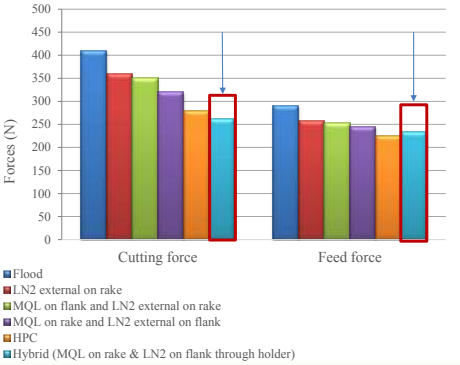

Results and analysis
Tool wear

- Flood:
  - Insert discoloration on the rake and flank.
  - Low heat extraction capacity → higher forces, temperature and tool damage.
  - Insert completely chipped and fractured (thermal expansion-driven stresses in the tool insert).
- LN2:
  - Reduction of the heat affected area due to its excellent heat extraction capacity.
- HPC:
  - Notable discoloration on flank face due to limited accessibility of the HPC jet.
- Hybrid:
  - Least discoloration on the flank and rake faces due to the enhanced cooling and accessibility.

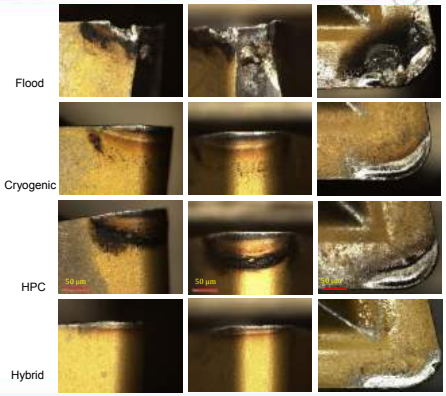

Results and analysis

Residual stresses in the subsurface layer

- Hybrid: Compressive RS (<300 µm from surface).
- Surface compressive stresses ~ -100 MPa for LN2 and Hybrid cooling.

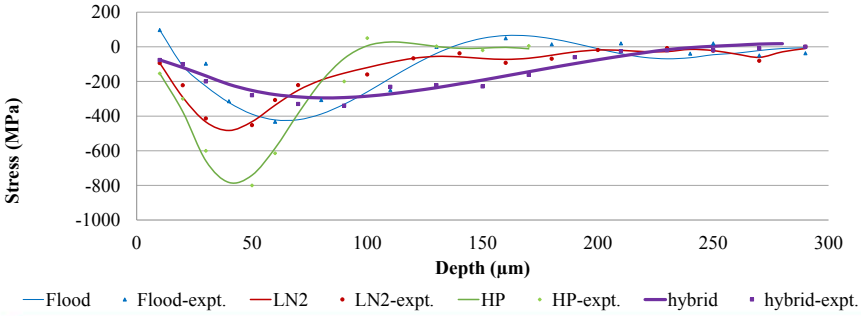

NRC·CNRC 21

NRC·CNRC NRC.CANADA.CA

Intelligent Tool Condition Monitoring (TCM)

National Research Council Canada | Conseil national de recherches Canada

Canada

Research Objectives and Methodology

Terminal objective: ***To develop a non-intrusive real-time sensor-based TCM system that can predict and prevent sudden tool chipping, as well as detect progressive tool wear to prevent machined part damage.***

↑Tool condition ↓Cutting conditions ↓System learning ↑Time response ↑Reliability ↑Practicality (AC)

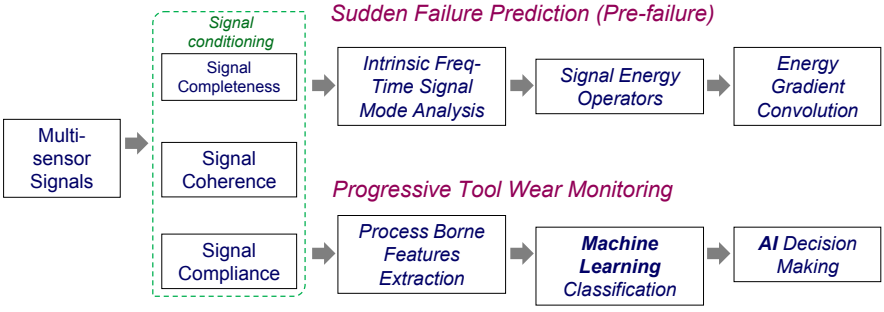

Reconfigurable multi-sensor Instrumentation

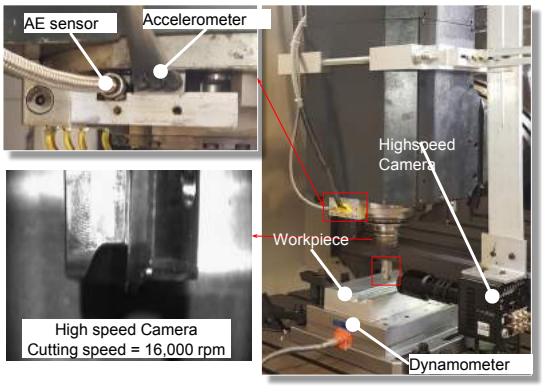

Real-time Intelligent Tool Condition Monitoring (I-TCM)

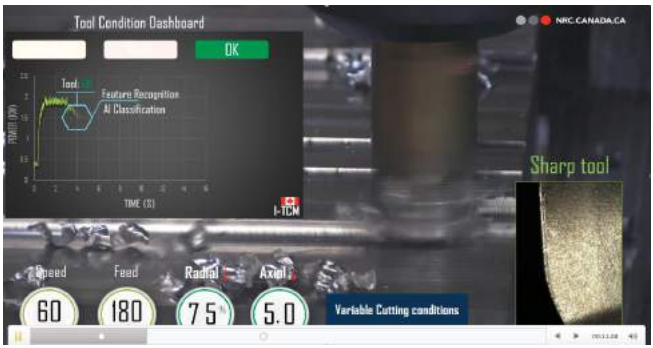

NRC·CNRC 25

Prefailure Detection - Milling Operations

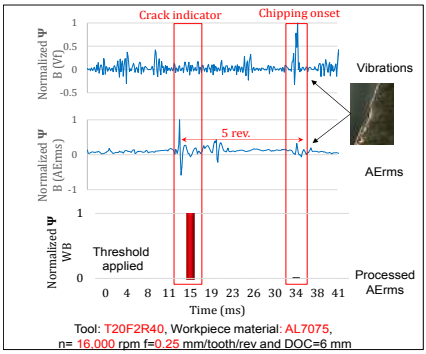

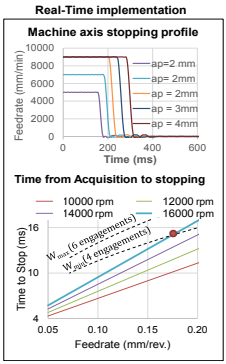

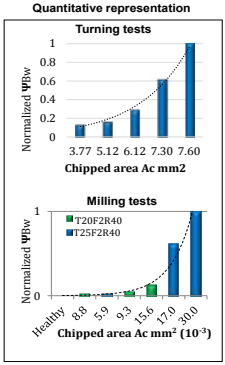

NRC·CNRC 9

NRC CNRC

NRC.CANADA.CA

Virtual Drilling of FRP Composites and Hybrid Stacks: Optimization of Tool Geometry

National Research Council Canada | Conseil national de recherches Canada

Canada

Motivation and Objectives

Motivation:

Industrial need for developing robust interactive prediction capabilities for:

- Tool design and optimization for drilling of FRPs and stacks to obtain defect-free parts.

Objectives:

Demonstrating the optimization capability based on a new generalized hybrid model predictions of *time variation* and *spatial distribution* of:

- The transient (and steady state) cutting forces → *cutting energy* E_c*:*
- Drilling-induced defects; *Considering the interaction between the complex tool geometry and the anisotropic laminar FRP structure.*

NRC·CNRC

Force Prediction Model

Inputs

- Material layup configuration
- Process Parameters (*n* and f_t)
- Tool geometry

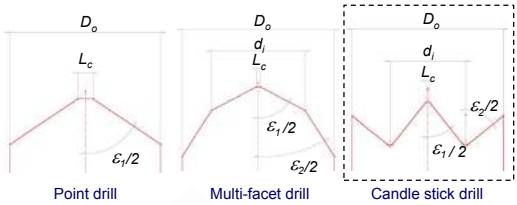

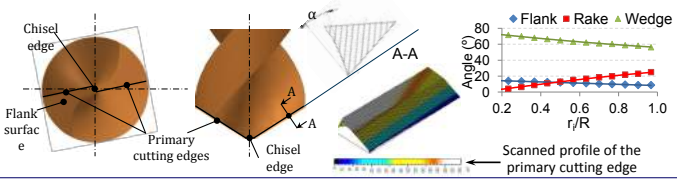

Prediction Model

Inputs

- Material layup configuration
- Process Parameters (*n* and f_t)
- Tool geometry

Process kinematics formulation

Tool-workpiece interaction

- Cutting edge sections
- Relative tool – workpiece position θ_e
- Formed chip dynamic geometry

Experimentally defined material properties

Hybrid mechanistic model

Empirical modules

- Frictional torque
- Material softening

***Output (Prediction)**: Cutting forces, torques and energy*

	Primary edges	*Chisel edge*
Force	$F_p(t) = \sum_{1}^{k} \sum_{1}^{i=N_p} K_{F,p,i}\{v_{c,i}, d_p(t), \theta_{e,p,i}, \alpha_i\}.\, d_p(t).\, L_{p,i}(t)$	$F_c(t) = \sum_{1}^{j=N_c} K_{F,c,j}\{v_r, d_c(t), \theta_{e,c,j}\}.\, d_{c,j}(t).\, L_{c,j}$
Torque	$T_p(t) = \sum_{1}^{k} \sum_{1}^{i=N_p} K_{T,p,i}\{v_{c,i}, d_p(t), \theta_{e,p,i}, \alpha_i\}.\, d_p(t).\, L_{p,i}(t)$	$T_c(t) = \sum_{1}^{j=N_c} K_{T,c,j}\{v_r, d_c(t), \theta_{e,c,j}\}.\, d_{c,j}(t).\, L_{c,j}$

Experimental Validation

- Machining center: 5-axis DMU-100P duo BLOCK®
- Spindle speed: 18,000 rpm, max feed rate: 50 m/min, power: 50kW.
- Force measurement: 4-component Kistler dynamometer (model: 9272).
- A FLIR SC8303 Infrared camera at the hole exits (ε_{tool}=0.34), (error=± 5%).

Axial feeds (mm/min)				
Rotational speed '*n*' (rpm)	Feed 'f_r' (mm/rev)			
	0.05	0.1	0.15	0.2
6000	300	600	900	1200
8000	400	800	1200	1600
10000	500	1000	1500	2000
12000	600	1200	1800	2400

- Minimum 2 replicates for each test.
- Three different tool geometries: 4x4x3x2

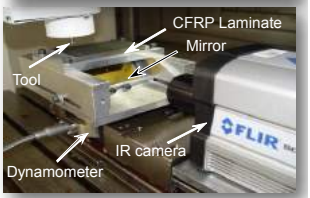

NRC·CNRC

Model Validation: Force and torque Predictions

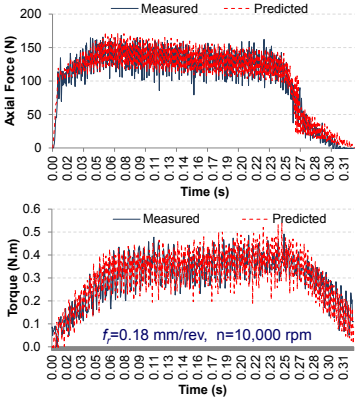

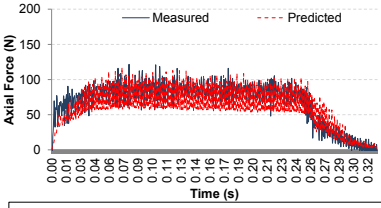

The prediction errors in the entrance, steady and exit stages:

- Axial Force: +5% to +15%,
- Torque: ±15%

with a confidence interval of 95%.

NRC·CNRC

Model Validation: delamination and thermal damage

- ✓ Process optimization
- ✓ Prediction of final part quality
- ✓ Tool design optimization

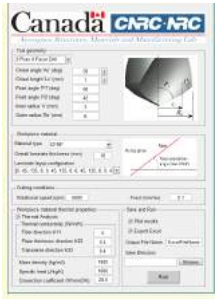

Prediction of final part delamination and thermal damage

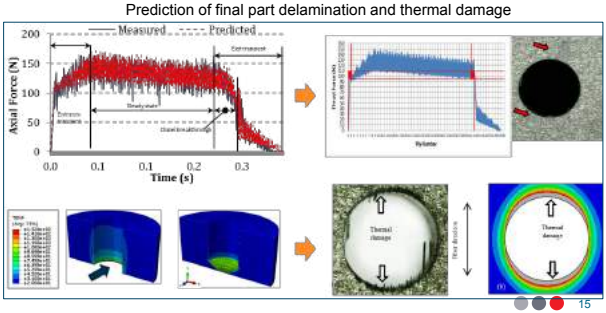

Tool Geometry Optimization

Tool	Levels	Diameter 'Do' (mm)	Inner diameter 'di' ratio 'di/Do'	Point angle 1 'ψ1' (deg)	Point angle 2 'ψ2' (deg)	Chisel length 'Lc' ratio 'Lc/do'	No. of Configurations
T1: Point Drill	1	2	--	45	--	0.25	
	2	6	--	90	--	0.5	
	3	10	--	135	--	0.75	
	No. of configurations	3	--	3	--	3	*27*
T2: Multi-facet drill	1	2	0.25	45	45	0.25	
	2	6	0.5	90	90	0.5	
	3	10	0.75	135	135	0.75	
	No. of configurations	3	3	3	3	3	*243*
T3: Candle stick drill	1	2	0.25	45	-45	0.25	
	2	6	0.5	90	-90	0.5	
	3	10	0.75	135	-135	0.75	
	No. of configurations	3	3	3	3	3	*243*

Parameter	Definition	Unit
D_o	Outer tool diameter	mm
d_i	Inner section diameter	mm
d_i/D_o	Inner to outer diameter ratio	--
ψ_1	Inner point angle	deg
ψ_2	Outer point angle	deg
L_c	Chisel edge length	mm
L_c/D_o	Chisel length to outer diameter ratio	--

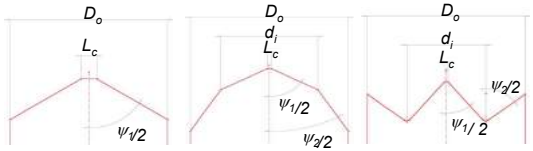

T1: Point drill T2: Multi-facet drill T3: Candle stick drill

Tool Geometry Optimization

Example optimization scheme demonstrated on T2

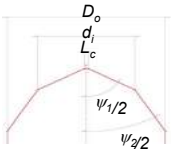

T2: Multi-facet drill

Configurations fulfilling objective

Objective: Fz < 110 N & Min. (Mz, Q, Tc)

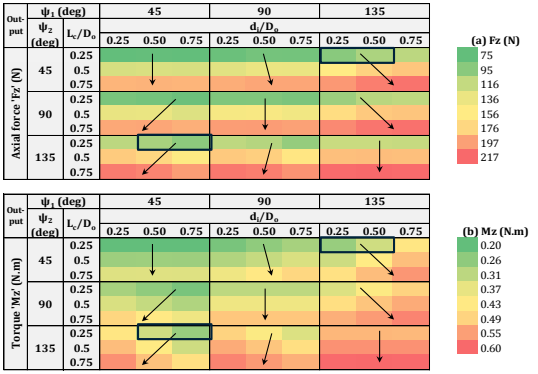

Representative maps for optimized conditions (f_t=0.18 mm/rev, n=10,000 rpm), @D_o=6mm

Tool Geometry Optimization

Example optimization scheme demonstrated on T2

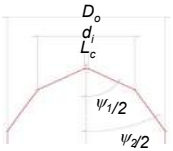

T2: Multi-facet drill

Configurations fulfilling objective

Objective: Fz < 110 N & Min. (Mz, Q, Tc)

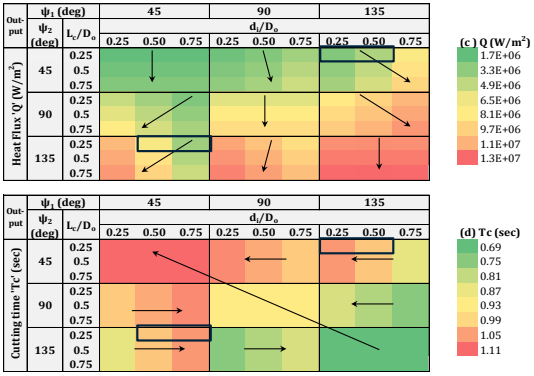

Representative maps for optimized conditions (f_t=0.18 mm/rev, n=10,000 rpm), @D_o=6mm

Tool Geometry Optimization

Example optimization scheme demonstrated on T2

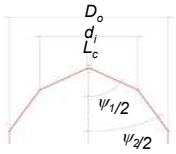

T2: Multi-facet drill

Configurations fulfilling objective

Objective: Fz < 110 N & Min. (Mz, Q, Tc)

Similar optimization was applied to T1 and T3

Configurations fulfilling objective

Parameter	Design 1	Design 2	Design 3	Design 4	Unit
D_o	6	6	6	6	mm
d_i	1.5	3	1.5	3	mm
d_i/D_o	0.25	0.5	0.5	0.75	--
ψ_1	135	135	45	45	deg
ψ_2	45	45	135	135	deg
L_c	1.5	1.5	1.5	1.5	mm
L_c/D_o	0.25	0.25	0.25	0.25	--
Force	75	95	95	75	N
torque	0.26	0.31	0.31	0.26	N.m
heat flux	1.70E+06	3.30E+06	3.30E+06	4.90E+06	w/m2
cutting time	1.05	0.99	0.99	1.05	sec

Tool Geometry Optimization

T2 resulted in the optimum values of force, torque and heat flux compared to T1 and T3

- Force reduced by 12% and 36%
- Torque reduced by 18% and 42%
- Heat flux by 66% and 75%

The drawback of the T2 design: relatively higher cutting time (increased by 30% and 14%).

Tool and configuration fulfilling objective

Parameter	T1	T2	T3	Unit
D_o	6	6	6	mm
d_i	--	1.5	4.5	mm
d_i/D_o	--	0.25	0.75	--
ψ_1	90	135	135	deg
ψ_2	--	45	45	deg
L_c	0.25	1.5	1.5	mm
L_c/D_o	1.5	0.25	0.25	--
Force	85	75	117.6	N
torque	0.317	0.26	0.45	N.m
heat flux	5.00E+06	1.70E+06	6.70E+06	w/m2
cutting time	0.812	1.05	0.92	sec

Concluding Remarks

The new developments in high performance cutting of difficult-to-cut aerospace materials are presented:

- **Superabrasive grinding:** demonstrated the advantages of long wheel life, good wheel form holding capability, and improved MMR in complex Ti-alloy aerospace components.
- **Integrated LAM and LSHT:** The benefits and feasibility of using the same laser source has been demonstrated through a 50% force reduction by LAM and the hard outer layer produced by LSHT without affecting the toughness of the bulk part.
- **Hybrid cryogenic cooling and MQL:** demonstrated sustainable and superior performance in improving tool life and surface integrity as compared to flood and high pressure cooling for cutting difficult-to-cut materials.
- **Smart tool wear and prefailure detection:** a breakthrough in TCM that combines reliable detection accuracy with minimized system learning.
- **Model-based tool geometry optimization:** approach has shown a unique digital capability for minimizing drilling forces and temperatures to eliminate part damage and enhance productivity.

NRC·CNRC

Future Directions

Superabrasive grinding:

- Precision machining of complex additive manufacturing aerospace parts
- Expand application to other difficult-to-cut materials (MMC, CMC and FRPs).

Integrated LAM and LSHT:

- Multi-axis laser-assisted milling
- Process optimization (e.g. laser power, beam size..) for max. surface integrity and part fatigue life.

Hybrid cryogenic cooling and MQL:

- Understanding the lubricating role of cryogens through the boundary film effect, and the control of material embrittlement for chip breakage and evacuation.
- Developing FE-CFD fluid-structure interaction models to enable effective coolant delivery in deep-hole drilling.

Smart tool wear and prefailure detection:

- Developing intelligent minimal deep learning approaches.
- Developing smart tools with robust embedded sensors and wireless transmission of signals.

Model-based tool geometry optimization:

- Optimization of new tools (e.g. superabrasive and ceramic) and processes (e.g. vibrational and orbital machining).
- Integration with smart real-time TCM to develop a new generation of effective cyber-physical adaptive machining.

NRC·CNRC

NRC CNRC

NRC.CANADA.CA

THANK YOU

Ahmad Sadek, Ph.D.
Team Lead, Advanced Machining
Aerospace Manufacturing Technologies Center (AMTC)
National Research Council Canada
5145 Avenue Decelles,
Montréal (QC) H3T 2B2
Email: ahmad.sadek@nrc-cnrc.gc.ca

National Research Council Canada | Conseil national de recherches Canada

Canada

Influence of the supplying technique of a sub-zero metalworking fluid on the performance of face turning of Ti-6Al-4V titanium alloy

Stephan Basten,
Research Assistant,
TU Kaiserslautern

Influence of the supplying technique of a sub-zero metalworking fluid on the performance of face turning of Ti-6Al-4V titanium alloy

20th Machining Innovations Conference for Aerospace Industry 2020 (MIC 2020)
December 2nd 2020, Hannover, Germany

S. Basten[a], B. Kirsch[a], K. Gutzeit[a], H. Hasse[b], J. C. Aurich[a]

a) Institute for Manufacturing Technology and Production Systems, TU Kaiserslautern, Germany
b) Laboratory of Engineering Thermodynamics, TU Kaiserslautern, Germany

Agenda

- Introduction and state of the art
- Experimental setup and cooling parameters
- Measuring techniques and measuring methodology
- Results and discussion
  - Tool temperature
  - Process forces
  - Crater depth and crater width
  - Surface roughness
- Conclusion and outlook

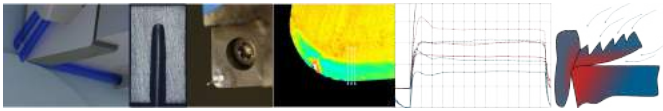

Introduction and state of the art

Cutting edge when machining titanium alloys [1].

Dual coolant supply on flank and rake surface in the context of turning [2].

- Machining of Ti-6Al-4V leads to high mechanical, thermal, and chemical loads on the cutting tool
  - Reducing the thermo-chemical load in the contact zone to minimize thermally induced wear
- Lower temperatures in the contact zone can be achieved by:
  - Use of cooling strategies that exhibit high cooling effects (cryogenic media, sub-zero MWF)
  - Variation of mass flow
  - Variation of supplying technique
- High nozzle exit velocities, nozzle geometry and position of the nozzles/ direction of the free jets have an influence on the cooling performance

[1] Armendia M, et al. Comparison of the machineabilities of Ti6Al4V and TiMETAL® 54M using uncoated WC–Co tools. J. Mater. Process. 2010;210(2):197–203.
[2] M'Saoubi R, et al. High performance cutting of advanced aerospace alloys and composite materials. CIRP Annals 2015; 64(2):557–580.

Introduction and state of the art

- LN_2-cooling: cryogenic temperature (-196 °C), film-boiling → low heat transfer coefficient
- CO_2-snow cooling: low temperature (-78.5 °C), solid-gasous → low heat transfer coefficient
- Emulsion: ambient temperature, liquid → high heat transfer coefficient
- Sub-zero MWF:
  - Liquid mixtures of polyhydric alcohols and water
  - High viscosity when refrigated
  - Low temperature (up to -50 °C), stable liquid state
    → High heat transfer coefficient

Introduction and state of the art

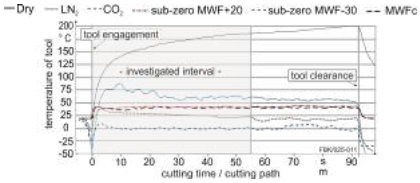

Temperature of tool when turning different cooling strategies [3].

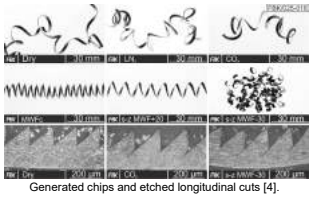

Generated chips and etched longitudinal cuts [4].

- Machining Ti-6Al-4V using sub-zero MWF:
  - lower tool temperatures
  - less tool wear

Influence of different nozzle positions and different free jet properties on the performance of sub-zero cooling approach?

Effect on the machining process or process results (e.g. tool wear, surface roughness)?

[3] Kirsch B, et.al. Sub-zero cooling: A novel strategy for high performance cutting. CIRP Annals 2018; 67(1):95–98.

Experimental Setup and cooling parameters

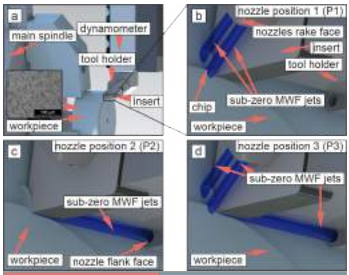

properties of the workpieces	tool and tool-geometry:
workpiece material: Ti-6Al-4V condition of material: stress relieved workpiece Ø = 80 mm Ø hole in rotational axis: 8 mm	indexable insert: CNMA 120408 cutting material: cemented carbides K20 (92.5% WC, 7.5% Co) coating: uncoated geometry: r_ε=0.8 mm, r_n=3-5 µm holder: DCLNL2525X12, γ=-6°, κ=95°, λ=-6°
parameter of face turning	**sub-zero metalworking fluid**
cutting speed v_c = variable v_c = 60 m/min and 120 m/min depth of cut a_p = 2 mm feed rate f = 0.2 mm/rev cutting time t_{c, 60m/min} = 12.44 s cutting time t_{c, 120m/min} = 24.88 s	sub-zero MWF: ethane-1,2-diol, water mass ratio: ζ_{ethane-1,2-diol,Wasser} = 1.72 g/g corrosion inhibition: disodium metasilicate EP/AW-additives: triisobutyl phosphate

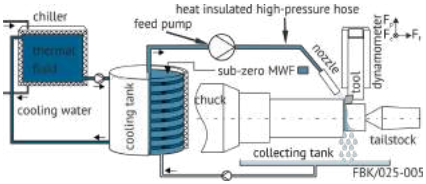

Sub-zero MWF supplying system integrated in the lathe.

Experimental Setup and cooling parameters

properties/parameter	P1+20	P1-30	P2+20	P2-30	P3+20	P3-30
number nozzles	2	2	1	1	3	3
diameter per nozzle in mm	1	1	1.3	1.3	1, 1.3	1, 1.3
distance nozzle orifice to contact zone in mm	7	7	17	17	7, 17	7, 17
supply temperature in °C	**+20**	**-29**	**+20**	**-29,5**	**+20**	**-28,9**
mass flow in kg/min	**a) 2.1 b) 4.2**	**a) 2.1 b) 4.2**	**a) 2.1 b) 4.2**	**a) 2.1 b) 4.2**	**a) 2.1 b) 4.2**	**a) 2.1 b) 4.2**
density in g/cm³	1.10	1.15	1.10	1.15	1.10	1.15
volumetric flow in l/min:	a) 1.90 b) 3.80	a) 1.83 b) 3.65	a) 1.90 b) 3.80	a) 1.83 b) 3.65	a) 1.90 b) 3.80	a) 1.83 b) 3.65
average nozzle exit velocity in m/s	a) 20.2 b) 40.3	a) 19.4 b) 38.9	a) 23.8 b) 47.7	a) 23.0 b) 45.8	a) ≈11 b) ≈22	a) ≈10.5 b) ≈21.0
kin. viscosity in mm²/s	5	75	5	75	5	75
Reynolds number (for a single nozzle)	a) 4930 b) 9860	a) 340 b) 680	a) 7580 b) 15160	a) 530 b) 1050	a) ≈3500 b) ≈7000	a) ≈250 b) ≈500

Investigated cooling parameters.

	Ti	Al	V	Fe	O	C	N	H	Res.
%	89.17	6.12	4.10	0.29	0.16	0.06	0.03	0.01	0.06

Chemical composition of the investigated batch of Ti-6Al-4V (wt%).

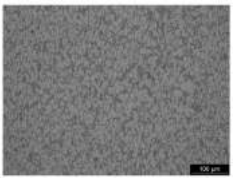

Microstructure of the investigated batch of Ti-6Al-4V.

Measuring techniques and measuring methodology

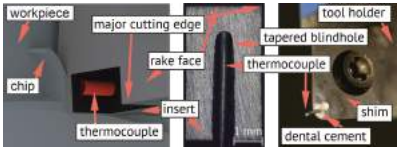

Measurement of the tool temperature at a distance of 1 mm to the contact zone.

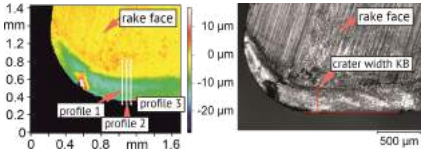

Methodology of the crater wear measurement of the cutting tool using structured-light 3D scanner (left) and optical microscopy (right).

- Tool temperature (thermocouple)
- Wear parameters according to ISO3685 (structured-light 3D scanner and optical microscope)
- Process forces (3-component dynamometer)

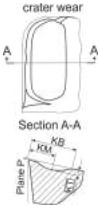

ISO 3865

Results and discussion – Tool temperature

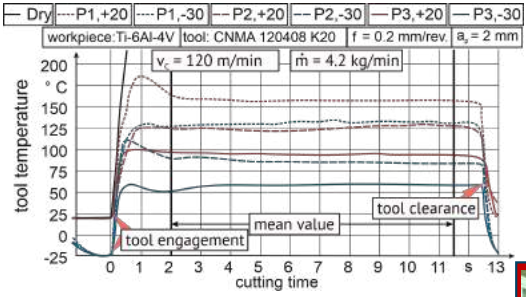

- Stationary zone: 2s after tool engagement until tool clearance
- Sub-zero MWF-30: lower temperature levels at consistant nozzle position
- Influence of nozzle position on cooling effect can be clearly seen

Results and discussion – Tool temperature

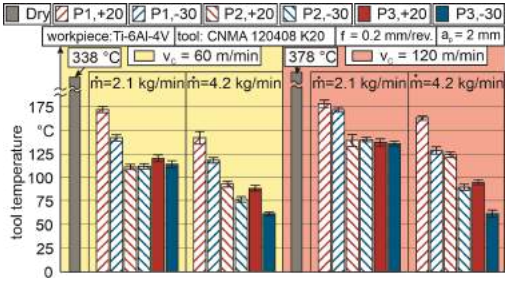

- Sub-zero MWF-30: High nozzle exit velocities to ensure better heat transfer coefficient compared to sub-zero MWF+20
- Highest possible wetted area leads to improvements regarding tool temperature

Measuring techniques and measuring methodology

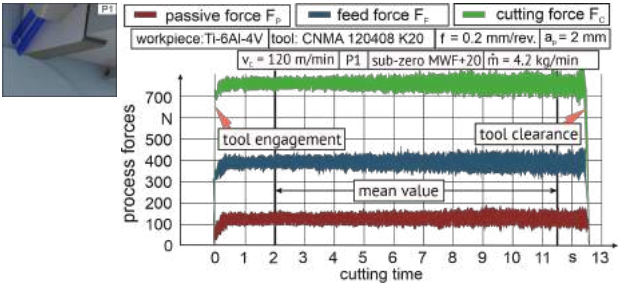

- Highest thermal load on tool is shown in this case
- Low peak-to-valley amplitudes
  → Robust workpiece clamping

Results and discussion – Process forces

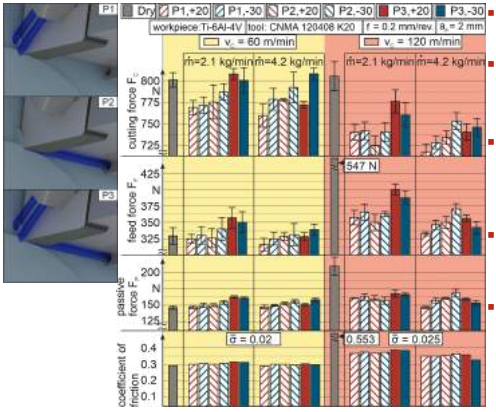

- Minor influences of cooling conditions on process forces
- Increasing cutting speeds:
  - cutting force ↓
  - Feed and passive force ↑
- Interacting effects: thermally induced softening of workpiece material and slightly decreasing depth of cut due to contraction of tool / workpiece
- Reduction of nozzle exit velocities when using multiple nozzle supplying technique must be considered
- CoF relatively constant at consistent cutting speed

Results and discussion – Crater depth and crater width

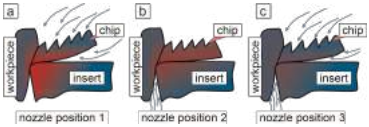

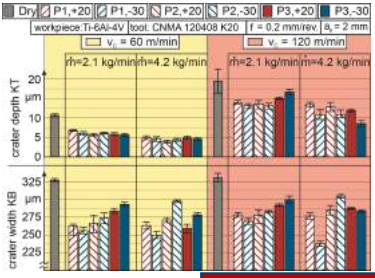

- Use of any cooling: KT and KB strongly reduced
- Supply along rake face (P1):
  - Higher temperature gradient between top side of chip and tool-work interface (thermally induced stress in chip increases)
- Supply along flank face (P2):
  - Lower temperature gradient between top side of chip and tool-work interface (thermally induced stress in chip decreases)
- Combined position of P1 and P2 (P3):
  - Superposing effects of P1 and P2

Results and discussion – Surface roughness

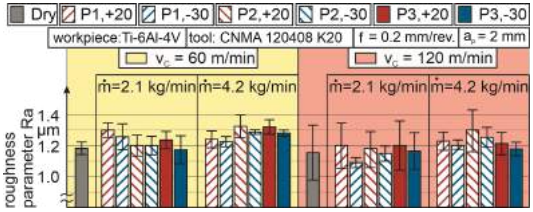

- Better surface roughness when using sub-zero MWF-30 compared to sub-zero MWF+20 for consistent nozzle position
- The lower the tool temperature, the lower the error bars
- Microscopic chatter marks may be reduced by lower temperatures in the workpiece
  - Increasing Young's modulus leads to less strong spring-back effect of Ti-6Al-4V

Conclusion

- Sub-zero MWF-30: Mass flow of approx. 4.2 kg/min should not be undercut in order to achieve a significantly higher cooling effect compared to coolant supplied at ambient temperature
- Most effective reduction of the tool temperature if multiple nozzles wet as many areas as possible simultaneously by impingement flow
- Improved chip formation by cooling top side of chip (higher thermally induced stresses)
- High cooling effect slightly improves surface roughness

Outlook

- Further investigation of the influence of nozzle position when machining Ti-6Al-4V at high cutting speeds with respect to tool life and chip breaking
- Analysis of possibilities to reduce springback effect of other titanium alloys

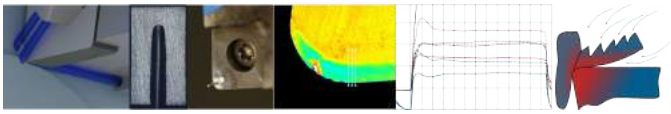

Acknowledgement

Funded by the Deutsche Forschungsgemeinschaft (DFG, German Research Foundation) – project number 172116086 - SFB 926. The authors also would like to thank Petrofer as well as Borg Warner Turbo Systems for the cooperation.

DFG Deutsche Forschungsgemeinschaft

CRC 926 MICOS Component Surfaces

PETROFER industrial oils and chemicals

BorgWarner Turbo Systems

Investigation of the influence of different hard coatings on chip formation and process forces when machining duplex steel 1.4462

Ante Glavas,
Research Assistant,
Rheinische Fachhochschule Köln

Rheinische Fachhochschule Köln
University of Applied Sciences

Institut für Werkzeug- und Fertigungstechnik
Prof. Dr.-Ing. M. Reuber
Prof. Dr.-Ing. W. Saxler

Investigation of the influence of different hard coatings on chip formation and process forces when machining duplex steel 1.4462

Ante Glavas, Benedikt Thimm, Tamara Teppernegg, Christoph Czettl

MIC Conference 2020
PZH Hannover, 02.12.2020

Structure

Investigation of the influence of different hard coatings on chip formation and process forces when machining duplex steel 1.4462

- Fundamentals – Hard coating
- Experimental investigations
- Analytical analysis
- Conclusion and outlook

Fundamentals - Hard coating

Use of hard coatings on cutting tools:

- Increase in thermal and mechanical resistance
- Reduction of friction between tool and workpiece

Schematic representation of separable layer systems

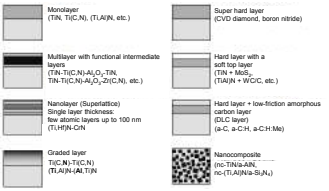

Source: Fertigungsverfahren 1 – Fritz Klocke, DBU Abschlussbericht 2018 – G. Erkens, B. Denkena

Properties of hard coatings:

- High surface hardness
- High temperature resistance
- High phase stability
- High chemical resistance to oxidation
- Low tendency to deform
- Low sliding friction between tool and workpiece

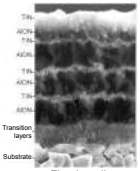

Fine lamellar multilayer

Conclusion:

- Hard coatings can have different thermo-physcial properties → influence on the process temperatures in the shear zones and impact on the chip formation
- For a mechanisms-oriented tool development it is necessary to understand these influences

Experimental investigations

Linear orthogonal cutting tests

Experiments were divided into two different test series:

- First test series: influence of coatings on sharp tools
- Second test series: influence of coatings on worn tools

Measurement values: Cutting Force F_c, Feed force F_f, chip thickness h'

Tools

- Indexable insert: SEKN 1203 AFN (standard cutting wedge)
- Cutting material: Cemented carbide (WC-Co)
- Coatings:
  - TiAlN (PVD)
  - TiN-TiCN-Al_2O_3 (CVD)
  - 4 µm layer thickness
  - → TiAlN shows a slightly lower thermal conductivity

Material

- X2CrNiMoN22-5-3
- Material number: 1.4462
- Austenitic-ferritic duplex steel
- Tensile strength R_m = 680 – 880 N/mm²
- Thermal conductivity λ = 15 W/mK

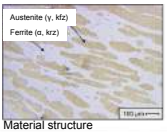

Material structure

Schematic representation of hardness measurement

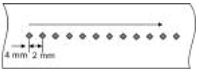

230 ± 4 HV

Experimental investigations

Linear orthogonal cutting test bench

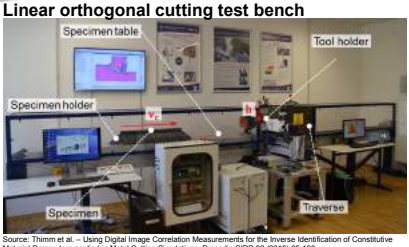

Source: Thimm et al. – Using Digital Image Correlation Measurements for the Inverse Identification of Constitutive Material Parameters applied in Metal Cutting Simulations. Procedia CIRP 82 (2019) 95-100.

Measurement values and adjustable parameters

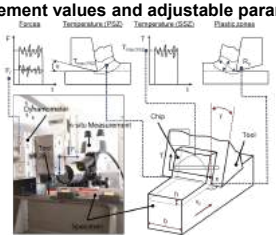

- Patented test bench for tests in orthogonal cutting as the basis for in situ determination of different measurement parameters
- Influence of: Cutting edge prepared tools (rounding, chamfer), wear protection layers, tool geometries, chip guide geometries
- Determination of: Cutting forces (dynamometer), temperatures in the primary and secondary shear zone (thermographic camera, pyrometer), strain rate in the primary shear zone, chip formation (high speed camera)

Experimental investigations

Experimental results – sharp tools

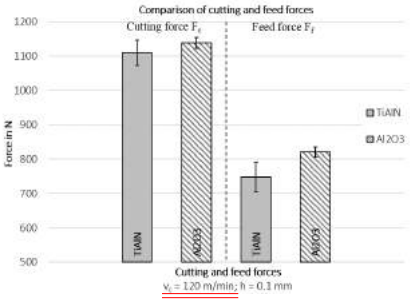

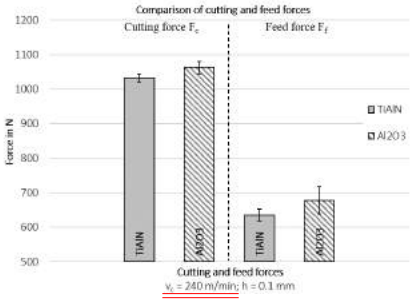

Conclusion: The mulitlayer-coating TiN-TiCN-Al_2O_3 leads to higher forces at both conditions. The difference in the cutting forces is smaller than in the feed forces for both conditions.

Experimental investigations

Influence of coatings on worn tools:

- To investigate the influence of friction in more detail, the coated indexable inserts were pre-worn using a grooving process
- Each insert was removed from the process after every 13 m length of cut and optically analysed by using a digital microscope
- Based on the optical measurement, two wear conditions were defined

Wear conditions:

- Primary wear occured on the rake face
- Small breakouts on the cutting edge
- TiN-TiCN-Al_2O_3 shows more material adhesion and breakouts

Coating **TiAlN**

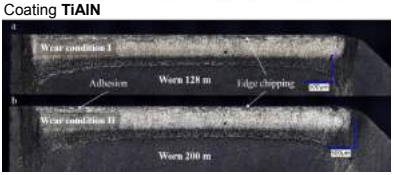

Coating **TiN-TiCN-Al_2O_3**

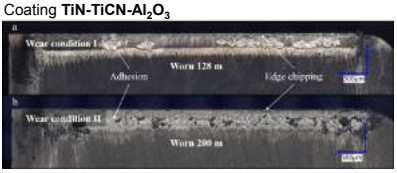

(a) Wear on the rake face after 128 m (wear condition I);
(b) Wear on the rake face after 200 m (wear condition II)

Experimental investigations

Experimental results – worn tools

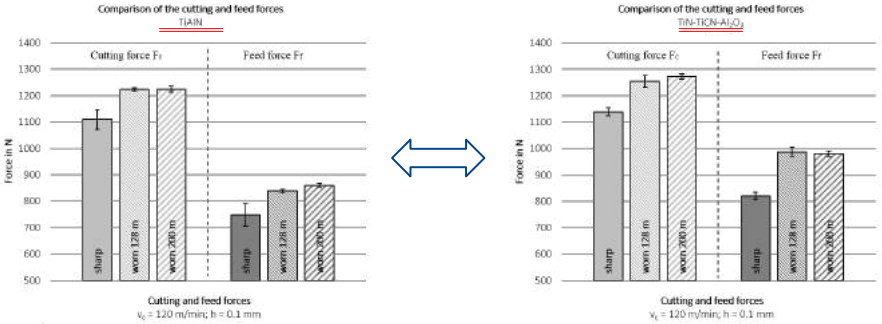

Conclusion: The pre-wear of the inserts leads to an increase in the cutting and feed force. The multilayer-coating TiN-TiCN-Al_2O_3 tends to higher feed forces.

Analytical analysis

Shear plane model according to Merchant

- The linear-orthogonal cutting tests allow the use of analytical relations derived from mechanistic models of orthogonal cutting
- Because experiment and model are close to each other, it is assumed that the basic relationships that Merchant derived for orthogonal cutting are valid
- In this way the shear flow stress and the friction angle in the primary and secondary shear zone were derived from the experimental results

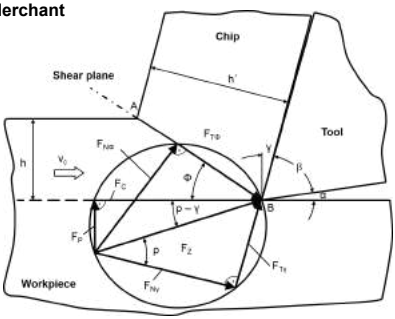

Source: Merchant ME. Mechanics of the Metal Cutting Process. I. Orthogonal Cutting and a Type 2 Chip.

Friction angle

$$\rho = tan^{-1}\left(\frac{F_f}{F_c}\right) + \gamma$$

Shear angle

$$tan\ \phi = \frac{cos\ \gamma}{\frac{h'}{h} - sin\ \gamma}$$

Shear flow stress

$$\tau_{AB} = \frac{\left(F_c * cos\ \phi - F_f * sin\ \phi\right) * sin\ \phi}{h * a_e}$$

Analytical analysis

Comparison of shear flow stress

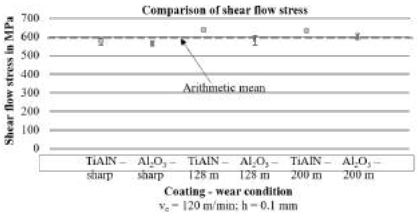

- Shear flow stress is comparable for almost all conditions
- This denotes that the deformation conditions in the primary shear zone were almost constant

Comparison of friction angle

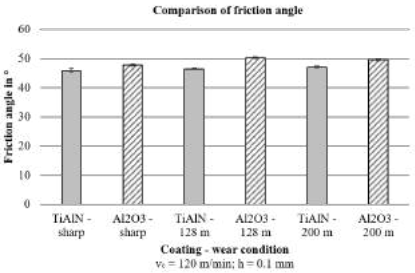

- Multilayer-coating TiN-TiCN-Al_2O_3 tends to the highest friction angle at all wear conditions
- Increase in wear leads to slightly higher friction angles

Conclusion and outlook

Conclusion

- Experimental analyses were carried out by using two different hard coatings (TiAlN and TiN-TiCN-Al_2O_3)
- Monolayer-coating TiAlN shows a slightly lower thermal conductivity
- Multilayer-coating leads to higher cutting and feed forces → differences in the forces were not caused by the deformation in the primary shear zone (nearly constant shear flow stress)
- Multilayer-coating leads to higher friction in the secondary shear zone
  - → lower thermal conductivity of the monolayer coating provides a higher thermal barrier and deflects more heat into the chip
  - → higher temperature in the secondary shear zone seems to reduce the friction effects

Outlook

- Determination of ploughing force due to the cutting edge roundness
- Influence of the coatings on the friction in the secondary shear zone (SSZ) → Temperature measurements with thermographic camera and pyrometer
- Surface analyses
- Numerical simulations

Influence of coatings on SSZ

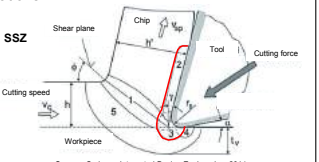

Source: Springer; Integrated Design Engineering, 2014

Rheinische Fachhochschule Köln

University of Applied Sciences

Thank you for your attention

iWFT
Institut für Werkzeug- und Fertigungstechnik
Prof. Dr.-Ing. M. Reuber
Prof. Dr.-Ing. W. Saxler

MIC2020

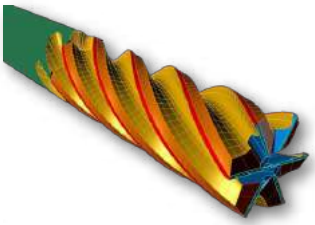

Ante Glavas, Benedikt Thimm, Tamara Teppernegg, Christoph Czettl

PZH Hannover, 02.12.2020

Development of a process-oriented tribological test rig for the performance assesment of tool coatings in turning of titanium Ti6Al4V

Petter Ploog,
Research Assistant,
TU Hamburg

Institute of Production Management and Technology

TUHH
Hamburg University of Technology

Machining Innovations Conference, Hanover, 02.12.2020

Development of a process-oriented tribological test rig for the performance assesment of tool coatings in turning of titanium Ti6Al4V

P. Ploog, W. Hintze, M. Bluehm, C. Möller

Funded by DFG Deutsche Forschungsgemeinschaft

MIC 2020
Turning of Ti6Al4V

Semi-finished Titanium

- high cutting temperatur
- high tool wear
- low removal rates

Turning Process

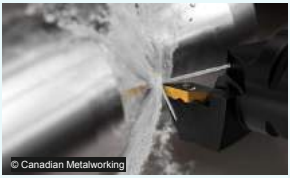

Finished Ti6Al4V Parts

Temperature active coatings

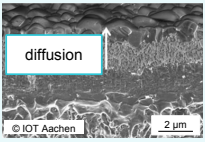

MIC 2020

Tribological Tests

Conventional Pin on Disk Test (POD-Test)

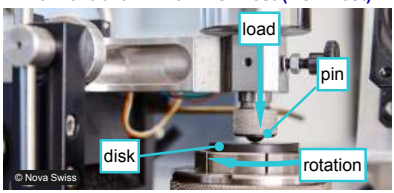

Standard: DIN 50324 / ASTMG99-17

- low temperatures in friction zone (no temperature gradient)
- closed friction system
- no temperature measurement in the contact zone
- pin consists of material to be machined
- disk is coated with coating to be tested

Temperatures during Turning

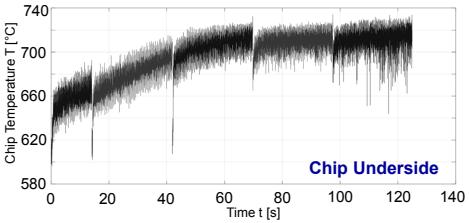

Cutting Insert

CNGP120408 (HW-K10)

Tool: HW-K10, CNGP 120408, α_{eff} = 6°, γ_{eff} = 2°, κ_r = 95°, r_β = 6+2 µm

Process parameters: a_p = 1.2 mm, f = 0.12 mm, v_c = 80 m/min, no coolant

MIC 2020

Proposed Experimental Rig for Open Friction Tests

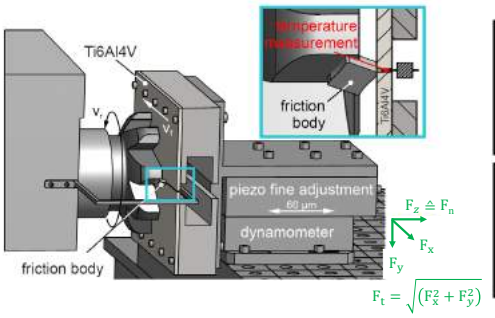

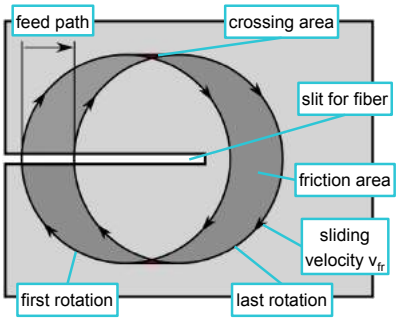

- open friction system (cycloid tool path)
- temperature measurement in the contact zone through two-colour pyrometer with high sample rate
- thermo-mechanical load adjustable to match either turning tool loads on rake- or clearance face respectively
- real cutting-tool replaces the pin from the classic POD tests
- piezo fine adjustment for constant normal forces F_n

MIC 2020

Derivation of Friction Test Conditions (1/2): Turning Experiments

Assumption of a sharp cutting edge i.e. cutting corner radius (r_β) ≪ chip thickness (h)

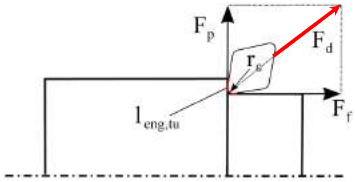

$$F_d = \sqrt{(F_p^2 + F_f^2)}$$

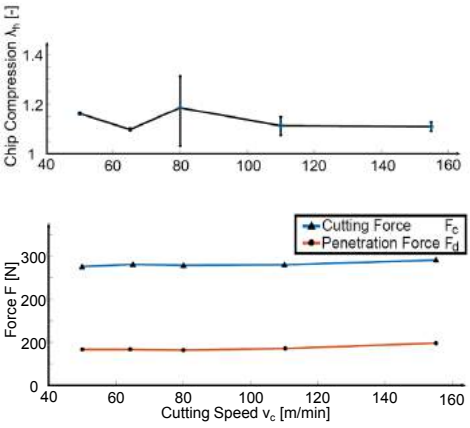

Tool: HW-K10, CNGP 120408, α_{eff} = 6°, γ_{eff} = 2°, κ_r = 95°, r_β = 6+2 µm

Process parameters: a_p = 1.2 mm, f = 0.12 mm, 65 m/min ≤ v_c ≤ 155 m/min, coolant

MIC 2020

Derivation of Friction Test Conditions (2/2): Force Separation

- Friction tests: mechanical load is set in terms of normal force $F_{n,fr}$ (to be determined)
- Determination of normal forces occuring on rake ($F_{n\gamma}$) and clearance face ($F_{n\alpha}$) during turning:

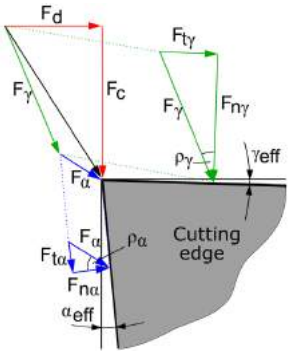

$$\vec{F}_c + \vec{F}_d = \vec{F}_{t\gamma} + \vec{F}_{n\gamma} + \vec{F}_{t\alpha} + \vec{F}_{n\alpha}$$

$$\rho_\gamma = \tan^{-1}(\mu_\gamma) = \tan^{-1}(F_{t\gamma}/F_{n\gamma})$$

$$\rho_\alpha = \tan^{-1}(\mu_\alpha) = \tan^{-1}(F_{t\alpha}/F_{n\alpha})$$

Input values

Values from turning process

Coefficients of friction for carbide & titanium

To be determined

Mechanical loads for friciton test

Normal forces to be set during friction tests: (assumed: $\mu_\alpha = \mu_\gamma = 0.2$)

$F_{n,\alpha}$ = 50 N

$F_{n,\gamma}$ = 287 N

MIC 2020

Experimental Setup of Tribological Tests on Fooke Endura 711 Linear

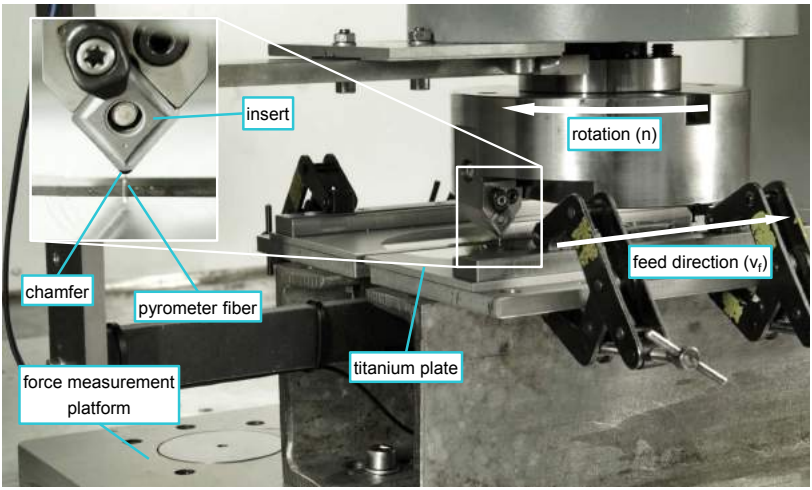

MIC 2020

Experimental Setup of Tribological Tests – Detail of Friction Zone

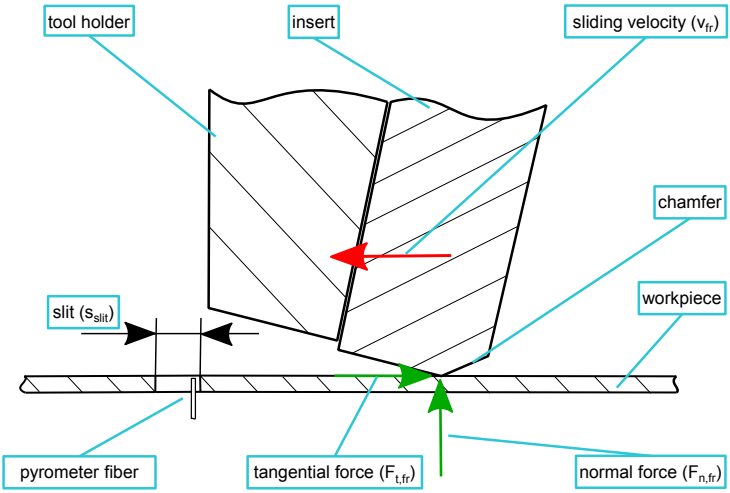

MIC 2020

Results and Discussion of Friction Tests – Tool Contact Length

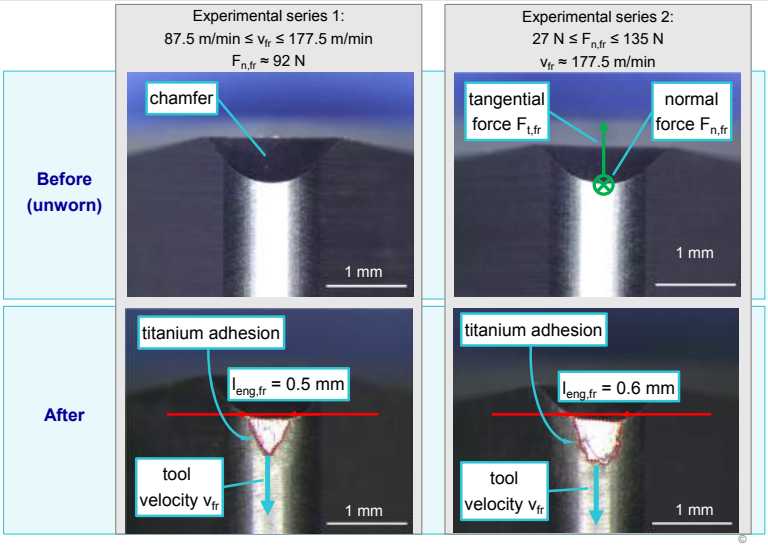

MIC 2020

Results and Discussion of Friction Tests – Thermal Loads

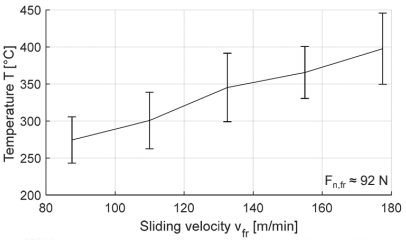

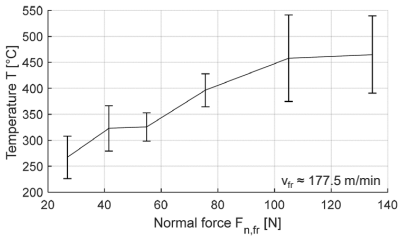

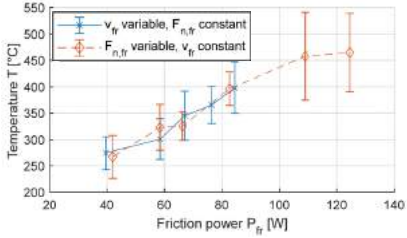

- Constantly rising temperatures with increasing sliding velocites v_{fr} and increasing $F_{n,fr}$
- Temperature depends mainly on friction power ($P_{fr} = F_{t,fr} \cdot v_{fr}$), which can be varied via v_{fr} or $F_{n,fr}$

Tool: HW-K10, CNGP 120408, α_{eff} = 38°, γ_{eff} = -38°

Parameters: 87.5 m/min ≤ v_{fr} ≤ 177.5 m/min, 27 N ≤ $F_{n,fr}$ ≤ 135 N, no coolant, path-controlled

MIC 2020

Results and Discussion of Friction Tests – Mechanical Loads

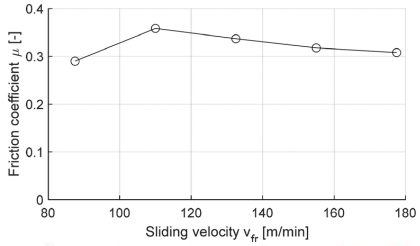

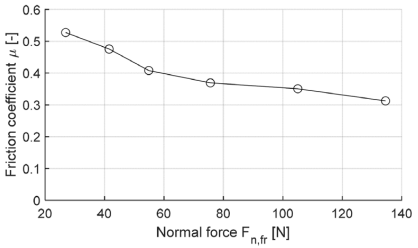

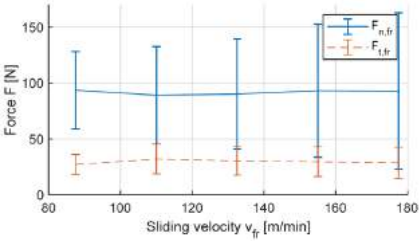

- Nearly constant friction coefficient μ for different sliding velocities v_{fr}
- Decreasing friction coefficient μ with increasing normal force $F_{n,fr}$

Tool: HW-K10, CNGP 120408, α_{eff} = 38°, γ_{eff} = -38°

Parameters: 87.5 m/min ≤ v_{fr} ≤ 177.5 m/min, 27 N ≤ $F_{n,fr}$ ≤ 135 N, no coolant, path-controlled

MIC 2020

Conclusion

- Presentation of a novel tribological test rig.
- Friction tests under realistic thermo-mechanical loads.
- Temperature depends mainly on the friction power P_{fr}.
- Further tests at higher sliding velocities should therefore be conducted to increase temperatures.
- Cutting tests could also be conducted on the test rig by simply reversing the direction of the rotation to increase temperature.

Funded by DFG Deutsche Forschungsgemeinschaft

Project: "Untersuchung temperaturaktiver, reibungsmindernder Schichtsysteme für die Drehbearbeitung von Titanlegierungen"
Project Number: 422345568 (GZ: HI 843/10-1)

MIC 2020
Contact

Thank you for your kind attention

Petter Ploog, M. Sc.
Reserch Assosiate
040 42 878 2820
petter.ploog@tuhh.de

Prof. Dr.-Ing. Wolfgang Hintze
Head of Production Technology
040 42 878 3051
w.hintze@tuhh.de

Institute of Production Management and Technology
Hamburg University of Technology
Denickestraße 17, 21073 Hamburg
www.tuhh.de/ipmt

MIC 2020
Confidential and proprietary document

Session 2 - Additive Manufacturing and Machining Innovations

IChallenges and innvative solutions in additive multi-material processing in the fields of powder, sensor integration and powder application systems

Julia Förster,
Research Assistant,
Fraunhofer IGCV

CHALLENGES AND INNOVATIVE SOLUTIONS IN ADDITIVE MULTI-MATERIAL PROCESSING IN THE FIELDS OF POWDER, SENSOR INTEGRATION AND POWDER APPLICATION SYSTEMS

Julia Förster, Maximilian Binder, Max Horn
Machining Innovations Conference Garbsen, December 02nd 2020

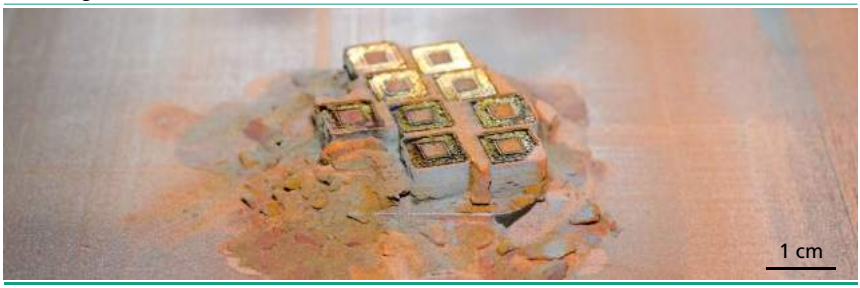

Fraunhofer IGCV

Agenda

1. Fraunhofer IGCV and the Multimaterial Center Augsburg
2. Multi-material laser beam melting process
3. Potentials and challenges
4. Summary and outlook

Fraunhofer IGCV

Agenda

1. **Fraunhofer IGCV and the Multimaterial Center Augsburg**
2. **Multi-material laser beam melting process**
3. **Potentials and challenges**
4. **Summary and outlook**

Fraunhofer IGCV

Together with the iwb of the TUM, 16 industrial-grade additive machines are operated in the community laboratory "AMLab".

Metal Working Systems

- Aconity One
  Ø 400 mm x 400 mm³
- EOS M290
  250 x 250 x 325 mm³
- EOS M400
  400 x 400 x 400 mm³
- Concept Laser M1 Cusing
  150 x 150 x 250 mm³
- SLM Solutions 125 HL
  125 x 125 x 125 mm³
- SLM Solutions 250 HL
  250 x 250 x 350 mm³
- Trumpf TruPrint 1000 GREEN
  Ø100 x 100 mm³
- Trumpf TruPrint 2000 Dual
  Ø200 x 100 mm³
- 14-Axes High-Pressure Cold Spray System
- 2 Wire-arc DED

Directed Energy Deposition (DED)

Plastic- / Sand Processing Systems

- Voxeljet VX1000
  1000 x 600 x 500 mm³
- Voxeljet VXC800
  800 x 500 x continuous
- Voxeljet VX500
  500 x 400 x 300 mm³
- Voxeljet Testachse
  110 x 250 x 95 mm³
- EOS Formiga P100
  200 x 250 x 330 mm³
- Stratasys F270
  305 x 254 x 305 mm³
- 3D Systems ProJet HD3000
  298 x 185 x 203 mm³
- Markforged Marc Two
  575 x 332 x 360 mm³
- RepRap X400 Pro V3
  390 x 400 x 330 mm³
- Sintratec Kit, Zortrax M300 Ultimaker 3 (3 pieces), Makerbots (15 pieces)

Prototyping-Systems

https://www.amlab.de/

4

AMLab iwb TUM Fraunhofer IGCV

The Multimaterial Center Augsburg is one of the largest additive manufacturing projects in Europe.

Goal	Additive manufacturing of mechatronic multi-material components
Budget	10 Technology projects with direct funding volume of 10 M. Euro, Total volume approx. 20 M. Euro
Technology	Focused technologies: Laser beam melting and cold gas spraying
Focus	Thematic Focus: Process Development, Product Development, Additive Production
Time	07/'17 — Today — 06/'22

Projektbeirat

Illustration of the project goal

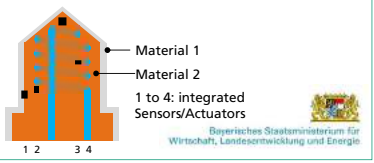

Fraunhofer IGCV

Agenda

1. Fraunhofer IGCV and the Multimaterial Center Augsburg
2. Multi-material laser beam melting process
3. Potentials and challenges
4. Summary and outlook

Fraunhofer IGCV

3-D multimaterial laser beam melting makes it possible to combine properties of different materials with each other in a targeted manner.

Material	Properties
Ti6Al4V	Biocompatibility Corrosion Resistance Specific Strength
CuCr1Zr	**Thermal Conductivity** Electrical Conductivity Ductility
AlSi10Mg	Specific Strength Electrical Conductivity
Ta	Osseointegration Biocompatibility
1.2709	Strength Hardness
…	…

Injection mould study in half-cut

Properties	Material
Biocompatibility Corrosion Resistance Specific Strength	Ti6Al4V
Thermal Conductivity Electrical Conductivity Ductility	CuCr1Zr
Specific Strength Electrical Conductivity	AlSi10Mg
Osseointegration Biocompatibility	Ta
Strength Hardness	**1.2709**
…	…

Image Source: Fraunhofer IGCV

Fraunhofer IGCV

Based on the presented findings, 3-D multi-material components can be manufactured at Fraunhofer IGCV.

Injector nozzle

3D-multimaterial-component

Fraunhofer IGCV

Agenda

1 Fraunhofer IGCV and the Multimaterial Center Augsburg
2 Multi-material laser beam melting process
3 Potentials and challenges
- 3.1 Sensor integration
- 3.2 Powder separation
- 3.3 Powder Application

4 Summary and Outlook

Fraunhofer IGCV

Agenda

1 Fraunhofer IGCV and the Multimaterial Center Augsburg
2 Multi-material laser beam melting process
3 Potentials and challenges
- 3.1 Sensor integration
- 3.2 Powder separation
- 3.3 Powder Application

4 Summary and Outlook

Fraunhofer IGCV

Implementation of sensors in AM components
Goal, motivation and implementation

Goal

Automated integration of sensors during the production of metallic components using PBF/LB-M

Motivation

- Automated production of sensor-monitored components
- Protection of the sensor through complete encapsulation
- Layer-by-layer structure allows integration at any time in the process at any point in the component
- Sensor-adapted enclosure can be produced directly

Implementation

- Interruption of the additive manufacturing process
- Removal of powder from cavity
- Inserting and wiring the sensor
- Resumption of the additive manufacturing process

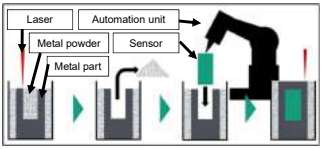

Fig.1: Concept for sensor integration

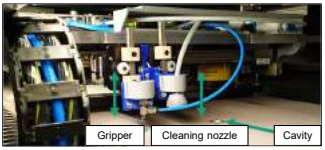

Fig.2: Automation unit for sensor integration

Fraunhofer IGCV

Implementation of sensors in AM components
Integration of weldable strain gauges

Strain gauge interated in tension rod (AlSi10Mg)

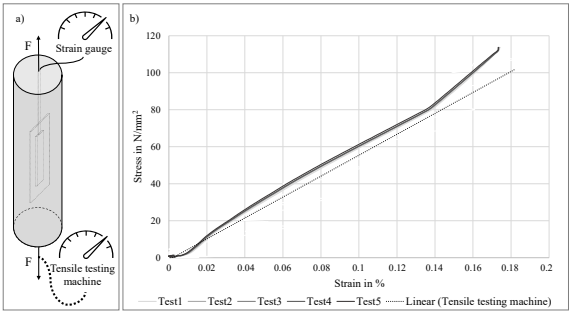

Application (IN718)

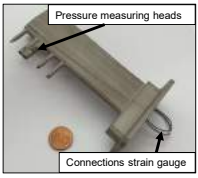

Fig.1: Rake of the company Vectoflow with integrated strain gauge

Fraunhofer IGCV

Agenda

Fraunhofer IGCV

Main challenge of multi-material PBF-LB powder process chain
Intermixture of processed materials

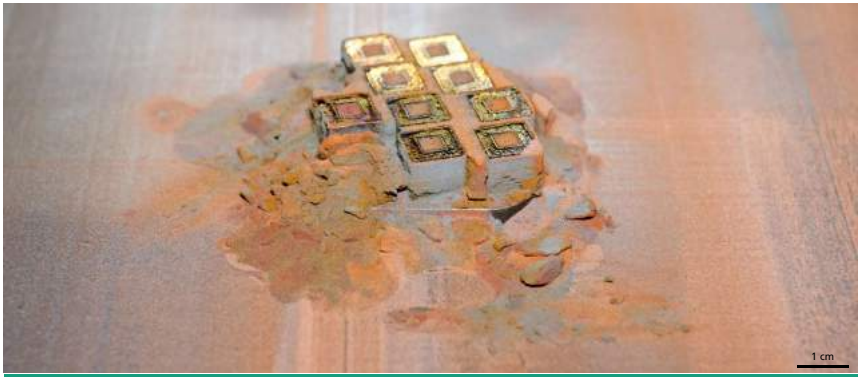

Fraunhofer IGCV

Criticality of foreign particles on part quality
Exemplary results for CW106C particles in 2.4668 (Inconel® 718)

Application[1]

Exemplary application: bi-metal rocket engine produced via Directed Energy Deposition by Launcher[1]

Cu- and Ni-base alloys are a relevant multi-material combination for aerospace applications.

Foreign particle induced defects

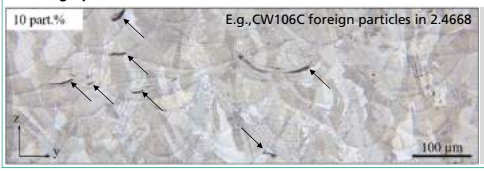

Foreign particles remaining in the powder material after reconditioning can lead to structural defects.

Influence of defects on part performance

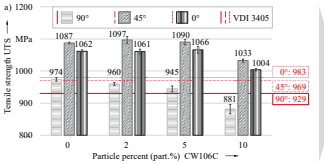

- Criticality of foreign particles and definition of thresholds are relevant research topics in multi-material PBF-LB
- E.g., up to 2 part.% CW106C in 2.4668 are tolerable in terms of static tensile strength.

[1]Image source: engineering.com

Fraunhofer IGCV

Agenda

Fraunhofer IGCV

Electrophotographic Powder Application for Laser Beam Melting
Potentials of Electrophotographic Powder Application for LPBF

Potentials

- Application speed and accuracy of a laser printer
- Independence from the flowability of the powder
- Expansion of the applicable particle spectrum
- Combination of a planar and selective application mechanism

Improvable* part quality through more precise powder application, higher resolution and increased build rate

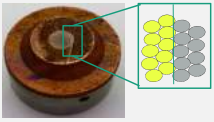

Processing of non-spherical powders as well as fine particles and particle size distributions possible

Switching between selective and planar powder application as well as multi-material processing for more than two materials with one mechanism possible

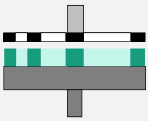

* Compared to nozzle- or blade-based application systems in the LPBF

Fraunhofer IGCV

Aspects of Developing a Powder Application Module based on Electrophotography for Additive Powder Bed based Processes

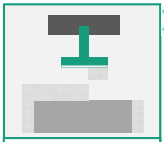

Powder Application by Electrophotography

1 **Charge generation**

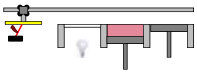

2 **Exposure**

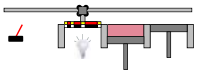

3 **Powder attraction**

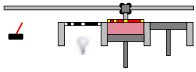

4 **Powder deposition**

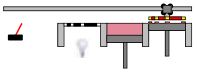

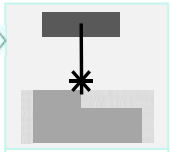

Solidification by Laser Beam Melting

Experimental investigations show the transferability of the electrophotographic principle to powder application in laser beam melting

Fraunhofer IGCV

Agenda

1. Fraunhofer IGCV and the Multimaterial Center Augsburg
2. Multi-material laser beam melting process
3. Potentials and challenges
4. Summary and Outlook

Fraunhofer IGCV

Summary and Outlook
Thank You Very Much for Your Attention.

Summary

- Multimaterial processing offers great potential for additive manufacturing
- **Sensor integration:** Successful integration of strain gauge into LPBF-tension rod
- **Powder separation:** Up to 2 particle percent of CW106C particles in Inconel 718 can be tolerated
- **Electrophotographic powder application**: Photoconductor is chargeable under LPBF-conditions

Outlook

- **Sensor integration**: Influence of process interruption with other materials and process parameters
- **Powder separation**: Influence of powder contamination needs individual case studies for specific applications and the considered material combinations
- **Electrophotographic powder application**: Further investigations to complete the process and implementation to LPBF-machine

I Look Forward to Your Questions and Comments!

M.Sc. Julia Förster
Research associate | Materials and Processes

Fraunhofer Institute for Casting, Composite and Processing Technology IGCV
Am Technologiezentrum 10 | 86159 Augsburg
Phone +49 821 90678-321 Fax -199

Julia.Foerster@igcv.fraunhofer.de
www.igcv.fraunhofer.de

Fraunhofer IGCV

Cryogenically Applied Support and Damping Structures for Chatter Suppression in the Machining of Thin-Walled Components

Eva Jaeger,
Research Assistant,
TU Dortmund

technische universität dortmund

MIC2020
20th Machining Innovations Conference for Aerospace Industry

ISF

Cryogenically Applied Support and Damping Structures for Chatter Suppression in the Machining of Thin-Walled Components

Eva Jaeger, Jonas Baumann, Dirk Biermann

Chatter suppression in the machining of thin-walled components

ISF

- Challenges in the aerospace industry
  - Increasing demand for lightweight and highly stressable components with complex geometries
  - Continuous increase of the chip removal volume under the boundary conditions of a production accuracy and quality
  - Dynamic effects cause undesired periodic relative movements between tool and workpiece (chatter oscillations)

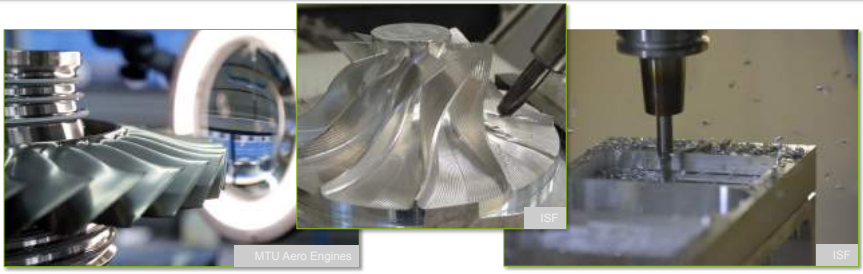

Influencing factors of process stability

Objective	Process stabilization				
Influencing factors [Munoa et al. 2016]	Structural stiffness enhancement	Structural damping enhancement	Regeneration disturbance	Process damping enhancement	Process parameter selection

Jaeger et al.

3

Cryogenically applied support and damping structures

Objective	Process stabilization				
Influencing factors [Munoa et al. 2016]	Structural stiffness enhancement	Process parameter selection	Regeneration disturbance	Process damping enhancement	Structural damping enhancement
Potential for influence	Support structures				Damping elements
Approach	Printed structures				Glued on masses

Jaeger et al.

Cryogenically applied support and damping structures

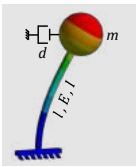

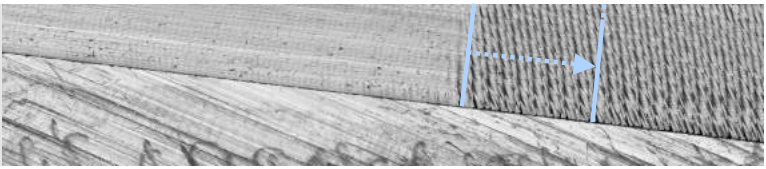

Objective	**Process stabilization**		
Influencing factors [Munoa et al. 2016]	Structural stiffness enhancement		Structural damping enhancement
Potential for influence	Support structures		Damping elements
Approach	**Cryogenically Applied Support and Damping Structures**		

Jaeger et al.

Experimental Setup and Procedure

- Procedure:
  - Spraying of a pressurized mixture of CO_2 and ice medium ($\dot{V}_{pump}$ = 10 ml/min)
  - Expansion at the nozzle, resulting in a temperature drop (Joule-Thomson effect, T = -79 °C)
  - Manual sprayed ice medium is fed into the snow jet externally ($\dot{V}_{man}$ = 54 ml/min)
- Operation modes:
  - I Cooling of the specimen by expanding CO_2
  - II Well adhering layer of ice
  - III Application of finer sprayed snow
- Measurement equipment:
  - Experimental modal analysis and FRF (*B&K* impulse hammer type *8204; M-E* laser triangulation sensor type *ILD2310-10*)
  - Air transmitted acoustic emissions (*Tascam* type *DR-40*)

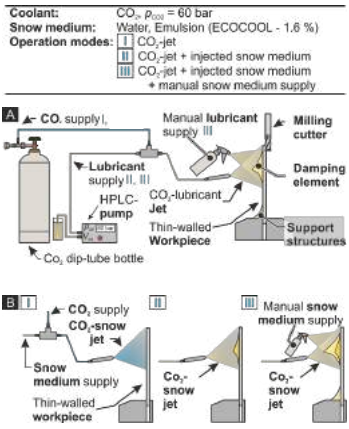

Jaeger et al. 6

Experimental Setup

ISF

Machine tool: Röders TEC 1000 **Workpiece:** EN AW-7075 (d = 3 mm, h = 45 mm, b = 50 mm)
Coolant: Liquid CO_2, $p \approx 60$ bar **Snow and ice medium:** Water and emulsion (ECOCOOL – 1.6%)
Operation modes: I : CO_2 (10s) II : CO_2 + lubricant through jet (10s) III : CO_2 + lubricant through jet + manual lub. (70s)

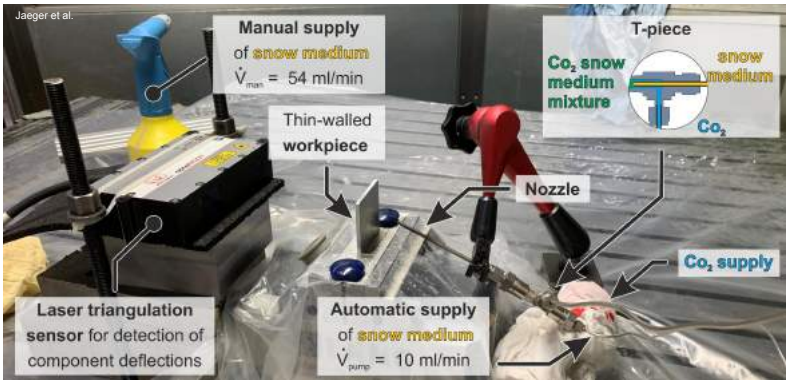

7

Cryogenic application of support and damping structures

ISF

Machine tool: Röders TEC 1000 **Workpiece:** EN AW-7075 (d = 3 mm, h = 45 mm, b = 50 mm)
Coolant: Liquid CO_2, $p \approx 60$ bar **Snow and ice medium:** Water and emulsion (ECOCOOL – 1.6%)
Operation modes: I : CO_2 (10s) II : CO_2 + lubricant through jet (10s) III : CO_2 + lubricant through jet + manual lub. (70s)

Light ice structure

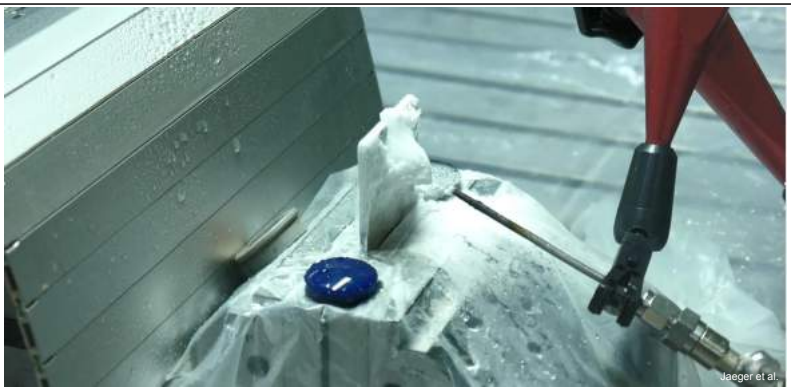

Dynamic behaviour of the workpiece

Machine tool: Röders TEC 1000 **Workpiece:** EN AW-7075 (d = 3 mm, h = 45 mm, b = 50 mm)
Coolant: Liquid CO_2, $p \approx 60$ bar **Snow and ice medium:** Water and Emulsion (ECOCOOL – 1.6%)
Operation modes: I : CO_2 II : CO_2 + lubricant through jet III : CO_2 + lubricant through jet + manual lub.

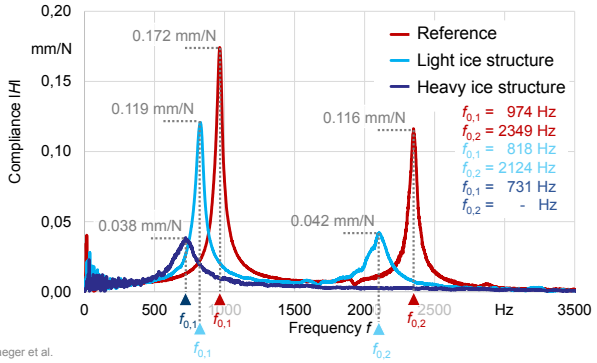

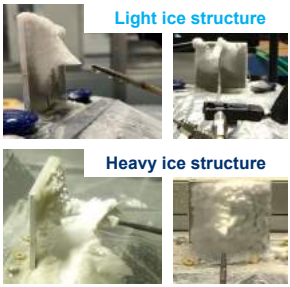

Jaeger et al. 9

Process design for the experimental evaluation

Simulation: **Workpiece:** EN AW-7075 (specific cutting force parameters)
Machining strategy: Down-milling **Spindel speed:** n = 4 000 - 20 000 min-1
Machining parameters: a_e = 1 mm ; z = 4 ; f_z = 0.05 mm

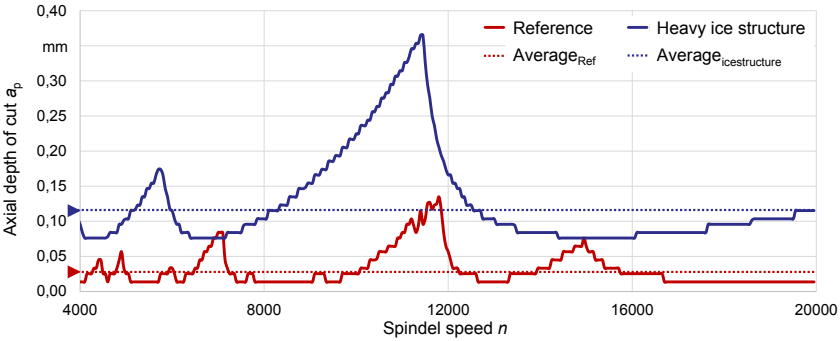

Jaeger et al. 8

Process design for the experimental evaluation

Simulation:
Machining strategy: Down-milling
Machining parameters: a_e = 1 mm ; z = 4 ; f_z = 0.05 mm

Workpiece: EN AW-7075 (specific cutting force parameters)
Spindel speed: n = 4 000 - 20 000 min-1

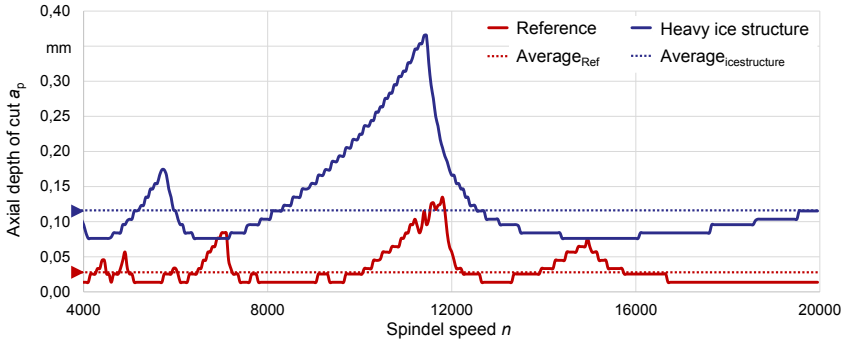

Jaeger et al. 8

Dynamic behaviour of the workpiece during milling

Machine tool: Röders TEC 1000
Milling tool: Gühring HSS end-mill (d = 8 mm, z = 4)
Coolant: Liquid CO_2, $p \approx 60$ bar
Operation modes: I : CO_2 II : CO_2 + lubricant through jet III : CO_2 + lubricant through jet + manual lub.

Workpiece: EN AW-7075 (d = 3 mm, h = 45 mm, b = 50 mm)
Process: n = 15 000 min^{-1}, f_z = 0.05 mm, a_e = 1 mm, a_p = 1 mm
Snow and ice medium: Emulsion (ECOCOOL – 1.6%)

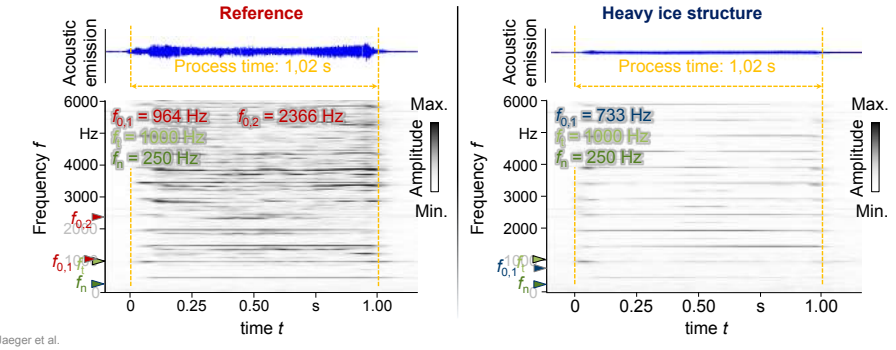

Jaeger et al. 12

Dynamic behaviour of the workpiece during milling

Machine tool: Röders TEC 1000
Milling tool: Gühring HSS end-mill (d = 8 mm, z = 4)
Coolant: Liquid CO_2, $p \approx 60$ bar
Operation modes: I : CO_2 (10s) II : CO_2 + lubricant through jet (10s) III : CO_2 + lubricant through jet + manual lub. (70s)

Workpiece: EN AW-7075 (d = 3 mm, h = 45 mm, b = 50 mm)
Process: n = 15 000 min^{-1}, f_z = 0.05 mm, a_e = 1 mm, a_p = 1 mm
Snow and ice medium: Emulsion (ECOCOOL – 1.6%)

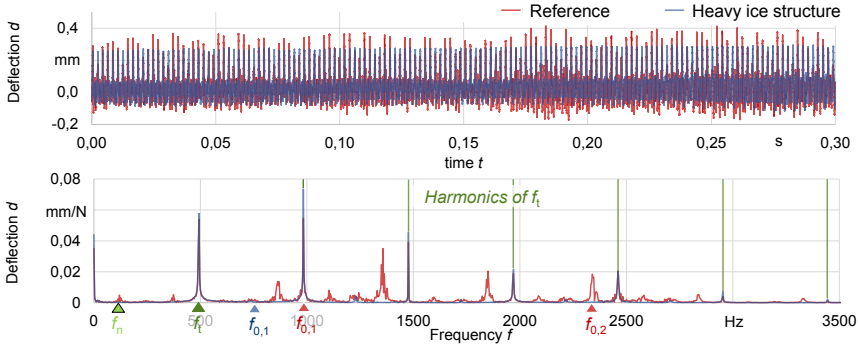

Conclusion and Prospects

- Conclusion:
  - Significant reduction of the compliance
  - Applied snow and ice elements melt off
  - Simple integration into existing machine concepts
- Prospects
  - Acquisition of fundamental knowledge
  - Production strategies for the generation of hybrid ice structures
  - Investigation of the influence of temperature on geometric deviations
  - Transfer to the application of more complex geometries

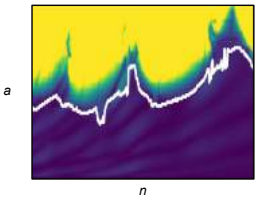

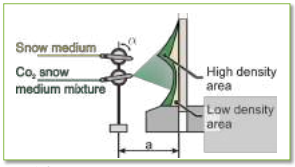

technische universität dortmund

MIC2020 20th Machining Innovations Conference for Aerospace Industry

ISF

Thank you for your kind attention!

Institute of Machining Technology
Baroper Str. 303
44227 Dortmund
Germany
www.isf.de
eva.jaeger@tu-dortmund.de

References

[Fraunhofer IPT] Nadine Winkelmann. Additive Manufacturing of Engine Components for Aviation https://www.springerprofessional.de/production---production-technology/basic-technologies/additive-manufacturing-of-engine-components-for-aviation/17033282. Accessed 27 October 2020.

[IFQ] Möhring, H.-C. ; Wiederkehr, P.; Baumann, J.; König, A.; Spieker, C.; Müller, M. Intelligent hybrid material slide component for machine tools. Journal of Machine Engineering, 17 (2017) 1, S. 17-30, ISSN 1895-7595 (Print), 2391-8071 (Online)

[Munoa et al. 2016] Munoa J, Beudaert X, Dombovari Z, Altintas Y, Budak E, Brecher C et al. Chatter suppression techniques in metal cutting. CIRP Annals - Manufacturing Technology 2016;65(2):785–808.

[Wan et al. 2018] Wan M, Dang X-B, Zhang W-H, Yang Y. Optimization and improvement of stable processing condition by attaching additional masses for milling of thin-walled workpiece. Mechanical Systems and Signal Processing 2018;103:196–215.

Near-net-shape trimming process by abrasive water jet cutting of high-performance workpieces for the aerospace industry

Robert Jaczkowski,
Research Assistant,
TU Berlin

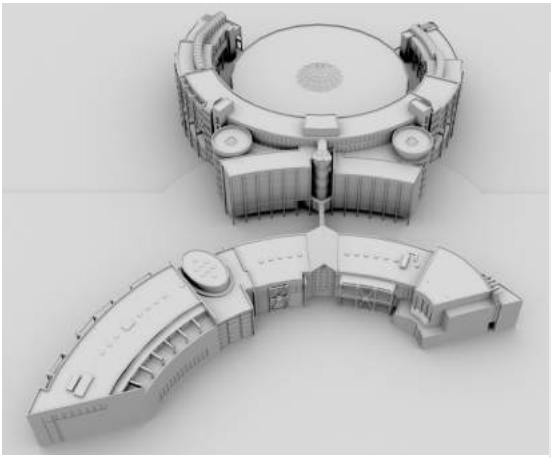

MIC2020 – December 2nd 2020

Near-net-shape trimming process by abrasive water jet cutting of high-performance workpieces for the aerospace industry

Waldemar Reder, M.Sc.

Technische Universität Berlin
Institute for Machine Tools and Factory Management (IWF)
Prof. Dr. h. c. Dr.-Ing. Eckart Uhlmann
Pascalstraße 8-9
10587 Berlin, Germany

Fraunhofer IPK
INSTITUT PRODUKTIONSANLAGEN UND KONSTRUKTIONSTECHNIK

IWF
INSTITUT WERKZEUGMASCHINEN UND FABRIKBETRIEB TECHNISCHE UNIVERSITÄT BERLIN

AGENDA

- Introduction
- Motivation
- Investigation
- Outlook
- Acknowledgment

TV tower Berlin,
Abrasive waterjet turning

Model of PTC Berlin,
Selective laser melting

Fraunhofer IPK
INSTITUT PRODUKTIONSANLAGEN UND KONSTRUKTIONSTECHNIK

IWF
INSTITUT WERKZEUGMASCHINEN UND FABRIKBETRIEB TECHNISCHE UNIVERSITÄT BERLIN

Introduction

The Production Technology Center (PTC) Berlin

Fraunhofer-Gesellschaft
Institute for Production Systems and Design Technology IPK

- **Corporate Management**
  Prof. Dr.-Ing. Holger Kohl
- **Virtual Product Creation**
  Prof. Dr.-Ing. Rainer Stark
- **Production Systems**
  Prof. Dr. h. c. Dr.-Ing. E. Uhlmann
- **Joining and Coating Technology**
  Prof. Dr.-Ing. M. Rethmeier
- **Automation Technology**
  Prof. Dr.-Ing. J. Krüger

Technische Universität Berlin
Institute for Machine Tools and Factory Management IWF

- **Sustainable Corporate Development**
  Prof. Dr.-Ing. Holger Kohl
- **Industrial Information Technology**
  Prof. Dr.-Ing. Rainer Stark
- **Machine Tools and Manufacturing Technology**
  Prof. Dr. h. c. Dr.-Ing. E. Uhlmann
- **Joining Technology**
  Prof. Dr.-Ing. M. Rethmeier
- **Industrial Automation Technology**
  Prof. Dr.-Ing. J. Krüger

Fraunhofer IPK
INSTITUT PRODUKTIONSANLAGEN UND KONSTRUKTIONSTECHNIK

IWF
INSTITUT WERKZEUGMASCHINEN UND FABRIKBETRIEB TECHNISCHE UNIVERSITÄT BERLIN

Introduction

Chair of Machine Tools and Manufacturing Technology

- Jet Machining
  - Close-contoured roughing of hard to machine materials using abrasive waterjet turning
  - Abrasive waterjet controlled depth milling
  - Development of process strategies for cleaning, de-coating, de-burring and pre-treatment of surfaces
  - Development of high-pressure liquid CO_2 jets for machining of hydrophobic materials


Abrasive waterjet turning


Abrasive waterjet milling


Waterjet cleaning


CO_2-cleaning


Liquid CO_2-cutting

Fraunhofer IPK
INSTITUT PRODUKTIONSANLAGEN UND KONSTRUKTIONSTECHNIK

IWF
INSTITUT WERKZEUGMASCHINEN UND FABRIKBETRIEB TECHNISCHE UNIVERSITÄT BERLIN

Motivation

State of the art

- High-performance materials used in aerospace industry lead to high tool wear and long process time in conventional machining
- Abrasive water injector jet cutting (AWIJC) is the most widespread variant of abrasive water cutting technologies
- AWIJC is mainly used for cutting sheet metal
- Benefits of AWIJC
  - Well suited for processing extremely hard materials
  - Characterized by a relatively low tool wear
  - Independent of material being processed

Turbine blades

©Jürgen Sommermeyer

Fraunhofer IPK
INSTITUT PRODUKTIONSANLAGEN UND KONSTRUKTIONSTECHNIK

IWF
INSTITUT WERKZEUGMASCHINEN UND FABRIKBETRIEB TECHNISCHE UNIVERSITÄT BERLIN

Motivation

Goals

- Automated pre-contouring of difficult to machine materials
- Pre-contouring of complex 3D geometries
  - Continuous cutting of outer material segments
  - Stepwise pre-contouring to final geometry
- Extension of machinable component spectrum
- Increasing usability of semi-finished product spectrum with solid bars and profiles

Trimming of a turbine blade using AWIJC

Fraunhofer IPK
INSTITUT PRODUKTIONSANLAGEN UND KONSTRUKTIONSTECHNIK

IWF
INSTITUT WERKZEUGMASCHINEN UND FABRIKBETRIEB TECHNISCHE UNIVERSITÄT BERLIN

Motivation

Systematic approach

- Detailed knowledge of cutting parameters is needed to compensate form and position errors though a corresponding path adaption with CAD-CAM control
- Development of automated trim path generation
- Development of new machine system to position the workpieces freely under the jet

➢ Automated pre-contouring of complex 3D geometries

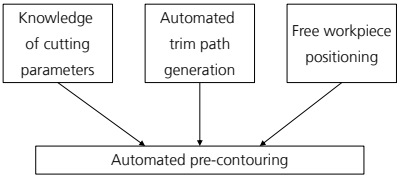

20th Machining Innovations Conference for Aerospace Industry 2020, December 2nd 2020 Page 8

Motivation

Systematic approach

- Detailed knowledge of cutting parameters is needed to compensate form and position errors though a corresponding path adaption with CAD-CAM control
- Development of automated trim path generation
- Development of new machine system to position the workpieces freely under the jet

➢ Automated pre-contouring of complex 3D geometries

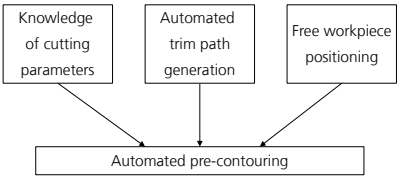

➔ First step is to provide a regression for predicting the shaft diameter of an abrasive water jet turned specimen

Investigation

Materials and methods

- Workpieces
  - Solid round bars with outer diameter of D = 60mm
  - Stainless steel of type X5CrNi18 (EN 1.4301)
- Water jet system based on a six-axis robot manipulator
  - Nozzle diameter d_p = 0.35 mm
  - Focusing tube diameter d_F = 1.02 mm

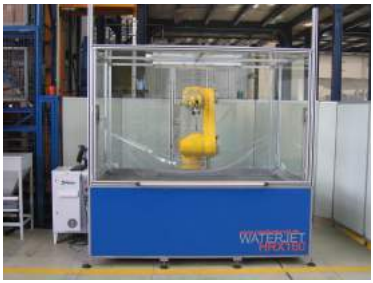

Waterjet HRX 160 with six-axis robot manipulator

Investigation

Materials and methods

- DOE with full factorial design
  - Variation of targeted shaft diameter d_E and volume removal rate VRR

Setting Parameter		Unit	Level of parameter variation		
Shaft diameter	d_E	mm	30	40	50
Volume removal rate	VRR	mm³/min	550	1100	1650
Jet pressure	p_a	MPa		280	
Abrasive flow rate	$\dot{m}_A$	g/min		500	
Rotational speed	n	rpm		20	

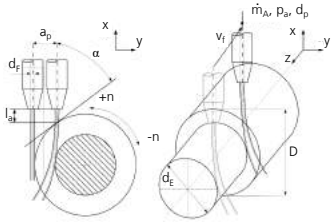

Stainless steel of the type X5CrNi18 (EN 1.4301) machined with AWJC turning

Investigation

Results

- Deviation from shaft diameter Δd_E increases with
  - Decreasing shaft diameter d_E
  - Increasing volume removal rate VRR
- Increasing of VRR leads to increasing waviness of workpiece surface
- Minimum deviation of 0.11 mm could be achieved
- Reduction of VRR leads to increasing machining time

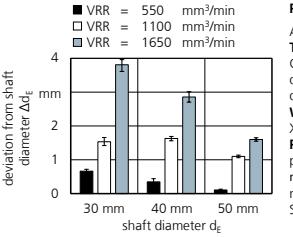

Process:
AWJC
Tools:
GMA Garnet , Mesh 80
d_O = 0.32 mm
d_F = 1.02 mm
Workpiece:
X5CrNi18
Process parameters:
p_a = 280 Mpa
$\dot{m}_A$ = 500 g/min
n = 20 rpm
Synchronous rotation

Fraunhofer IPK
INSTITUT PRODUKTIONSANLAGEN UND KONSTRUKTIONSTECHNIK

IWF
INSTITUT WERKZEUGMASCHINEN UND FABRIKBETRIEB TECHNISCHE UNIVERSITÄT BERLIN

Investigation

Results

- Regression to predict deviation from the targeted shaft diameter d_E:

$$\Delta d_E = -1.315\ \text{mm} + 1.35\cdot10^{-2}\cdot d_E + 5.115\cdot10^{-3}\frac{\text{min}}{\text{mm}^2}\cdot\text{VRR} + 7.5\cdot10^{-5}\frac{\text{min}}{\text{mm}^3}\cdot d_E\cdot\text{VRR}$$

- Accuracy decreases with increasing cutting depth and volume removal rate VRR

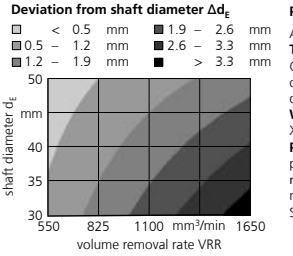

Process:
AWJC
Tools:
GMA Garnet , Mesh 80
d_O = 0.32 mm
d_F = 1.02 mm
Workpiece:
X5CrNi18
Process parameters:
p_a = 280 Mpa
$\dot{m}_A$ = 500 g/min
n = 20 rpm
Synchronous rotation

Fraunhofer IPK
INSTITUT PRODUKTIONSANLAGEN UND KONSTRUKTIONSTECHNIK

IWF
INSTITUT WERKZEUGMASCHINEN UND FABRIKBETRIEB TECHNISCHE UNIVERSITÄT BERLIN

Outlook

- Investigations are the foundation for trimming with new technology
- Influence of process parameters for abrasive waterjet turning identified and transferred into regression
- Further investigations for AWIJC with very flat cutting angles and different techniques for cutting off finished workpieces
- Aim to compensate form and position errors though a corresponding path adaption with CAD-CAM control

Trimming of a turbine blade using AWIJC

Different techniques for cutting off finished workpieces with AWIJC

Fraunhofer IPK
INSTITUT PRODUKTIONSANLAGEN UND KONSTRUKTIONSTECHNIK

IWF
INSTITUT WERKZEUGMASCHINEN UND FABRIKBETRIEB TECHNISCHE UNIVERSITÄT BERLIN

Acknowledgement

- This presentation is based on results acquired in the project ZF4067143LL9, which is kindly supported by the AiF Projekt GmbH.

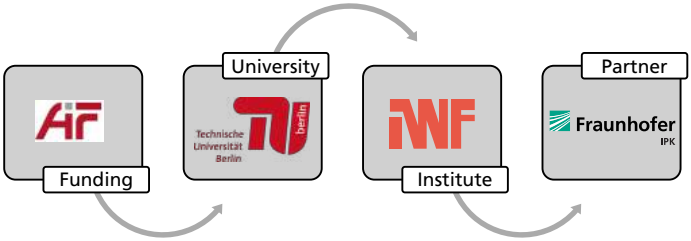

Fraunhofer IPK
INSTITUT PRODUKTIONSANLAGEN UND KONSTRUKTIONSTECHNIK

IWF
INSTITUT WERKZEUGMASCHINEN UND FABRIKBETRIEB TECHNISCHE UNIVERSITÄT BERLIN

Contact Details

Technische Universität Berlin
Institute for Machine Tools and Factory Management (IWF)
Chair of Machine Tools and Manufacturing Technology
Prof. Dr. h. c. Dr.-Ing. Eckart Uhlmann
Office PTZ 1
Pascalstr. 8 - 9
10587 Berlin

Waldemar Reder, M.Sc.
Research Engineer

Phone: +49 30 314 79344
E-Mail: reder@iwf.tu-berlin.de

Fraunhofer IPK
INSTITUT PRODUKTIONSANLAGEN UND KONSTRUKTIONSTECHNIK

IWF
INSTITUT WERKZEUGMASCHINEN UND FABRIKBETRIEB TECHNISCHE UNIVERSITÄT BERLIN

Fundamental study on cutting temperature in high speed cutting of difficult to cut materials

Takashi Ueda,
Research Assistant,
Nagoya University, Japan

MIC2020

Fundamental study on cutting temperature in high speed cutting of difficult-to-cut materials

by
Takashi Ueda, Kensuke Suzuki and Eiji Shamoto

Presenting author: Faculty of Mechanical Engineering, Institute of Science and Engineering, Kanazawa University, Japan.
Email: ueda2004@staff.kanazawa-u.ac.jp

MIC Procedia (2020) 086-092

NAGOYA UNIVERSITY

1

MIC2020

1. Introduction

Back ground:

The equations derived by Kronenberg and Shaw cannot evaluate the influence of thermal properties of cutting tool on the cutting temperature since they do not contain the thermal properties of it.

Main purpose of this paper :

1. We derive the evaluating equation to present the influence of cutting conditions and the thermal properties of the workpiece/tool on the cutting temperature by the dimensional analysis.
2. We carried out the cutting experiments to confirm the propriety of the equation.

NAGOYA UNIVERSITY

2

MIC2020

2. Derivation of evaluating equation by dimensional analysis

We assume that the cutting temperature θ is affected by the physical quantities of total cutting energy Q, volumetric heat capacity ρc, and thermal conductivity λ.
Then, the cutting temperature θ is expressed by the following equation

$$f_1(\theta, Q, \rho c, \lambda) = 0 \qquad (1)$$

where, f_1, f_2, f_3 ・・・ are functions.

NAGOYA UNIVERSITY

MIC2020

2.2.1 Model of interaction region between workpiece and cutting tool

We assume that the cutting region consists of the workpiece region and the cutting tool region, and the chip is regarded as a part of the workpiece.

The cutting energy Q generated in the interaction region is divided roughly into the energy Q_w and the energy Q_t.

Then, the following relation is held.

$$Q = Q_w + Q_t \qquad (2)$$

Q_w: the energy which flows into the workpiece

Q_t : the energy which flows into the cutting tool

When heat partition coefficients of cutting energy are denoted by ξ_w and ξ_t , Q_w and Q_t are given by

$$Q_w = \xi_w Q \ , \quad Q_t = \xi_t Q$$

Substituting these equations into Eq.(2), we get

$$\xi_w + \xi_t = 1 , \qquad (3)$$

where ξ_w and ξ_t are non-dimensional constants.

NAGOYA UNIVERSITY

MIC2020

The volume of metal removed per unit time Z is given by

$$Z = a\, f\, v\,. \tag{4}$$

Using the specific cutting energy *ks*, the total cutting energy Q is expressed by

$$Q = Z\, ks = a\, f\, v\, ks\,. \tag{5}$$

Consequently, Q_w and Q_t are given by

$$Q_w = \xi_w Q \;=\; \xi_w a\, f\, v\, ks, \tag{6}$$

and

$$Q_t = \;\xi_t\, Q = \xi_t a\, f\, v\, ks. \tag{7}$$

NAGOYA UNIVERSITY

MIC2020

2.2.2 Temperature of workpiece-1

Let us consider the cutting temperature of the workpiece θ_w.

θ_w is expressed by this equation.

$$f_2(\,\theta_w\,, Q_w\,, \rho_w c_w\,, \lambda_w) = 0 \tag{8}$$

Q_w : the energy which flows into the workpiece

$\rho_w c_w$: the volumetric heat capacity of the workpiece

λ_w : the thermal conductivity

Substituting $Q_w = \xi_w a\, f\, v\, ks$ into Eq.(8), we get the fundamental equation

$$f_2(\theta_w, v, (a\, f), (\xi_w ks)\,, \rho_w c_w\,, \lambda_w) = 0. \tag{9}$$

Using the dimensional matrix of Eq.(9) and Π(Pi) theorem,

$$f_2(\Pi_1, \Pi_2) = 0, \tag{10}$$

Π_1 and Π_2 are products of dimensionless quantities.

NAGOYA UNIVERSITY

MIC2020

2.2.2 Temperature of workpiece-2

Then, Π_1 is presented by this equation

$$\Pi_1 = \theta_w^{x_1} v^{y_1} (af)^{z_1} (\xi_w ks)^{r_1} (\rho_w c_w) \quad (11)$$

As Π_1 is a dimensionless product,

$$[\Pi_1] = [\ \Theta\ ]^{x_1} [\ L\ T^{-1}]^{y_1} [\ L^2\ ]^{z_1} [\xi\ H\ L^{-3}\ ]^{r_1} [\ H\ L^{-3}\Theta^{-1}\ ] = 0$$

Using this relation, we can get

$$\Pi_1 = \theta_w (\xi_w ks)^{-1} (\rho_w c_w) = \frac{\theta_w (\rho_w c_w)}{\xi_w ks} \quad (12)$$

Applying the same method to Π_2, we get

$$\Pi_2 = \theta_w^{x_2} v^{y_2} (af)^{z_2} (\xi_w ks)^{r_2} \lambda_w. \quad (13)$$

From this equation,

$$\Pi_2 = \theta_w v^{-1} (af)^{-1/2} (\xi_w ks)^{-1} \lambda_w = \frac{\theta_w \lambda_w}{v(af)^{1/2} \xi_w ks} \quad (14)$$

NAGOYA UNIVERSITY

MIC2020

2.2.2 Temperature of workpiece-3

Substituting Π_1 and Π_2 into Eq.(10), we get

$$f_2 \left(\frac{\theta_w (\rho_w c_w)}{\xi_w ks}, \frac{\theta_w \lambda_w}{v(af)^{1/2} \xi_w ks} \right) = 0. \quad (15)$$

From the simplest combination of these two products, we get

$$\theta_w = C_1 \cdot \xi_w ks \frac{v^{1/2} a^{1/4} f^{1/4}}{(\rho_w c_w)^{1/2} \lambda_w^{1/2}}, \quad (16)$$

where C_1 is a dimensionless constant.

NAGOYA UNIVERSITY

MIC2020

2.2.3 Temperature of cutting tool

Then, θ_t is expressed by this equation

$$f_3(\theta_t, Q_t, \rho_t c_t, \lambda_t) = 0 . \quad (17)$$

Q_t : the energy which flows into the cutting tool

$\rho_t c_t$: the volumetric heat capacity of cutting tool

λ_t : the thermal conductivity

Substituting $Q_t = \xi_t a f v ks$ into Equation (17), we get

$$f_3(\theta_t, v, (a f), (\xi_t ks), \rho_t c_t, \lambda_t) = 0 . \quad (18)$$

As a result, the temperature of the cutting tool is expressed by this equation

$$\theta_t = C_2 \cdot \xi_t ks \frac{v^{1/2} a^{1/4} f^{1/4}}{(\rho_t c_t)^{1/2} \lambda_t^{1/2}} , \quad (19)$$

where C_2 is a dimensionless constant.

NAGOYA UNIVERSITY

MIC2020

2.2.4 Evaluating function of cutting temperature

At the interaction region between the workpiece and the cutting tool, we can consider that these two temperatures are equal

$$\theta_w = \theta_t \ (= \theta) \quad (20)$$

Substituting Eqs. (16) and (19) into Eq.(20) and using Eq.(3), we get heat partition coefficients ξ_w and ξ_t,

$$\xi_w = \frac{(\rho_w c_w)^{1/2} \lambda_w^{1/2}}{(\rho_t c_t)^{1/2} \lambda_t^{1/2} + (\rho_w c_w)^{1/2} \lambda_w^{1/2}} , \quad (21)$$

and

$$\xi_t = \frac{(\rho_t c_t)^{1/2} \lambda_t^{1/2}}{(\rho_t c_t)^{1/2} \lambda_t^{1/2} + (\rho_w c_w)^{1/2} \lambda_w^{1/2}} . \quad (22)$$

Consequently, we get the cutting temperature.

$$\theta = C_3 \frac{ks\, a^{1/4} f^{1/4} v^{1/2}}{(\rho_t c_t)^{1/2} \lambda_t^{1/2} + (\rho_w c_w)^{1/2} \lambda_w^{1/2}} , \quad (23)$$

where C_3 is a dimensionless constant.

NAGOYA UNIVERSITY

MIC2020

Simplification of "*ks*"

This figure is the experimental result in this reference.

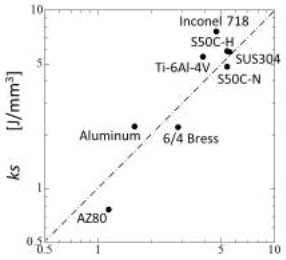

$q_c = \rho_w c_w \theta_m$ [J/mm³]

Fig.12 *ks* – q_c relation

[3] Ueda, T., Hirai, Y., Uto, S., Shamoto, E., Studies on cutting temperature by dimensional analysis, Transactions of the JSME, Vol.85, No.869; 2019.p.1-14.

$q_c = \rho_w c_w \theta_m$

q_c is specific energy which is needed to increase chip temperature to melting point of workpiece material.

From this figure, there is a relation $ks \approx q_c$ in metal turning.

This equation means that a large part of specific cutting energy *ks* is consumed to make the chip.

We assume that $ks \propto q_c \ (= \rho_w c_w \theta_m)$ can be used.

MIC2020

Simplification of "ρc"

Table 2 Physical properties of workpiece material

			Ti-6Al-4V	AISI1050	Inconel718	AISI304
Melting point	θ_m	℃	1660	1400	1300	1410
Thermal conductivity	λ_w	W/(m・K)	7.6	44	11	16
Density	ρ_w	kg/m³	4420	7840	8200	7920
Specific heat	c_w	J/(kg・K)	537	492	440	499
Volumetric heat capacity	$\rho_w c_w$	J/(mm³・K)	0.00237	0.00386	0.00361	0.00395
Thermal diffusivity	$\alpha_w=\lambda_w/\rho_w c_w$	mm²/s	3.20	11.4	3.05	4.05

Table 3 Physical properties of cutting tool

			Al_2O_3 Alumina	WC Carbide	Bi-A Bidemics	Bi-B Bidemics	Bi-C Bidemics
Thermal conductivity	λ_t	W/(m・K)	17	63	58	76	100
Density	ρ_t	kg/m³	4000	14400	12700	14900	15000
Specific heat	c_t	J/(kg・K)	900	200	280	200	200
Volumetric heat capacity	ρc_t	J/(mm³・K)	0.00360	0.00288	0.00356	0.00298	0.00300
Thermal diffusivity	$\alpha=\lambda_t/\rho c_t$	mm²/s	4.72	21.88	16.31	25.50	33.33
HV hardness	HV		1750	1600	2500	2500	2500

The relation $\rho_t c_t / \rho_w c_w \approx 1$ can be used.

MIC2020

Simplification of Eq.(23)

Substituting these relations into Eq.(23), we finally get

$$\frac{\theta}{\theta_m} = C_4 \frac{1}{\alpha_t^{1/2} + \alpha_w^{1/2}} a^{1/4} f^{1/4} v^{1/2} \qquad (24)$$

$\alpha_t = \frac{\lambda_t}{\rho_t c_t}$, $\alpha_w = \frac{\lambda_w}{\rho_w c_w}$: thermal diffusivity

C_4 : dimensionless constant

Equation (24) holds for $\theta \leq \theta_m$

Consequently, from Eq.(24), we can get the information about the influence of cutting conditions, thermal properties of workpiece/tool material on cutting temperature.

MIC2020

Experimental set-up

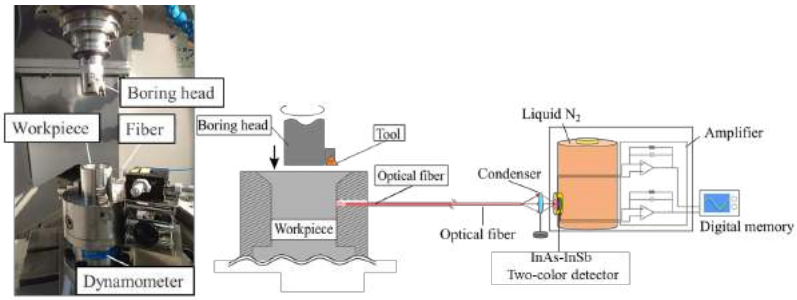

MIC2020

Typical output waves of two-color pyrometer

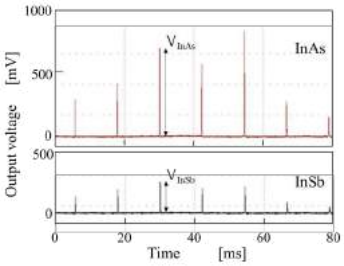

NAGOYA UNIVERSITY

15

MIC2020

Frequency characteristics of pyrometer

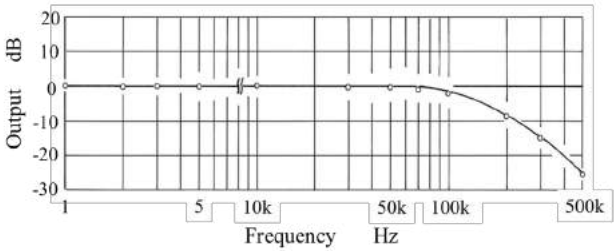

NAGOYA UNIVERSITY

16

MIC2020

Experimental conditions

Table 1 Experimental conditions

Cutting speed	v	m/min	50 ~ 800
Depth of cut	a	mm	0.05 ~ 0.15
Feed rate	f	mm/rev	0.1 ~ 0.3

NAGOYA UNIVERSITY

17

MIC2020

Influence of cutting speed on cutting temperature

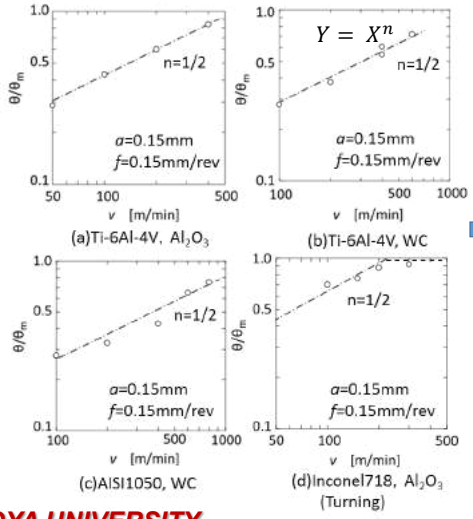

From these figures, the propriety of the following equations is confirmed.

$\theta/\theta_m \propto v^{1/2}$

NAGOYA UNIVERSITY

18

MIC2020

Influence of depth of cut and feed rate on cutting temperature

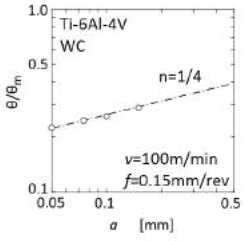

(a) Depth of cut

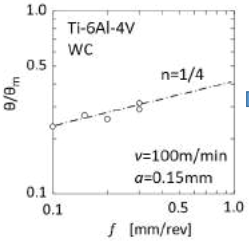

(b) Feed rate

$\theta/\theta_m \propto a^{1/4}$
$\theta/\theta_m \propto f^{1/4}$

NAGOYA UNIVERSITY

19

MIC2020

Influence of a, f, v on cutting temperature

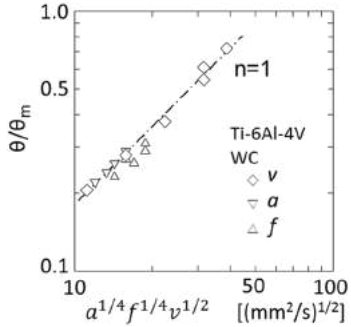

$\theta/\theta_m \propto (a^{1/4} f^{1/4} v^{1/2})$

NAGOYA UNIVERSITY

20

MIC2020

Influence of thermal properties of workpiece/tool material on cutting temperature

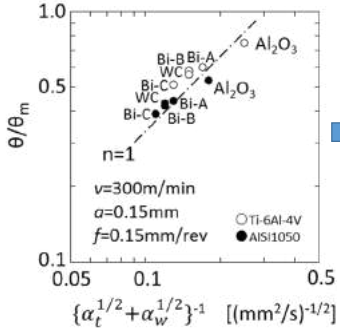

$$\theta/\theta_m \propto \frac{1}{\alpha_t^{1/2}+\alpha_w^{1/2}}$$

NAGOYA UNIVERSITY

21

MIC2020

Influence of cutting conditions (*a*, *f*, *v*), thermal properties of workpiece/tool material on cutting temperature

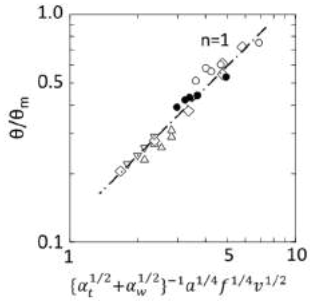

$$\theta/\theta_m \propto \frac{1}{\alpha_t^{1/2}+\alpha_w^{1/2}} a^{1/4} f^{1/4} v^{1/2}$$

NAGOYA UNIVERSITY

22

MIC2020

Conclusions

1. An evaluating function to present the overall influence of these elements on temperature is derived by the dimensional analysis.

2. Our evaluating function consists of physical quantities of cutting speed, depth of cut, feed rate, specific cutting energy, and thermal conductivity and volumetric heat capacity of the workpiece/tool.

3. The derived function is useful to evaluate the overall influence of these physical quantities on the cutting temperature.

NAGOYA UNIVERSITY

In-process Virtual Quality Monitoring

Shashwat Kushwaha,
Research Assistant,
Katholieke Universiteit Leuven, Belgium

KU LEUVEN

In-process

Virtual Quality Monitoring

-Shashwat Kushwaha
02.12.2020
MIC 2020, Hannover, Germany

Current industrial practice/process

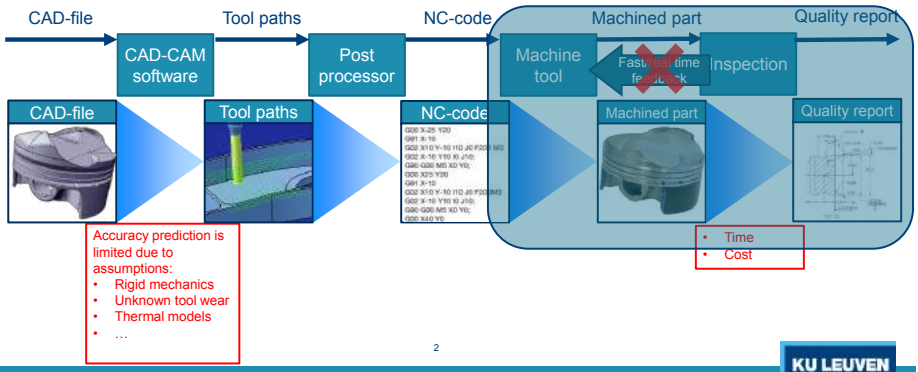

2

KU LEUVEN

Proposed workflow

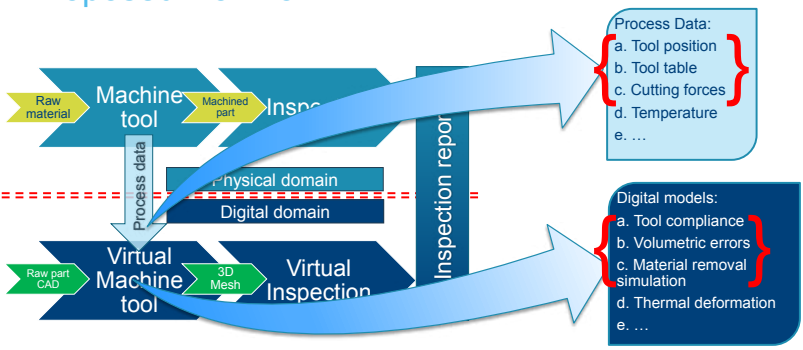

3

KU LEUVEN

Compliance map

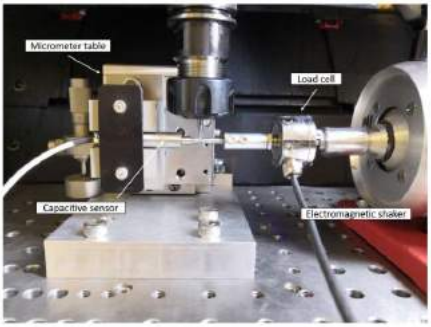

Static compliance measurement

- Compliance of the tool centre point as a function of machine's working volume

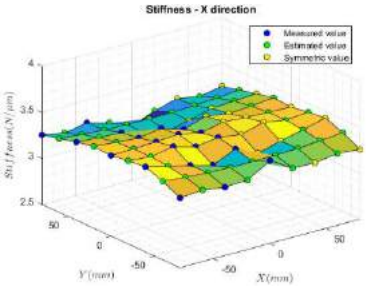

4

KU LEUVEN

Estimation of tool deviation

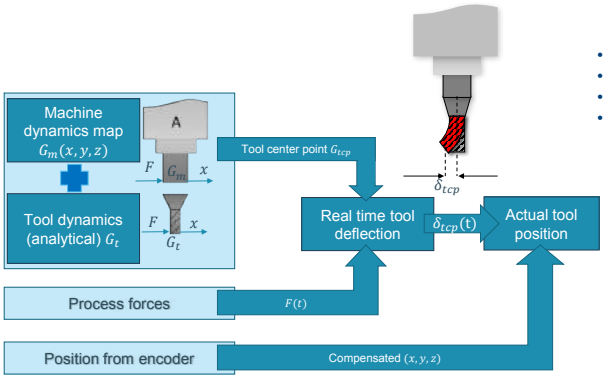

- Tool dynamics valid for 0-200 Hz
- Analog data sampling at 1 kHz
- Position at 200 Hz
- Encoder at 500 Hz

5

KU LEUVEN

Validation

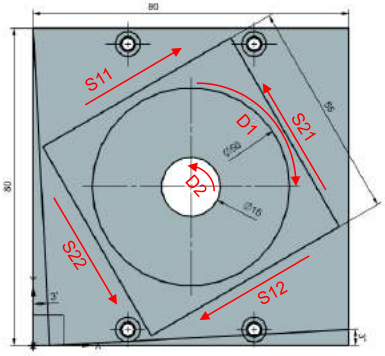

Feature	Cut type	Cutter compensation	Nominal dimension [mm]	Expected deviation
S1	Down	On	55	+
S2	Up	Off	55	~
D1	Down	On	50	+
D2	Down	On	15	-

6

KU LEUVEN

Validation: Dimensional deviations

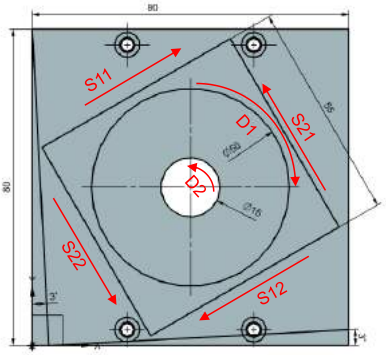

Feature	Nominal dimension [mm]	Expected deviation	CMM [mm] (deviation from nominal)	Virtual measurements [mm] (deviation as compared to CMM)
S1	55	+	55.0289 (+0.0289)	55.037 (+0.0081)
S2	55	~	54.9901 (-0.0099)	55.001 (+0.0109)
D1	50	+	50.0311 (+0.0311)	50.038 (+0.0069)
D2	15	-	14.9659 (-0.0341)	14.958 (-0.0079)
		Mean error as compared to CMM		0.0085

KU LEUVEN

Validation: Geometric tolerances

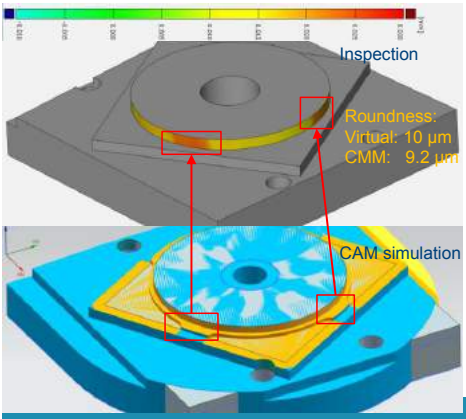

- High speed analog data is used to refine feature
- Improved geometric tolerances

KU LEUVEN

Faster outlook on results

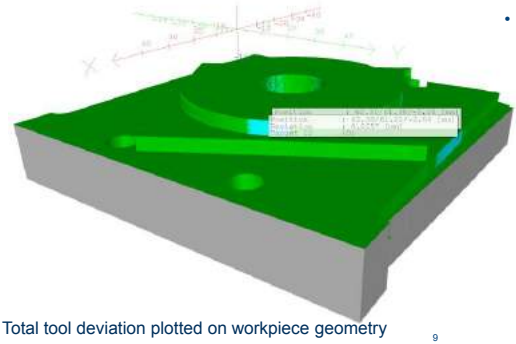

Total tool deviation plotted on workpiece geometry

- High speed analog data is used to refine feature
- Improved geometric tolerances

9

KU LEUVEN

Conclusion and future outlook

- Real time virtual machining (0.4 hours vs 3.25 hours of machining)
- Static and dynamic compliance map (analogous to volumetric error compensation map)
- Tool deviation estimation (max uncertainty ± 2.5 µm)

- Refine existing models
- Add more models, e.g. thermal, workpiece deformation
- Closed-loop machining
- Streamline hardware integration

10

KU LEUVEN

Design and Manufacturing Strategy of a Back-to-back Test Rig for Investigation of Ultra High Cycle Fatigue Strength regarding Tooth Root Strength in Aerospace Applications

ohannes Lövenich,
Research Assistant,
RWTH Aachen

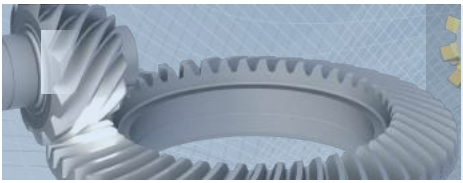

Design and Manufacturing Strategy of a Back-to-back Test Rig for Investigation of Ultra High Cycle Fatigue Strength regarding Tooth Root Strength in Aerospace Applications

Johannes Lövenich M.Sc. RWTH

Werkzeugmaschinenlabor (WZL) der RWTH Aachen
Lehrstuhl für Werkzeugmaschinen
Prof. Dr.-Ing. C. Brecher
J. Brimmers M.Sc. M.Sc.

20th Machining Innovations Conference for Aerospace Industry 2020 (MIC 2020), December 2nd 2020, Hannover, Germany

Fraunhofer IPT WZL | RWTH AACHEN UNIVERSITY

Structure

Fraunhofer IPT WZL | RWTH AACHEN UNIVERSITY

Introduction and Motivation

Extended SN-Curve and classification of aviation gear units

Pratt & Whitney PW1000G (A320neo)

- i ca. 3:1
- n_{Fan}: 3500 rpm
- n_{ND}: 10000 rpm
- P: 22.4 MW

Rolls Royce Ultrafan®

- P: 74.4 MW

Planet

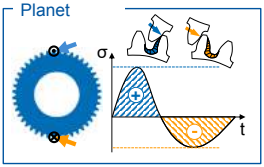

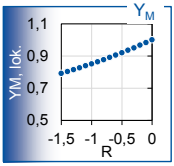

Example calculation D-Check

n_{Planet}: 10000 rpm
t_{check}(D-Check): 20000 h
N_{Planet}(20000h): 2.4×10^{10} LC
Maximum Take off Power (MTOP)

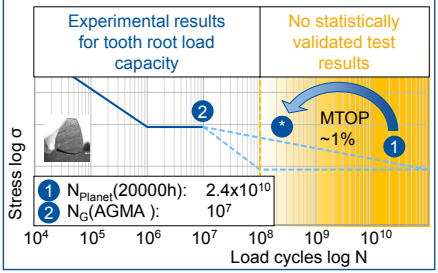

Fraunhofer IPT | WZL RWTH AACHEN UNIVERSITY

Structure

Fraunhofer IPT | WZL RWTH AACHEN UNIVERSITY

Fundamentals of Gear Investigation

Overview Damages on Gears

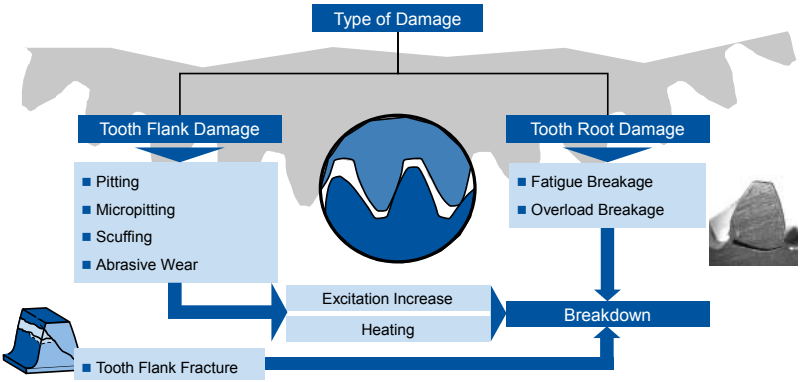

5 © Werkzeugmaschinenlabor WZL / Fraunhofer IPT

Fraunhofer IPT WZL RWTH AACHEN UNIVERSITY

Fundamentals of Gear Investigation

Gear testing methods and standardized back-to-back test rig

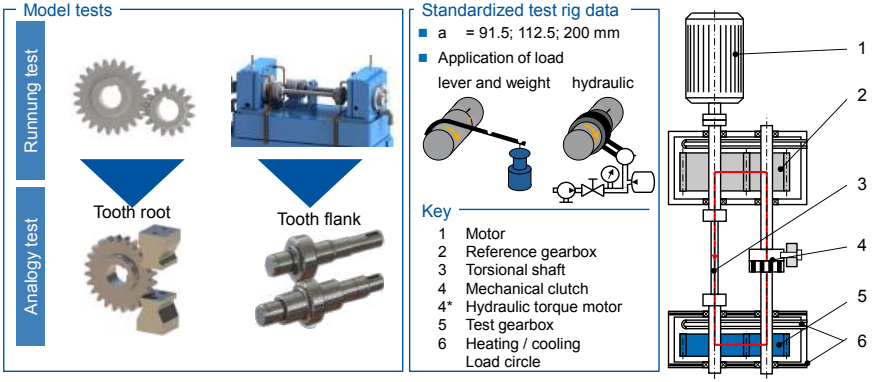

6 © Werkzeugmaschinenlabor WZL / Fraunhofer IPT

Fraunhofer IPT WZL RWTH AACHEN UNIVERSITY

Structure

Fraunhofer IPT WZL | RWTH AACHEN UNIVERSITY

Tooth root Load capacity in UHCF range

SN-Curves for material behaviour in the UHCF range

Duplex SN-Curve (SAKAI)

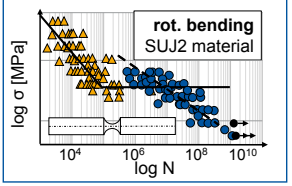

Crack initiation

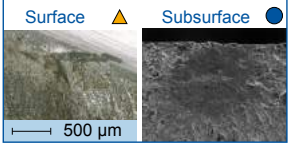

Late tooth root fractures (SCHURER)

Gear geometry:

- m_n: 1.5 mm
- b: 8 mm
- z: 59/61
- α: 20°
- β: 0°

Material data:

- Material: 20MnCr5
- Surface: shot peened
- Heat treat.: case hardening

Pulsator:

- f: 70-110 Hz

Back-to-back test rig:

- a: 91.5 mm
- n_{pinion}: 3400 rpm
- R: 0

Back-to-back tests (SCHURER)

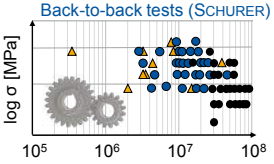

Pulsatortests (SCHURER)

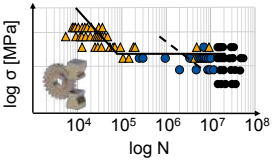

Fraunhofer IPT WZL | RWTH AACHEN UNIVERSITY

Tooth root Load capacity in UHCF range

Calculation model Murakami

Stress Ratio

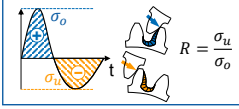

Vickers hardness

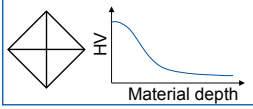

Inclusionsize

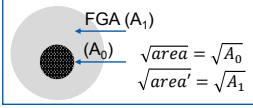

MURAKAMI

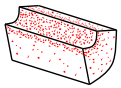

Surface Failure

$$\sigma_w = 1{,}56 \cdot \frac{HV + 120}{(\sqrt[2]{area})^{\frac{1}{6}}} \cdot \left[\frac{1-R}{2}\right]^{\alpha}$$

Subsurface Failure

$$\sigma_w = 1{,}43 \cdot \frac{HV + 120}{(\sqrt[2]{area})^{\frac{1}{6}}} \cdot \left[\frac{1-R}{2}\right]^{\alpha}$$

with

$$\alpha = 0{,}226 + HV \cdot 10^{-4}$$

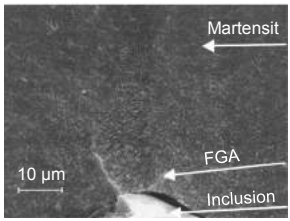

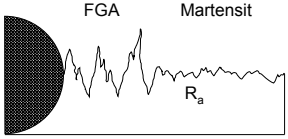

Fraunhofer IPT | WZL | RWTH AACHEN UNIVERSITY

Structure

Fraunhofer IPT | WZL | RWTH AACHEN UNIVERSITY

UHCF test rig concept

Test rig overview

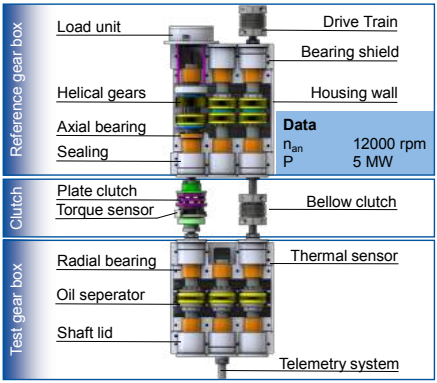

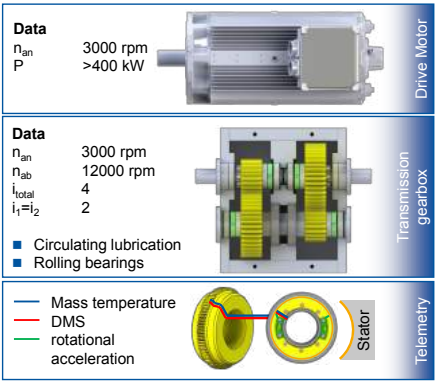

Fraunhofer IPT WZL RWTH AACHEN UNIVERSITY

UHCF test rig concept

Lubrication and power losses

Bearing Lubrication

#	n	T_{in} [°C]	T_{out} [°C]	P_{loss} [kW]	Q_{oil} [l/min]
1	4	45	63	18	34
2	8	45	59	14	34
3	2	45	61	13	20
	14			210	448

Gear Lubrication

#	n	T_{in} [°C]	T_{out} [°C]	P_{loss} [kW]	Q_{oil} [l/min]
4	2	140	100-170	50	73
5	2	45	55-75	50	73
	4			200	292

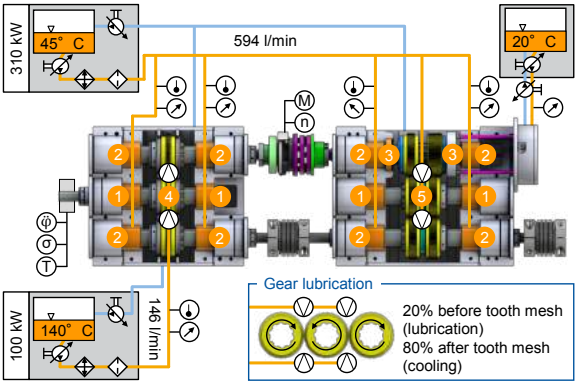

Fraunhofer IPT WZL RWTH AACHEN UNIVERSITY

UHCF Test rig concept
Load application system

Concept for load application

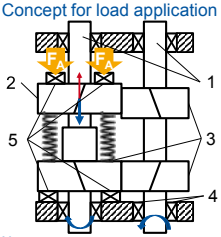

Key
- 1: Shafts
- 2: Sliding helical gear
- 3: Fixed helical gear
- 4: Radial bearing
- 5: Axial bearing
- F_A Axial force
- **Loading** / Unloading

Design

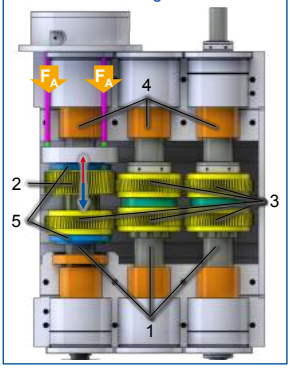

Operation and function
- Due to the journal bearings, the system must be started up loadfree and can only be tensioned at test speed
- Double helical gears for compensation of axial forces

Manufacturing challenges
- Imprecise manufacture of the double helical gears to each other leads to an uneven load distribution and a wandering contact pattern which leads to vibration excitation of the system
- Vibrations in the system can cause damage to the sensitive measuring technology and the journal bearings

Fraunhofer IPT | WZL RWTH AACHEN UNIVERSITY

Structure

Fraunhofer IPT | WZL RWTH AACHEN UNIVERSITY

Manufacturing challenges

1 Shiftable double helical gears

- Precise manufacture of the helical gears to each other
- Low friction surfaces on the splined shaft profile (PECVD)

2 Fixed double helical gears

- Precise manufacture of the helical gears to each other
- Very high depth of spline hub (>160 mm)
- Possible Production technology: eroding

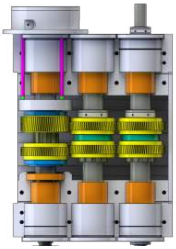

3 Balancing and concentricity of the shafts

- High demands on the concentricity of the shafts
  - High length of l = 1.3 meters
  - Low-distortion hardening through long-term nitriding (t > 80h)
- Balancing of the shafts before every test

4 Bearing seats

- Precise manufacture of the bearing seats to each other through spindles with large bearing distance of a > 1m

Fraunhofer IPT | WZL | RWTH AACHEN UNIVERSITY

Manufacturing concept

Production chain for reference gears

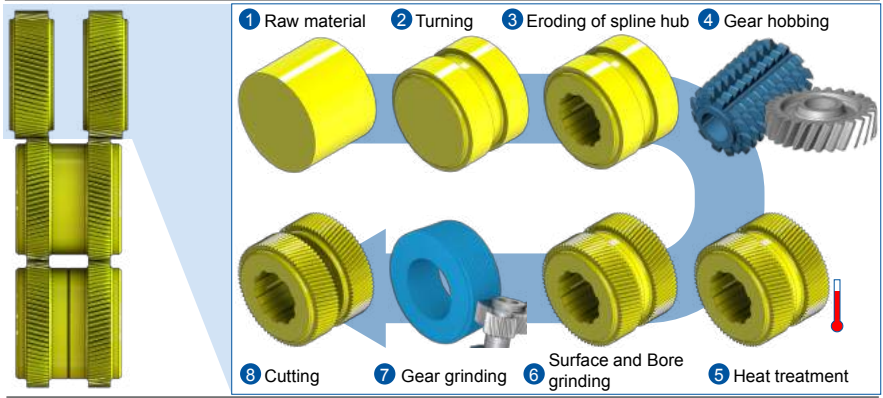

Fraunhofer IPT | WZL | RWTH AACHEN UNIVERSITY

Structure

1	Introduction and Motivation
2	Fundamentals of Gear Investigation
3	Tooth root load capacity in UHCF range
4	UHCF test rig concept
5	Manufacturing challenges and concept
6	**Summary and Outlook**

Fraunhofer IPT WZL | RWTH AACHEN UNIVERSITY

Summary and Outlook

Summary

- Standard bracing test rigs do not allow economic testing of gears in the performance class of aviation applications up to the UHCF range
- In the UHCF range, there is a shift of the crack starting point from the surface below it, so that the material purity plays a very important role in aerospace gears → New material models have to be developed
- The high power and speed of the test rig leads to manufacturing challenges
  - Double helical gears (axial force compensation)
  - High concentricity of the shafts

Outlook

- Currently the production of the test rig and the assembly and commissioning of a lower-performance prototype is in progress
- Next year the main test rig will be set up and then UHCF tests up to N > 10^8 will be performed
- Based on the results of the tooth root load capacity tests, a calculation model for the behavior of gears under alternating load in the UHCF range is created in combination with standard samples

Fraunhofer IPT WZL | RWTH AACHEN UNIVERSITY

Contact Details

Jens Brimmers M.Sc. M.Sc.

WZL Aachen GmbH
Steinbachstr. 25
52074 Aachen

☎ +49 241 / 56 622 304

✉ j.brimmers@wzl-aachen-gmbh.de

For the WZL of RWTH Aachen University:

Johannes Lövenich M.Sc.

Werkzeugmaschinenlabor WZL der RWTH Aachen
Campus-Boulevard 30
52074 Aachen

☎ +49 241 / 80 27 996

✉ j.loevenich@wzl.rwth-aachen.de

Project homepage: www.match4turbo.de

Fraunhofer IPT

WZL | RWTH AACHEN UNIVERSITY

In-process quality monitoring during turning based on high frequency machine data

Alexander Fertig,
Research Assistant,
TU Dortmund

In-process quality monitoring during turning based on high frequency machine data

Alexander Fertig, Christoph Bauerdick, Matthias Weigold

Garbsen | 02. December 2020
20th Machining Innovations Conference for Aerospace Industry

Agenda

Introduction and objective

TU DARMSTADT

Manual inspection

- staff intensive
- error-prone
- cost-intensive
- offline

Additional sensors

- cost-intensive
- installation costs
- high maintenance effort
- most common approach in research

Internal data

Objective

- automated
- cost-effective (no additional sensor technology)
- in-process

Sources: [CHIN20], [WILL20], [EMAG13]

Investigation whether and to what conclusions about occurring defects in raw workpieces can be detected by using only high-frequency internal drive data

Experimental configuration

TU DARMSTADT

Environment and data acquisition

Experimental environment

- Machine Tool: EMAG VLC 100 Y

Source: [EMAG13]

- Control system: IndraMotion MTX
- Recording solution: Efficiency Workbench with an industrial PC
- Sampling frequency: up to 500 Hz (Interpolationcycle)
- Process: Machining process of a control disc for coaxial pumps

Efficiency Workbench (EWB)

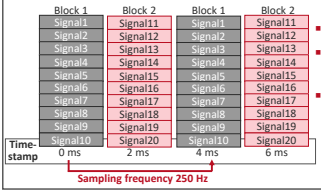

- SERCOS signals
- Alternately recording of 10 signals per block
- Resulting frequency for sampling of 20 signals: 250 Hz

Recorded internal drive signals

Current	Torque/Force	Actual position	Power, Voltage
X, Y, Z, spindle	X, Y, Z, spindle	X, Y, Z	spindle

+ NC block

Databasis: 20 process parallel recorded internal drive signals

Experimental configuration

TU DARMSTADT

Setup and sesign

Experimental setup

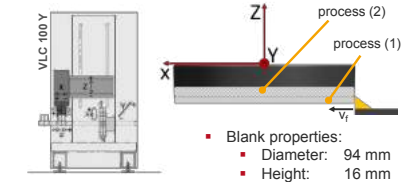

- 2 face turning processes
- Blank properties:
  - Diameter: 94 mm
  - Height: 16 mm
  - Material: 8CrMo16

Experimental parameters

Process	a_p in mm	v_c in m/min	f in mm/rev
1)	1.3	180	0.3
2)	1.5	180	0.3

Simulated defects

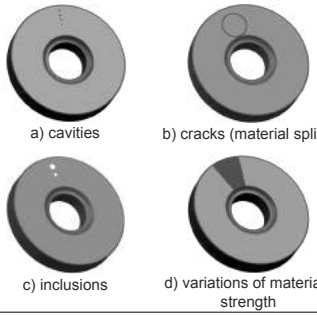

a) cavities b) cracks (material splits) c) inclusions d) variations of materials strength

First two turning processes of considered control disc were examined with simulated defects in blanks

Data analysis

TU DARMSTADT

Internal drive signals and interim conclusion

Internal drive signals

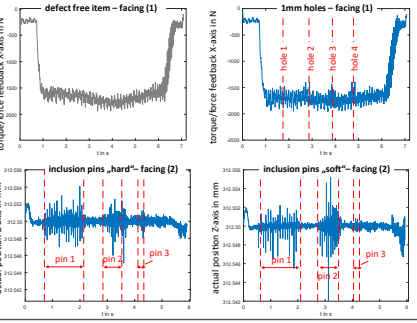

Interim conclusion

- Holes, inclusions and variations of material strengths can be detected by using internal drive data
- Cracks too small for detectable impacts in the data
- Machine internal signals not equally suitable for the detection of component defects
- higher sampling rates enable detection of smaller defects

Reduction to 10 relevant signals to achieve sampling rates of 500 Hz with EWB

Higher sampling frequencies allow detection of smaller defects

Feature reduction and analysis

TU DARMSTADT

Correlation and collinearity

Correlation

- Calculation of correlations coefficients between recorded signals: $r_{xy} = \frac{s_{xy}}{s_x s_y} = \frac{\sum(x_i - \bar{x})(y_i - \bar{y})}{\sqrt{\sum(x_i - \bar{x})^2 \sum(y_i - \bar{y})^2}}$
- Five data packages of error-free blanks
- 8 pairs of signals identified with $|r_{xy}| \geq 0.95$
- Correlated signals generated from the same data basis

First signal	Second signal
Torque/force feedback value (Y)	Process torque/force value (Y)
Torque/force feedback value (Y)	Phase current U (Y)
Phase current U (Y)	Process torque/force value (Y)
Phase current V (Y)	Process torque/force value (Y)
Torque/force feedback value (X)	Process torque/force value (X)
Torque/force feedback value (Y)	Phase current V (Y)
Phase current U (Y)	Phase current V (Y)
Torque/force feedback value (Z)	Process torque/force value (Z)

Collinearity

- Variance inflation factor (VIF): metric for multicollinearity
- Iterative calculation of the VIF for each signal:
  1. VIF for all signals for process (1) and process (2)
  2. Removing signal with highest VIF
  3. Continuing iteration until none of signals has a VIF >10
- Counting prevalence of naming a signal as collinear independent for all workpieces for final comparison

Top 10 signals	Prevalence VIF<10 in %:	facing (1)	facing (2)
Actual position (Y)		100	100
Phase current U (spindle)		100	100
Phase current U (X)		100	100
Phase current V (spindle)		100	100
Phase current V (X)		100	100
Phase current U (Z)		100	98.7
Phase current U (Y)		94.7	97.4
Phase current V (Z)		96.1	92.1
Torque/force feedback value (Z)		94.7	90.8
Torque/force feedback value (spindle)		2.6	19.7

Correlation and collinearity analysis as support for signal reduction process

Feature reduction and analysis

TU DARMSTADT

Signal reduction and feature analysis

Procedure

- Calculation of features from error-free and defective blanks for each signal
- Analysis of time-domain and frequency domain features
- Classification with a Ridge-Classifier
- Determination of Top10 signals based on classification results

Time-domain features

- Calculation of 14 time-domain features, which a most commonly used in machine monitoring systems

Poor classification results with miss classification rates of nearly 50 %

Frequency-domain features

Cepstrum

$$c_x = \frac{1}{2\pi}\int_{-\pi}^{\pi} \ln\left|X\left(e^{j\omega}\right)\right| e^{j\omega n} d\omega$$

Spectral Kurtosis

$$Kurt\,(X) = \frac{\mu_4}{\sigma^4} = \frac{E[(X-\mu)^4]}{(E[(X-\mu)^2])^2}$$

- Weighted error score: $e_{P,w} = g_f + w * f_g = g_f + 5 * f_g$

  $g_f \triangleq$ false positives $f_g \triangleq$ false negatives $w \triangleq$ weight
- Sum of $e_{P,w}$ for process (1) and process (2) for each signal

Top10 signals for further classification approaches

Cepstrum and spectral kurtosis provide best results for determination of Top10 signals

Feature reduction and analysis

TU DARMSTADT

Result of feature reduction

Ranking	Signal	Sum
1	Phase current U (X)	0
2	Phase current U (X)	1
3	Phase current V (X)	1
4	Process torque/force value	1
5	Process torque/force value	1
6	Phase current V (X)	5
7	Power (spindle)	5
8	Actual position (Y)	8
~~9~~	~~Phase current U (spindle)~~	~~13~~
~~10~~	~~Torque/force feedback (spindle)~~	~~16~~
localization	Actual position (Z)	31
localization	Actual position (X)	34

Selection of the Top8 signals with additional 2 localization signals

Classification approaches

TU DARMSTADT

Binary classification based on envelope curves

Classification approach

- Calculation of envelope curves from 30 good workpieces
- Entering all data sets of the remaining workpieces

Positive results with 3 major failures: one cavity, one crack, and one hardened workpiece

Power (spindle) –process (1)

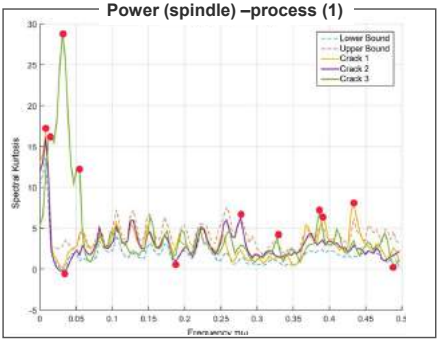

Classification Approach based on envelope curves shows weaknesses

Classification approaches

Binary classification based on a Convolutional Neural Network (CNN)

Time-Frequency Representations using „Velocity Synchronous Linear Chirplet Transform“ (VSLCT)

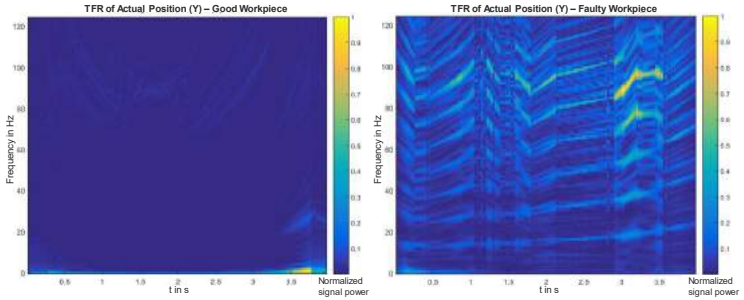

Transformation of time-series data to image data

Classification approaches

Binary classification based on a Convolutional Neural Network (CNN)

Convolutional Neural Network

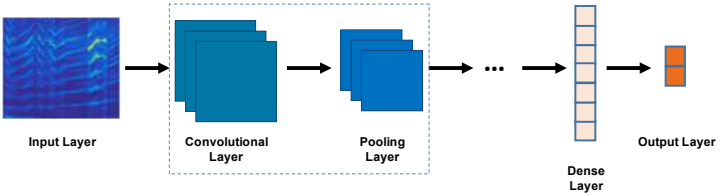

ParameterS:

- CNN from the Python library Keras [FRAN18]
- 16 Convolutional layers
- Kernel size: 5x5
- 32 filter per layer
- Global-Max-Pooling
- Split of dataset: randomly, 80/20 training/test

All test workpieces were classified correctly

Conclusion

Summary and outlook

Summary

- Approach for developing an in-process quality monitoring system based on machine tool data
- Analysis of faultless and defective workpieces during face turning processes
- High frequency data acquisiton of internal drive data (250 Hz)
- Identification of Top10 signals for defect classification based on
  - Correlation and collinearity analysis
  - Frequency domain feature analysis
  - Classification results based on ridge classification
- Two approaches for classification developed an evaluated:
  - Binary classification based on envelope curves
  - Classification with a CNN based on VSCLT

Outlook

- Higher sampling frequencies in further investigations
- Expectation to detect even smaller defects
- Deployment of models for online analysis

Thank you for your kind attention!!

Please do not hesitate to contact us.

Alexander Fertig
Institute of Production Management, Technology and Machine Tools
Technical University of Darmstadt

Otto-Berndt-Straße 2
64287 Darmstadt

Phone.: +49 61 51 | 16 29973
Fax: +49 61 51 | 16 20087
E-Mail: a.fertig@ptw.tu-darmstadt.de
Internet: www.ptw.tu-darmstadt.de

Sources:
[CHIN20] https://www.chinaimportal.com/blog/thailand-quality-inspection-companies/
[WILL20] https://www.willtec.de/sensorik/
[EMAG13] EMAG GmbH & Co. KG: EMAG VLC 100 Y im Schnitt, Salach, 2013

Innovative processes and machine tool components for aerospace industry

Alexander Krödel,
Head of Department Manufacturing Processes,
Leibniz Universität Hannover

IFW
Institut für Fertigungstechnik
und Werkzeugmaschinen
Prof. Dr.-Ing. Berend Denkena

Innovative processes and machine tool components for aerospace industry

Dr.-Ing. A. Krödel

2nd December 2020

Leibniz Universität Hannover
Produktionstechnisches Zentrum Hannover

Challenges and limiting factors in aerospace industry

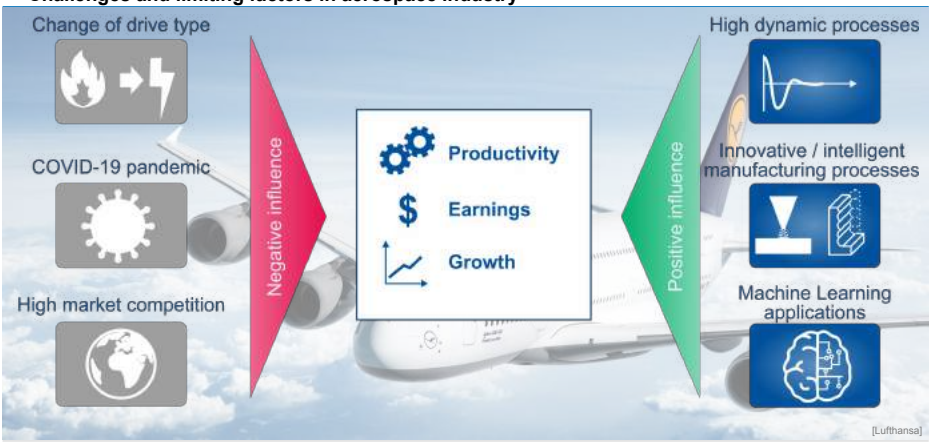

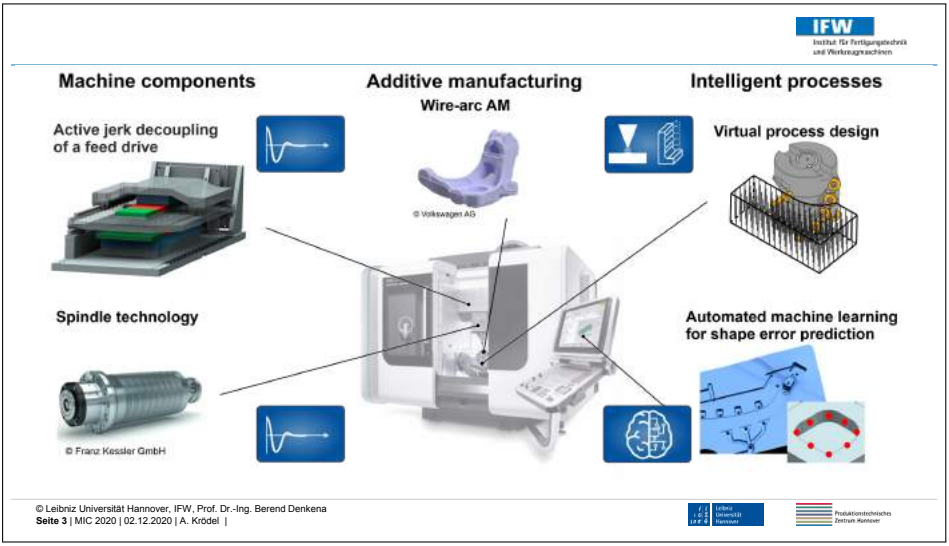
IFW
Institut für Fertigungstechnik und Werkzeugmaschinen
Machine components
Additive manufacturing
Wire-arc AM
Intelligent processes
Active jerk decoupling of a feed drive
© Volkswagen AG
Virtual process design
Spindle technology
© Franz Kessler GmbH
Automated machine learning for shape error prediction
© Leibniz Universität Hannover, IFW, Prof. Dr.-Ing. Berend Denkena
Seite 3 | MIC 2020 | 02.12.2020 | A. Krödel |

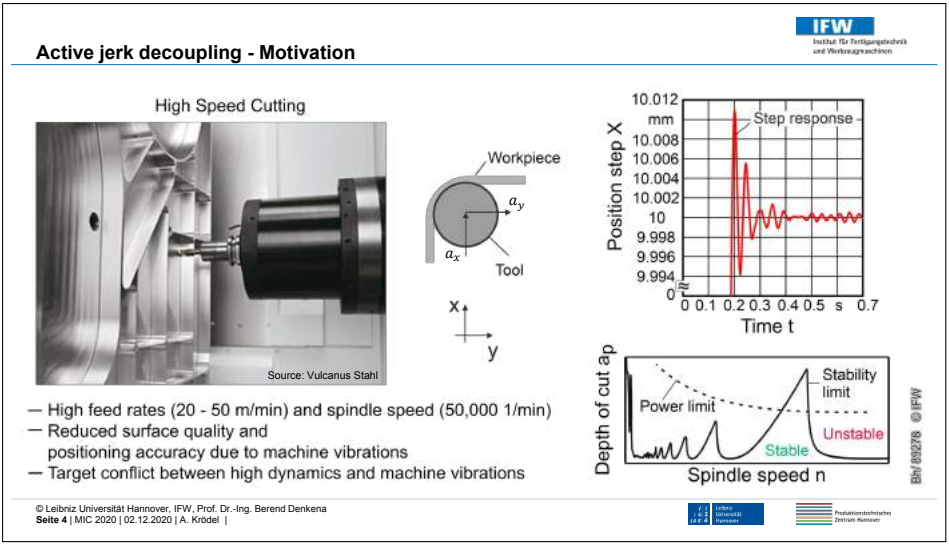
IFW
Institut für Fertigungstechnik und Werkzeugmaschinen
Active jerk decoupling - Motivation
High Speed Cutting
Source: Vulcanus Stahl
Workpiece
a_y
a_x
Tool
x
y
10.012
mm
10.008
10.006
10.004
10.002
10
9.998
9.996
9.994
Position step X
Step response
0 0.1 0.2 0.3 0.4 0.5 s 0.7
Time t
Depth of cut ap
Power limit
Stability limit
Stable
Unstable
Spindle speed n
— High feed rates (20 - 50 m/min) and spindle speed (50,000 1/min)
— Reduced surface quality and positioning accuracy due to machine vibrations
— Target conflict between high dynamics and machine vibrations
Bh/ 89276 © IFW
© Leibniz Universität Hannover, IFW, Prof. Dr.-Ing. Berend Denkena
Seite 4 | MIC 2020 | 02.12.2020 | A. Krödel |

Active jerk decoupling - Design

Active jerk decoupling concept

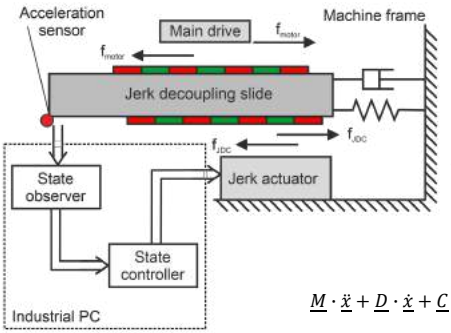

Active jerk decoupled direct drive

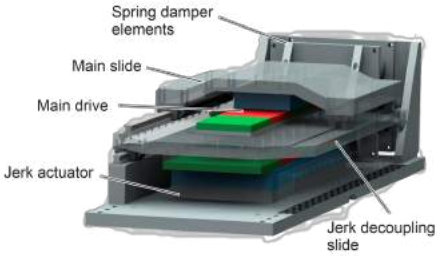

$$\underline{M} \cdot \ddot{\underline{x}} + \underline{D} \cdot \dot{\underline{x}} + \underline{C} \cdot \underline{x} = \begin{bmatrix} -1 & 1 \\ 0 & -1 \end{bmatrix} \cdot \begin{bmatrix} f_{motor} \\ f_{JDC} \end{bmatrix}$$

Bh/89264 © IFW

Source: Ph.D. Thesis Peter Hesse (2008), Oliver Gümmer (2014)

Active jerk decoupling - Effect

Cross table test rig

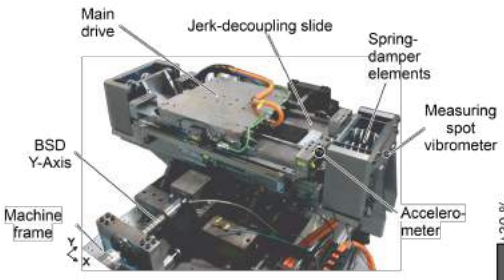

Frame vibration by 120 mm positioning step

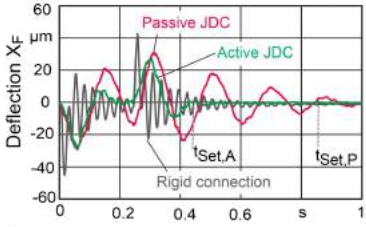

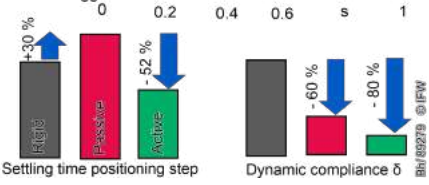

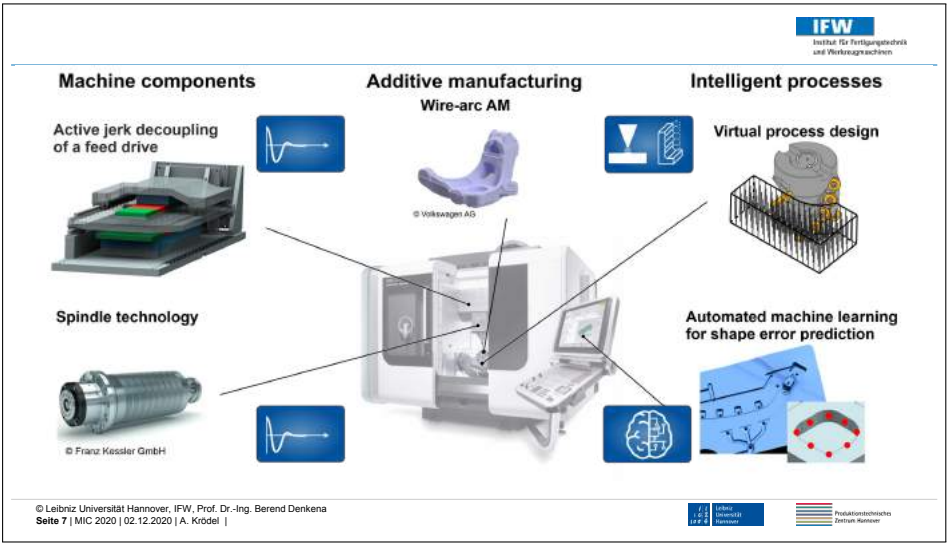
IFW
Machine components
Additive manufacturing
Intelligent processes
Active jerk decoupling of a feed drive
Wire-arc AM
© Volkswagen AG
Virtual process design
Spindle technology
© Franz Kessler GmbH
Automated machine learning for shape error prediction
© Leibniz Universität Hannover, IFW, Prof. Dr.-Ing. Berend Denkena
Seite 7 | MIC 2020 | 02.12.2020 | A. Krödel |


IFW
Hybrid spindle - motivation
Structural components
Titanium parts
HPC
Aluminium parts
HSC
Switchable Spindle enables productive machining on HSC and HPC with an universal machine tool
Requirement:
Adaption of spindle preload
Lufthansa
[Lufthansa]
© Leibniz Universität Hannover, IFW, Prof. Dr.-Ing. Berend Denkena
Seite 8 | MIC 2020 | 02.12.2020 | A. Krödel |

Hybrid spindle – Design of the adaptive preload element

Switchable hybrid spindle

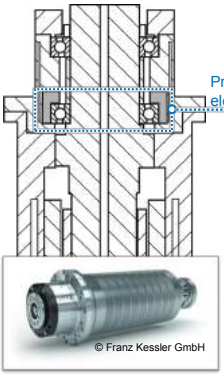

Adaptive preload element

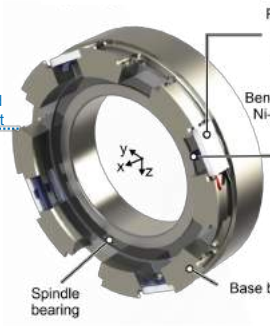

Operation principle

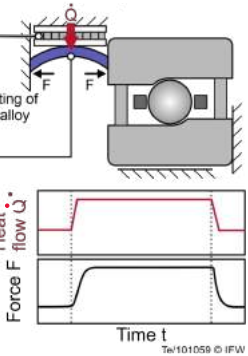

- Conversion of initiial preload force for HSC configuration
- Creating additional preload for HPC configuration

Hybrid spindle – Effect of the adaptive preload element

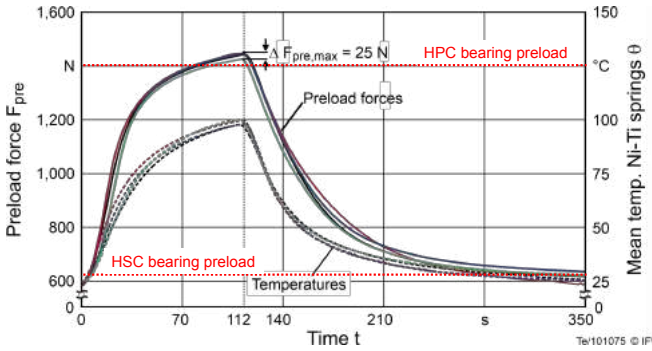

Energy efficient P = 80 W

Simple Design

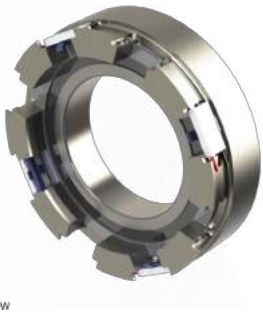

The adaptive preload element is suitable for use in the hybrid spindle

IFW
Institut für Fertigungstechnik und Werkzeugmaschinen

Machine components

Active jerk decoupling of a feed drive

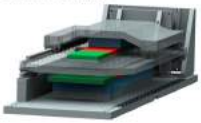

Spindle technology

© Franz Kessler GmbH

Additive manufacturing

Wire-arc AM

© Volkswagen AG

Intelligent processes

Virtual process design

Automated machine learning for shape error prediction

IFW
Institut für Fertigungstechnik und Werkzeugmaschinen

Additive Manufacturing

SLM
Selective Laser Melting

© DMG Mori

© SLM Solutions

LMD
Laser Metal Deposition

© DMG Mori

© Trumpf

WAAM
Wire Arc Additive Manufacturing

© Aircraft Philipp Group

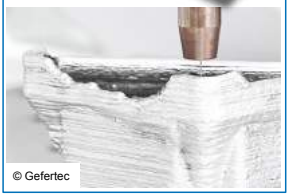

© Gefertec

Surface quality — **Productivity**

Process chain

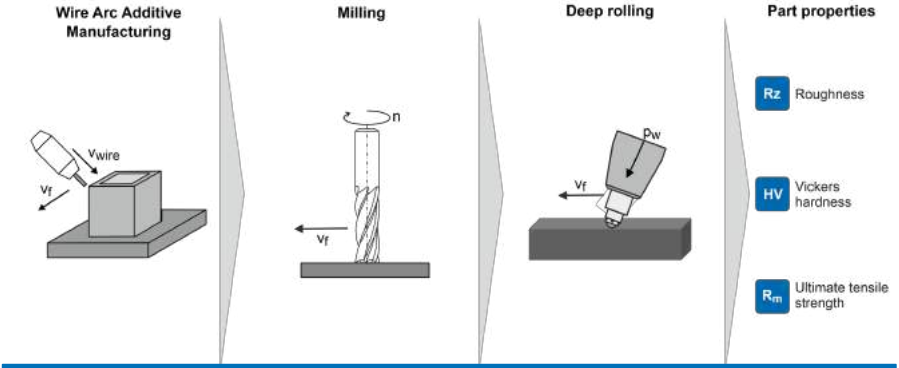

Investigation on the effects of mechanical finishing on WAAM part properties

Mechanical properties determined by tensile tests

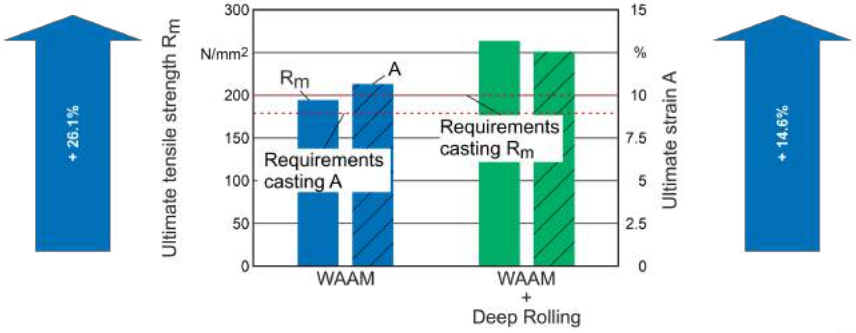

Deep rolling improves ultimate tensile strength R_m and ultimate strain A

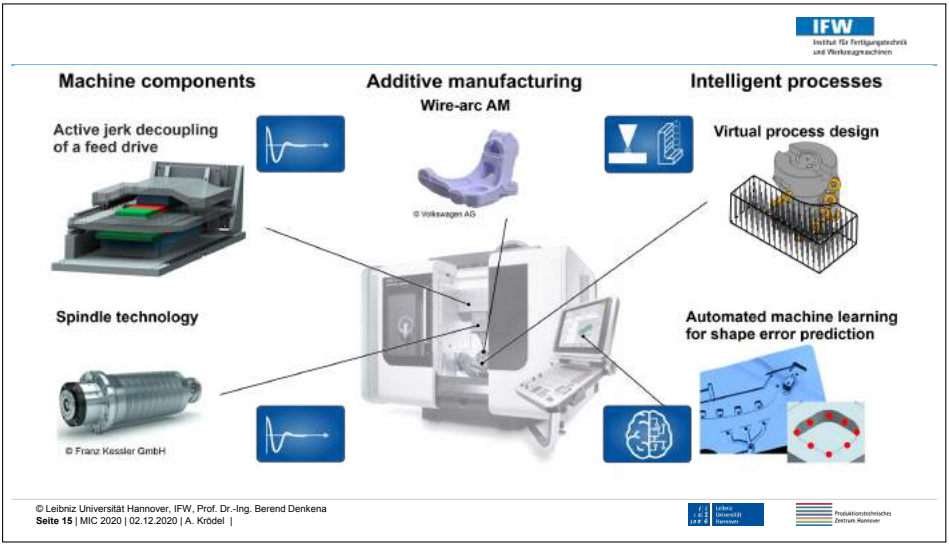
IFW
Machine components
Additive manufacturing
Intelligent processes
Active jerk decoupling of a feed drive
Wire-arc AM
© Volkswagen AG
Virtual process design
Spindle technology
© Franz Kessler GmbH
Automated machine learning for shape error prediction
© Leibniz Universität Hannover, IFW, Prof. Dr.-Ing. Berend Denkena
Seite 15 | MIC 2020 | 02.12.2020 | A. Krödel |

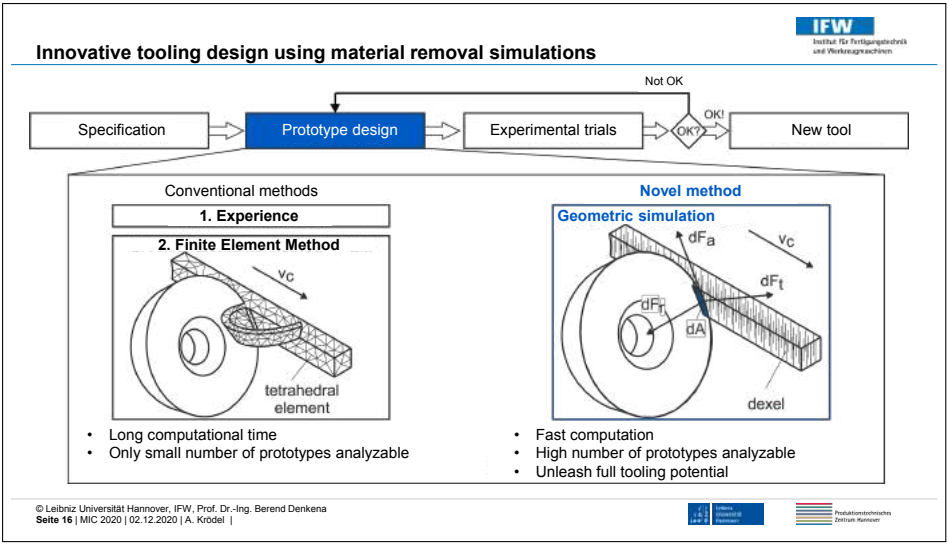
IFW
Innovative tooling design using material removal simulations
Not OK
Specification
Prototype design
Experimental trials
OK?
OK!
New tool
Conventional methods
1. Experience
2. Finite Element Method
vc
tetrahedral element
Long computational time
Only small number of prototypes analyzable
Novel method
Geometric simulation
dFa
vc
dFt
dFr
dA
dexel
Fast computation
High number of prototypes analyzable
Unleash full tooling potential
© Leibniz Universität Hannover, IFW, Prof. Dr.-Ing. Berend Denkena
Seite 16 | MIC 2020 | 02.12.2020 | A. Krödel |

Example: Simulation based design of a novel porcupine milling cutter

Conventional porcupine milling cutter

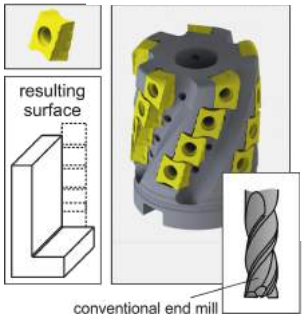

Prototype

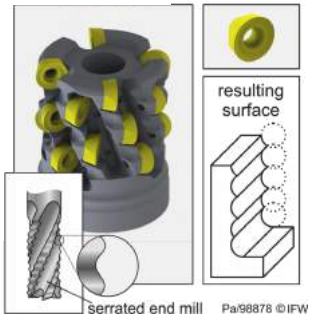

Productivity gain by reducing the radial force F_r

2. iteration geometry

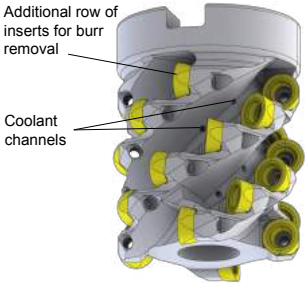

D = 50 mm

Comparison of radial force

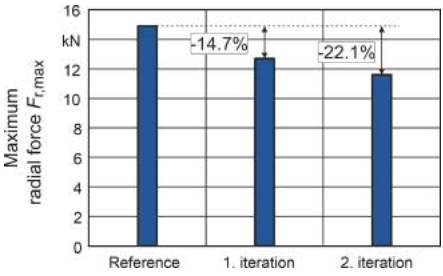

Machining titanium with optimized prototype

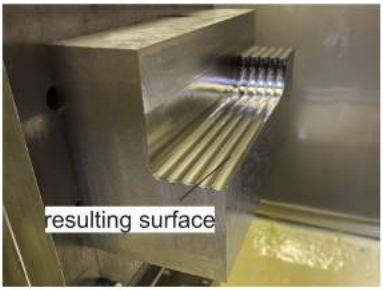

Process	Process parameters			
Milling	Cutting speed	v_c = 45 m/min	Cutting depth	a_p = 40 mm
Ti-6Al-4V	Feed per tooth	f_z = 0,15 mm	Cutting width	a_e = 30 mm

Pa/102881 © IFW

Announcement: spin-off from IFW

Start: December 2020

Founder:
Karolin Fricke
Arne Mücke
Oliver Pape

Product: Material removal simulation

Software for tool and process design

Soft-Sensor for offline and online process monitoring

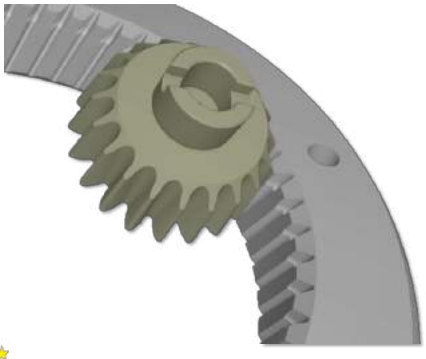

Contact:
Oliver Pape, pape@ifw.uni-hannover.de

Funded by:

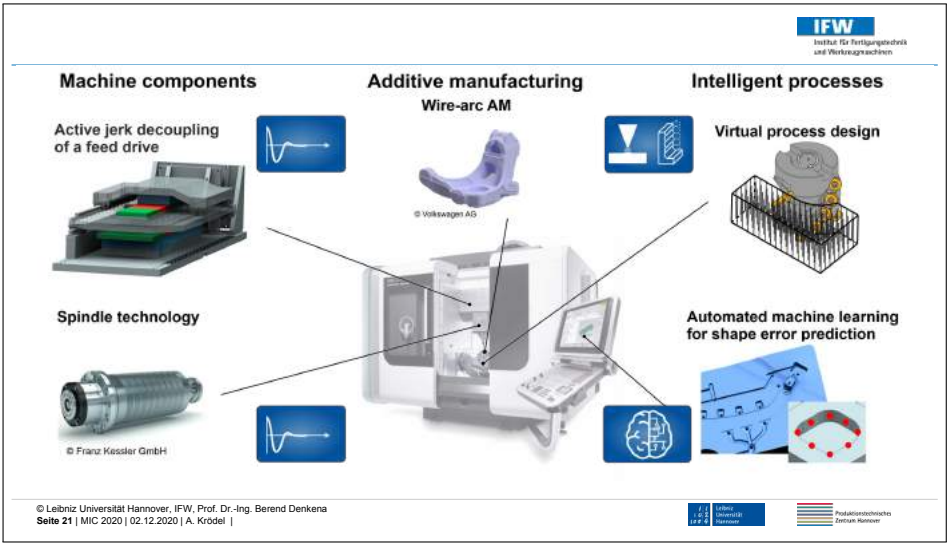
IFW
Machine components
Additive manufacturing
Intelligent processes
Active jerk decoupling of a feed drive
Wire-arc AM
© Volkswagen AG
Virtual process design
Spindle technology
© Franz Kessler GmbH
Automated machine learning for shape error prediction
© Leibniz Universität Hannover, IFW, Prof. Dr.-Ing. Berend Denkena
Seite 21 | MIC 2020 | 02.12.2020 | A. Krödel |

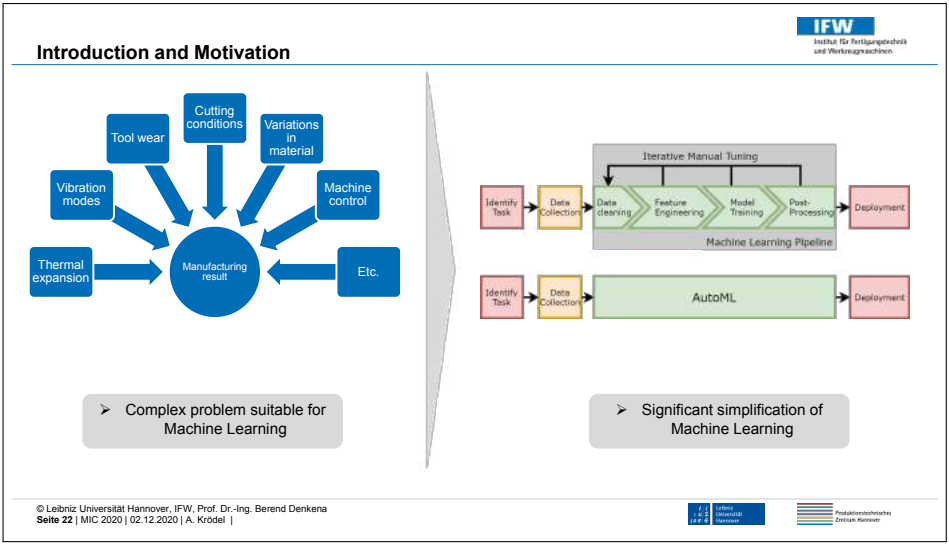
IFW
Introduction and Motivation
Tool wear
Cutting conditions
Variations in material
Vibration modes
Machine control
Thermal expansion
Manufacturing result
Etc.
Iterative Manual Tuning
Identify Task
Data Collection
Data cleaning
Feature Engineering
Model Training
Post-Processing
Deployment
Machine Learning Pipeline
Identify Task
Data Collection
AutoML
Deployment
Complex problem suitable for Machine Learning
Significant simplification of Machine Learning
© Leibniz Universität Hannover, IFW, Prof. Dr.-Ing. Berend Denkena
Seite 22 | MIC 2020 | 02.12.2020 | A. Krödel |

Results

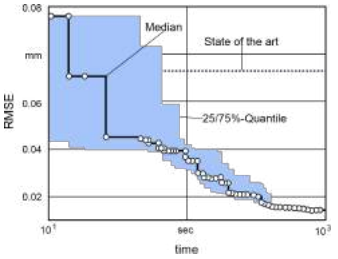

➢ Outdoing of conventional ML within minutes

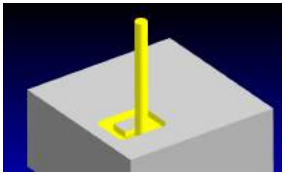

➢ Consideration of tool wear with simulation data (Set 2) significantly improves predictions

Simulation data